# Optimal Cruise Control of Heavy-Haul Trains Equipped with Electronic Controlled Pneumatic Brake Systems

by

**Ming-Shan Chou**

Submitted in partial fulfillment of the requirements for the degree

Master of Electronic Engineering

in the

Faculty of Engineering, Built Environment and Information Technology

UNIVERSITY OF PRETORIA

Aug 2005

# Optimal Cruise Control of Heavy-Haul Trains Equipped with Electronic Controlled Pneumatic Brake Systems

by

**Ming-Shan Chou**

Department: **Electronics Engineering**
Faculty of Engineering, Built Environment and Information Technology

Degree: **M. Eng (Electronics)**

**Keywords**: ECP, train control, closed-loop control, LQR, reconfigurable control, model validation, parameter tuning, optimised control.

## Summary

In this study a closed-loop cruise controller to minimise the running costs of the heavy-haul train is proposed. The running costs of a heavy-haul train are dependent on its travelling time, maintenance costs and energy consumption during the trip. The Coallink train with the new train technologies, Distributed Power (DP) traction and Electronically Controlled Pneumatic (ECP) brake system, is the centre of the study.

A literature study on existing train control, both passenger and heavy-haul trains, is carried out to build up a knowledge base. Many different techniques for train handling were observed, their features in relation to heavy-haul ECP trains are discussed.

From these backgrounds, a comprehensive longitudinal train model is proposed and successfully validated with real-life data from Spoornet. In the model, both static and dynamic in-train forces are studied, as well as energy consumption. This is possible by modelling each locomotive and wagon as an individual unit. The equations of motion for the train with coupled units and additional non-linearities, such as traction power limits, are considered.

An open-loop controller for maintaining equilibrium velocity is designed. During transient velocity changes, a transient controller for calculating the required additional acceleration and deceleration is designed and validated.

Because locomotive traction settings are only available in discrete notches, quantisation conversion from force into notches results in input chattering. In addition, during brake to traction transitions, the locomotives receive a sudden traction demand which results in spikes in in-train forces. To avoid these problems, input filtering is performed for these inputs.

Closed-loop controllers based on LQR method, optimised for in-train forces, energy consumption and velocity regulation respectively, are designed and compared. To overcome the communication constraints, a fencing concept is introduced whereby the controller is reconfigured adaptively to the current track topology. Different train configurations in terms of availability of additional control channels for both traction and braking are compared, as well as their effects on dynamic and static in-train force. These configurations are unified, distributed and individual traction and brake controls.

The results from these different configurations are compared to recorded train data and given in this study. From the results, it is found that the closed-loop controller optimised for in-train force is able to provide the best overall improvement out of the three controllers.

# Optimale Spoedbeheer van 'n Swaar-vrag Trein met Elektronies Beheerde Pneumatiese Briekstelsels

deur

**Ming-Shan Chou**

Departement: **Elektroniese Ingenieurswese**
Elektriese, Elektroniese en Rekenaar-Ingenieurswese Fakulteit

Degree: **M.Eng(Elektroniese)**

**Sleutelwoorde**: ECP, trein beheer, geslote-lus beheer, LQR, her-konfigureerbare beheer, model validasie, parameter instelling, optimale beheer.

## Opsomming

In hierdie studie word n geslote-lus spoed beheerstelsel wat die bedryfkostes van n swaar-vrag trein minimeer voorgestel. Die bedryfskoste van n hoe las trein is afhanklik van die trein se reistyd and energieverbruik vir die reis sowel as van die onderhoudskoste. Die Coallink trein met sy DP (Distributed Power) trek-krag en ECP (Electronically Controlled Pneumatic) briek stelsels was die fokus van hierdie studie.

n Literatuur-studie oor bestaande passasiers en swaar-vrag trein beheerstelsels is gedoen. Daar is opgemerk dat daar, ten spyte van die groot verskeidenheid metodes vir treinbeheer, geen bestaande beheerstelsels vir lang swaar-vrag ECP treine is nie.

Met hierdie agtergrond is n realistiese trein-model afgelei en suksesvol met Spoornet data bevestig. Die model is gebruik om statiese en dinamiese binnetreinse kragte en energie verbruik te ondersoek. Dit is moontlik gemaak deur elke lokomotief en wa as n individuele eenheid te modeleer. Die vergelykings vir die trein met gekoppelde eenhede is afgelei.Additionele nie-lineariteite bv.trek-krag limiete is ook in ag geneem.

n Ope-lus beheer-stelsel om die trein teen n ekwilibrium spoed laat beweeg is ontwerp .n Beheerstesel om die nodige versnellings tydens spoed-veranderings uit te werk is ook ontwerp en gevalideer.

Die feit dat die lokomotief se trek-krag instellings net sekere diskrete waardes aanneem lei tot inset kwettering. Gedurende die briek tot trek-krag transisie benodig die lokomotief skielik trek-krag wat tot pieke in die binne-treinse kragte lei. Die insette word gefilter om hierdie probleme te voorkom.

Verskillende geslote-lus beheerstelsels,wat op die LQR metode gebaseer is, is ontwerp en met mekaar vergelyk. Die beheer-lusse is vir binne-treinse kragte, energie-verbruik en spoed beheer geoptimeer. Om kommunikasie begrensinginge te oorkom word n omheinings-konsep gebruik waarin die beheerstelsel vir elke spoor topologie aangepas word. Verskillende konfigurasies ten opsigte van additionele kanale vir trek-krag en briek beheer is vergelyk en hulle invloed op statiese en dinamiese binne-treinse kragte is ondersoek.

Die resultate van hierdie verskillende konfigurasies is met bestaande trein data vergelyk.Daar is gevind dat n geslote-lus beheerstelsel wat binne-treinse kragte optimeer die beste algehele verbetering toon.

# Abbreviations

**AAR** Association of American Railroad

**ATP** Automatic Train Protection

**DP** Distributed Power traction system

**ECP** Electronically Controller Pneumatic Brake system

**GIS** Geographical Information System

**GPS** Global Positional System

**HST** High-Speed Train

**DD** Distributive Drive

**PPD** Pull-Push Drive

# Contents

# Chapter 1

# Introduction

## 1.1 Background

Heavy-haul trains are an important means of long distance transportation. They provide a more economical option than air transport and are more reliable than their road transport counterparts.

The railway provider Spoornet, utilises heavy-haul trains on its Coallink line to transport coal to Richard's Bay for export.

Since late 1990's, Coallink trains have already reached the maximum train length and wagon size permitted by the narrow-gauge railway system. To improve throughput on the line, Spoornet plans to roll out brake and traction systems upgrade on all Coallink trains.

An Electronically Controlled Pneumatic (ECP) brake and a Distributed Power (DP) system are the two new train technologies that are geared to improve performance and reduce travelling time.

The three running costs specified by the railway industry are: travelling time, energy consumption and maintenance costs. The shorter the travelling time, the more traffic can be allowed on the line, thus increasing the carrying capacity. Hence, it is economical for the railway company if the train travels to its destination as fast as possible.

Another reason why travelling time is important is that shipping companies charge heavy fines for late deliveries. Late railway deliveries delay cargo ship departures, resulting in fines from the ports for additional time spent in the dock.

The largest basic running cost of a train is its energy consumption. In diesel lines, the cost is directly proportional to the amount of fuel used. In the Coallink line, electrical locomotives are employed. Since both traction and braking use energy, it is desirable to minimise the control effort as far as possible in order to reduce the running costs of the train.

Safety is very important for railway company. Excessive wear on train parts such as brake blocks and couplers result in need for frequent maintenance. This requires more downtime and leads to extra costs for replaced and repaired parts. It would be more economical if the train was driven as carefully as possible so that the wear could be minimised, thus reducing maintenance costs.

## 1.2 Motivation

Spoornet wishes to deploy ECP and DP technologies in order to improve throughput on the Coallink line and to reduce overall running costs.

The ultimate goal of Spoornet is to operate a train consisting of 800 wagons. Current Coallink trains consist of 200 wagons.

No cruise controller exists for ECP-equipped heavy-haul trains. Due to its long length and large mass, Coallink trains pose many challenges for train modelling and controller design. This research examines many of these challenges and proposes solutions to both the modelling and the cruise control problems.

## 1.3 Objectives

The main objective of this project is to design a cruise controller for a Coallink train. The cruise controller should be able to reduce the running costs of the train.

Travelling time of the train can be reduced by following the speed limits very closely. Thus, improving velocity regulation of the cruise controller will results in decreasing the train's travelling time.

An optimal controller that utilises fewer and smaller control actions will reduce energy consumption of the train.

Lastly, since the highest maintenance costs are due to coupler system damage resulting from large in-train forces, a controller that is able to minimise these forces will reduce wear and damage on the aforementioned system. This would translate to a reduction in the maintenance costs of the train.

Thus, the optimal cruise controller should have the following characteristics: good velocity regulation, efficient utilisation of control actions and in-train forces minimisation.

## 1.4 Outlines

This study is divided into three main topics, discussed in six chapters. The knowledge base of the study consists of background information and a review of existing train controllers. These themes are covered in Chapters 2 and 3 respectively.

Both passenger and heavy-haul train controls, ranging from low-level adhesive controls to high-level cruise-controls, are studied in Chapter 3.

Coallink trains are described in chapter 2 and Chapter 4 in detail to allow better understanding of the train dynamics.

Model design and verification, in conjunction with the corresponding controller designs are discussed extensively in Chapters 4, 5 and 6. Results from

the verified simulation are shown and discussed in Chapter 7.

## 1.5 Contributions

On the research side, the study of existing methods provides an overview of train control methodologies. The two main contributions of this study are the verified model and closed-loop controller design.

The train model is validated with actual train data. This allows the modelling methods to be verified and provides a solid foundation for the train controller design.

The closed-loop controller brings online optimal control to heavy-haul train for the first time. The tunability of the controller allows adaptive control via human selection. By selecting a more appropriate set of weights for the current track condition, the driver can improve the controller performance.

The tunability can be further investigated into possible online learning adaptive control whereby parameters are tuned automatically. In practise, this would be done by the driver, in conjunction with the computer assisted optimised control.

The results shown in this study represent a unique study of different train configurations and their impact on running costs such as in-train forces and energy consumption. Since performance indices are given, railroad operators would only have to add its own logistic costs to these results to complete the feasibility study for train configurations.

# Chapter 2

# Background

## 2.1 Coallink Line

The main strength of South African export lies in its mineral exports, rare metals such as platinum and gold as well as energy sources such as coal. As most mines are situated far inland, heavy-load capable transportation system is required to move the minerals to the coast where it will be exported via the sea. Economical and fast, the railway system has been proven to be the most efficient way of transportation for these heavy loads.

Of all the minerals, coal plays an important role in export. In 2000/2001, coal export brought in R11 billion (US$1.7 billion) in foreign exchange earning. Coallink, the Spoornet coal export rail from Ermelo to Richard's Bay, contributes greatly in bringing this impressive income for the country.

With the initial construction completed in 1976, the Coallink railway has gone through numerous upgrades, with the last construction completed in 1989. The original capacity of 21 million tons a year, carried by diesel locomotives and 76 wagons, was soon upgraded to carry over 60 million tons with the current configuration of 200 wagons by 1989. The 580 km railway carries the coal, also known as black gold, from 44 coal-rich mines in Mpumalanga to the harbours in Richard's Bay in the province of KwaZulu-Natal. During the journey, the railway passes through some 37 concrete-lined tunnels that run 44 km in total and 137 bridges before reaching its destination.

Since late 1990's the Coallink system has reached the maximum capacity due to the increase in demands. Both the train length as well as wagon size have reached the maximum allowed by the specification of the narrow-gauge railway system. Various upgrades on the railway system, *i.e.*, the depots and the trains, are now being considered to increase the capacity to 69 million tons a year.

## 2.2 Train Structure

### 2.2.1 Locomotive

54 Class 10E direct current (DC) locomotives and 112 alternating current (AC) locomotives, such as the 7E1 locomotives, are used to haul the 200 jumbo wagons across the Coallink line. At the marshalling yard in Ermelo, the train control current is switched from DC to AC for the remaining journey to the port. Due to the combinational use of DC and AC lines, both AC and DC locomotives are employed. A 10E AC locomotive is shown in Fig. 2.1. Each locomotive has three bogies. A bogie is a set of wheels and suspension system.

Figure 2.1: Class 10E locomotives (Spoornet, 2003).

Traction efforts of a locomotive are controlled via notch settings. Regenerative braking, or dynamic brake, is also available as one of the possible notches. Each notch setting represents a certain traction force value, depending on the current speed. The traction effort versus velocity graph of

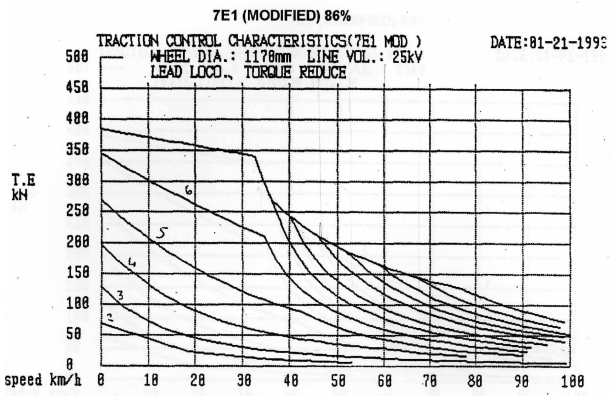


Figure 2.2: Traction effort versus velocity graph for the 7E1 AC locomotive (Spoornet, 2003).

the 7E1 locomotive, currently employed on the Coallink line, is shown in Fig. 2.2.

Pneumatic brake is available in the locomotives. Due to the limit on the amount of energy each wheel can dissipate, regenerative braking is preferred over pneumatic brake to prevent wheel lock up. The energy from regenerated brake is converted into heat energy by the resistor bank on the locomotive whereas pneumatic brake uses the wheel for this energy conversion. For example, the maximum energy each wheel can dissipate is 60 kW, while the maximum rating for regenerative braking in the 7E1 locomotive is 3000 kW, nearly ten times the 360 kW the six wheels can dissipate. The only exception is when the train needs to come to a complete stop at low speeds where regenerative braking has no braking efforts, shown in Fig. 2.3.

### 2.2.2 Wagons

The type of wagon used in Coallink trains is the jumbo type. Each wagon has an axle load of 24 tons and is capable of 84 ton of payload, making the overall mass of the wagon 104 250 kg. The wagons are known as rotary dump wagon. The wagons consist of two bogies. Fig. 2.4 shows a picture of a CCL-8 wagon that is currently upgraded with ECP brake system.

Each wagon is equipped with one or two equalising reservoirs. These reservoirs are charged to a specific pressure at the beginning of the trip. A brake

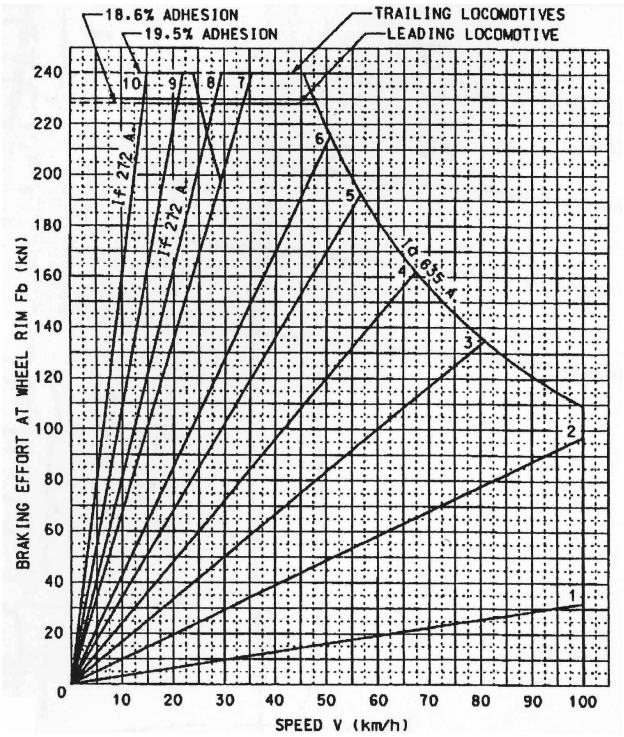


Figure 2.3: Dynamic brake effort versus velocity graph for the 7E1 AC locomotive (Spoornet, 2003).


Figure 2.4: CCL-8 wagon (Spoornet, 2003).

pipe runs throughout the whole train and is kept at the same pressure as the reservoir. The brake control valve in the brake system compares the pressure from both the brake pipe and the equalising reservoir. If the decrease in brake pipe pressure and its rate exceeds a certain threshold, the brake control valve tries to equalise the two pressures by letting the excess pressure from the equalising reservoir into the brake cylinder, hence applying the brake. This will stop when the equalising reservoirs pressure has dropped to the same level as the brake pipe. This mechanism allows a fail-safe braking system whereby any sudden loss of pressure in the brake pipe will cause an immediate application of the emergency brake.

The brake application signal travels down the brake pipe around the speed of sound, in practice around 280 $ms^{-1}$. This equals to a delay around 10 s for the signal to travel from the front locomotive to the very last wagon for a 200 wagon train.

Once brake is applied, any subsequent brake application of the same magnitude or smaller could trigger kick-off. Kick-off is the undesired brake application at the rear end of train due to the uneven brake pipe pressure. To avoid this, the brake system needs to be fully charge before the next brake application. Typical time required to fully charge a 200 wagon train is around 15 minutes after a full-service brake.

Each Coallink train consists of two hundred wagons, stretching over 2.5 km. The train is pulled by a maximum of four or six locomotives, depending on the type of locomotive used. The 11E locomotives have a continuous rating 3800kW in powering mode compared to 3000kW rating for the 7E1, thus only four 11E locomotives are required. These locomotives are connected as a group at the front of the train in the current configuration.

Four wagons are connected with rigid bars to form a group, called a rake. Each group of wagons is connected with each other and with the locomotives via elastic-like connectors, or couplers. This type of grouping reduces the free-slack introduced by couplers.

## 2.3 Running Costs

The three major running costs of a train are: travelling time, energy consumption and maintenance cost due to in-train force. Travelling time and energy consumption are directly proportional to the travelling speed and the traction efforts applied. In-train forces are the forces experienced by the couplers joining adjacent cars. Excessive pulling and pushing forces, or draft and buff forces, can damage these couplers. Given the fact that there could be a coupler between every single car in a 206 car train, maintenance cost could run high. The term car refers to any wheeled unit in the train that can be either a locomotive or a wagon.

The biggest problem experienced during the operation of the heavy-haul trains is the in-train forces in the couplers that link the wagons and locomotives and between wagons. Due to the extra long train length (in excess of 2.5 km) and the heavy load (the full load in excess of 104 tons) in each wagon, the in-train forces can be enormous during acceleration and deceleration of the train. The current pneumatic braking system uses pressure waves to transmit braking control signals to all the wagons. The process is slow and is not spontaneous among the wagons. This attributes to additional in-train forces during braking. Excessive in-train forces result in excessive strains in the couplers, which then require frequent maintenance check and replacement.

While ideally all three costs should be minimised, in practice improving one area often means sacrificing the other two costs. For example, it is impossible to achieve higher travelling speed with reduced traction efforts to obtain both optimal travelling time and optimal energy consumption. Different situation might also place much greater importance on one factor while overlook the rest. For example, a train late for shipment needs to get to the harbour as soon as possible since the fine for late delivery is enormous. In this case, considerations of in-train forces and fuel consumption are less important in comparison.

The developed closed-loop controller takes this into consideration by allowing parameter tuning for the optimal targets. Thus the driver could dynamically change the weights of importance on the three factors as the situation deems.

## 2.4 Electronically Controlled Pneumatic brake system and Distributed Power

In the current pneumatic controlled brake system (Garg and Dukkipati, 1984), signal propagation of the pressure wave used is limited to the speed of sound. This results in long delay as the length of the train typically exceeds 2.5km. Due to this brake signal delay, the train experiences uneven braking whereby the front part of the train will brake before the end of the train. The reverse applies when the brake is released. Another limitation is that the cars could not brake individually due to the way the brake pipe pressure is used for both brake signal transmission and brake force supply.

These factors hinder the performance of the brake system, resulting in increase in braking time and very large in-train forces in some cases.

The new electronic controlled pneumatic (ECP) brake system, defined by the Association of American Railroads (AAR) (AAR, 2002) and discussed in Kull (2001), is designed to provide control flexibility that was not possible with the existing brake system. The new ECP system replaces the pneumatic brake control with electronic signals, allowing almost simultaneous brake control by wire and ultimately individual brake setting for each car. The actual brake force will still be applied pneumatically, only the control signal will be electronically transmitted.

The advantages of ECP are clear: faster response time and spontaneous braking across the whole train. The latter is a major advantage as it distributes the energy dissipated during braking evenly across all the wheels in the train. With the old system, the front end of the train often has to dissipate most of the energy since they brake earlier. This results in uneven wear of the brake system and a limitation on the maximum brake level. Another advantage is that because brake pipe is no longer used to send brake signals, successive brake applications are no longer limited by the charging time.

In theory, individual brake control would be the most efficient. In practice, ECP system needs to overcome two problems before efficiency can be improved. First, true individual control is not possible due to computation and bandwidth constraints. In AAR specification, ECP communication line can have up to 32 channels, clearly insufficient for 200 individual wagon brakes. Secondly, the current manual control does not take advantage of the addi-

tional control inputs.

Distributed power system is another promising technology. The AAR stipulates that with human driver, only two consists are allowed. Consists are group of locomotive that received the same control settings. However, with computer assisted control, AAR removed this restriction.

This opens up numerous opportunities to locomotive placements. It could be found that it is more efficient to spread the locomotives across the whole train. While impossible with human control, an automated controller could be used to improve running efficiency of the train.

However, this also opens up to numerous new optimisation problems. The previously mentioned locomotive placement is the most important one. To utilise such options, logistic side of train traffic will also be affected. The benefits will need to be weighed against the new costs. For example, does the improvement from spreading locomotive placements justify the additional time required to shuffle the wagons around? Such questions require considerable knowledge into the logistic side of the Coallink system and much further research to determine the actual benefits.

In this study, the DP system will mostly work with the two group setup, whereby the two sets of locomotives are found in the front and rear of the train, the wagons in between them.

## 2.5 Current Controller

Although the response time of the braking system has been improved through the introduction of the ECP braking system, one problem still remains: the cruise control system. To achieve a certain velocity, various factors such as current velocity, acceleration, wheel slip and current railway gradient need to be taken into account before the required action, *i.e.*, acceleration, braking and partial braking, can be decided upon. Currently, the available control systems for the traction and braking are open loop controllers that do not take the aforementioned factors into consideration. It is up to the driver to make these decisions based on his experience and knowledge. Although humans are more versatile than any modern control system, the performance of the driver is not guaranteed to be consistent every time. Neither are the

decisions made by driver necessarily the most efficient and these could differ from person to person. The training of the driver takes a substantial period of time, while most drivers can only be trained for a section of the track.

In the current operation, the driver sits in the front locomotives and operates the rest of the train via notch settings and brake levels. Traffic controls are read visually by robot-like indicators along the track. Track conditions such as large incline section are memorised by drivers. Often one driver would only be responsible for a section of the track that he is familiar with.

## 2.6 Project Objectives

This project is focused on the closed-loop controller of the heavy-haul train. Research on existing methods will be fundamental to the development of the controller. Passenger trains in comparison to heavy-haul trains, consist of many advance control systems. Thus research in both fields will have to be considered.

Controller design is impossible without knowledge of the model itself, whether it may be only sets of input and output data or the actual mechanism. To do this, train parameters needs to be determined, many of which are not steadily available. Some of the parameters change as train configuration changes. A model structure will have to be picked and subsequently the identification of the required parameters.

To be able to design closed-loop controller, the train first will have to reach some kind of equilibrium state. To achieve a steady speed, an open-loop controller is used. This controller will be responsible for maintaining the train at the desired speed or even determine the required acceleration or deceleration.

With the DP system, more than one locomotive control groups, or consists, are possible. ECP also allows wagon to be controlled individually. The controller will have to be generic to allow changes in train configurations.

Lastly, the closed-loop controller must be designed with tuning flexibility to allow weights for the three running costs to be changed online. This is a necessary feature that allows the driver to better assess the current

condition and make the necessary modification to the controller performance accordingly.

# Chapter 3

# Existing Methods

Train design can be classified into two classes: passenger train and heavy-haul train. The main difference lies in the mass and the length of the train. Passenger trains consist of fewer cars and are considerably lighter than heavy-haul trains. The different objectives of the two thus result in different research directions.

Research in passenger trains tends to focus on the comfort, various methods to reduce the vibrations and oscillations felt by the passenger. Advanced controllers are common since passenger train locomotives and wagons are updated with the latest technology more frequently.

In comparison heavy-haul train design is more conservative. Adoption to new advancements is slow, due to the stronger focus on safety and proven reliable technology. The demand for improvement is also less since competition from other transportation medium are limited, as railroad transportation still remains more economical means of heavy-haul transport. Passenger transportation faces a tougher competition from air and road transportation.

In this study, literatures on the control system on both fields were considered, ranging from high speed train controller (Yang and Sun, 2001) to safety brake control for heavy-haul trains (Watanabe and Takashige, 1994).

The main approaches to the general train control in the literature are: optimal control and robust control. Each approach has its weakness and strength. While most of these approaches were extensive, none of them was designed

with the ECP braking system in mind. Rather than trying to come up with a controller that meets all the requirements, each approach tackled one specific feature of the problem. These features included, but are not limited to, fuel consumption, in-train forces, adhesive force, speed restriction and non-consistent slopes.

# 3.1 Optimal Control Method

## 3.1.1 Introduction

Howlett (1996) proposed an optimal control strategy for the scenario where a train has to travel between two stations within a certain time limit via a non-constant slope path while minimising energy usage. The method places strong emphasis on the fuel consumption. The method was discussed further by Khmelnitsky (2000).

## 3.1.2 Methodology

Howlett's design was based on the performance characteristics of a particular GM diesel-electric locomotive. The general traction force of a diesel-electric locomotive is shown in Fig. 3.1. The locomotive has eight traction control settings; each determines a constant rate of fuel supply to the diesel motors. It can be seen that the traction force is inversely proportional to the speed, *i.e.*, acceleration is less at higher speed. Although the particular graph only applies to the specific locomotive, similar graphs can be found for most AC and DC locomotives.

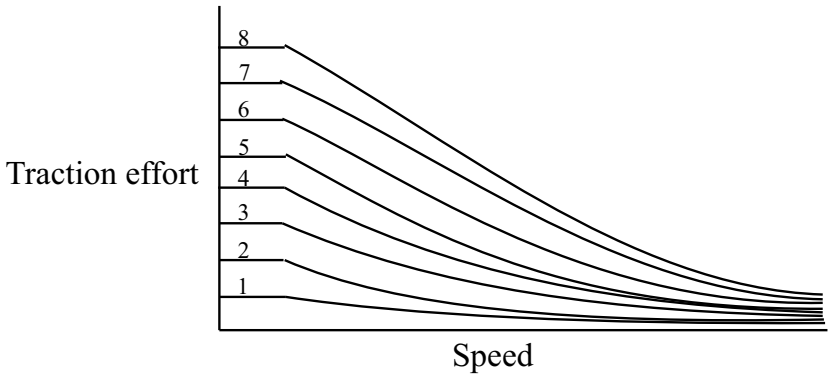


Figure 3.1: Traction force versus speed of a typical diesel-electric locomotive.

The locomotive model proposed by Howlett uses a finite sequence of traction and one brake setting. For simplification, a negative traction force is used to represent braking force. The whole train was modelled as a point mass, shown in Fig. 3.2.

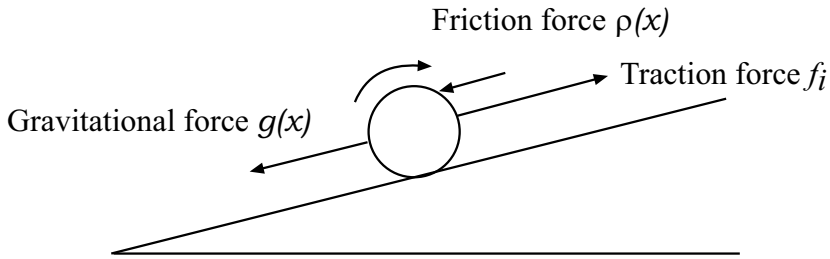


Figure 3.2: Force diagram for the optimal strategy.

The equations of motion for the train are given as follow

$$\begin{aligned} \frac{dx}{dt} &= v, \\ \frac{dv}{dt} &= \frac{Hf_i}{v} + K_j - \rho(x) + g(x), \end{aligned}$$

where $x$ is the distance along the track, $v$ is the velocity of the train, $f_i$ is the traction force, $K_j$ is the constant braking force if brake was applied, $\rho(x)$ is the frictional force, $H$ is a constant from the traction graph and $g(x)$ is the resistance force due to the track gradient. Mass of the train was eliminated from both side of the equation.

Note the equations of motion is only valid for non standstill case.

The optimal control strategy applies control at various discrete points. The total distance is then divided up into segments as follows,

$$0 = x_0 \leq x_1 \leq x_2 \leq x_3 \leq \cdots \leq x_{n+1} = X,$$

where $x_0$ is the initial point and $x_{n+1}$ is the end point $X$. Thus one could define a subset

$$j(k+1)_{k=0,1,\ldots,n},$$

where $j(k+1)$ is the control setting on the interval $(x_k, x_{k+1})$.

The cost function for the optimal strategy is then given as

$$J = \sum_{k=0}^{n} f_{j(k+1)} \tau_{k+1},$$

where $f_{j(k+1)}$ is the traction force for that specific interval and $\tau_{k+1}$ is the time taken for the train to move across the interval $(x_k, x_{k+1})$.

The true gradient can be represented as a piecewise-constant gradient. This was done for computational and theoretical reasons as optimal control method was used. Thus the interval $(0, X)$ can be divided into

$$0 = h_0 \leq h_1 \leq h_2 \leq \cdots \leq h_{p+1} = X,$$

where the resistance force due to track grade $g(x)$ is constant on each subinterval $(h_r, h_{r+1})$. This subintervals of gradient is not directly related to the control signal subintervals $(x_k, x_{k+1})$, although one would choose the control signal subintervals based on the gradient information of the track.

### 3.1.3 Results

The results obtained by Howlett (Howlett, 1996) are given below from a proprietary algorithm, Metromiser, where the optimal points were determined. The results are shown in Fig. 3.3 and Fig. 3.4 for a level track and a small valley, respectively.

It can be seen that the result from the level track coasts longer at the end than the small valley results. For the small valley, the train requires less traction action initially. More frequent traction actions were required after it completed the uphill climb of the valley.

It was shown that the most fuel-efficient strategy is the speed-holding strategy. Another result is that the power-efficient traction setting is the maximum traction setting. The Metromiser result showed an improvement in travelling time and a 14% fuel efficiency.

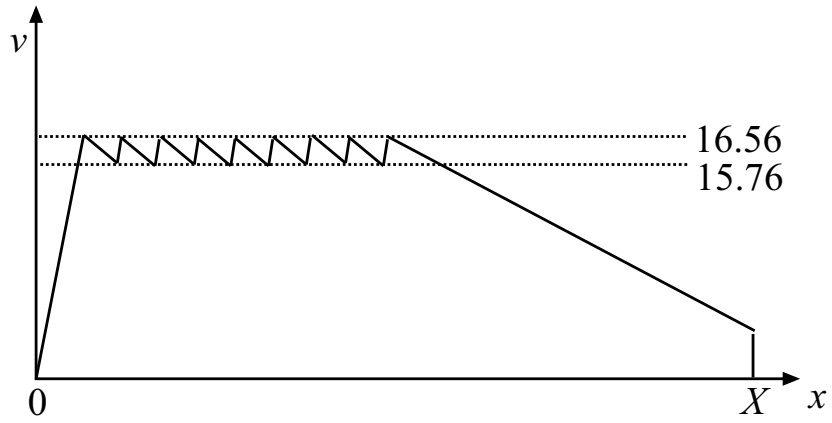


Figure 3.3: Speed profile of the optimal type on level track.

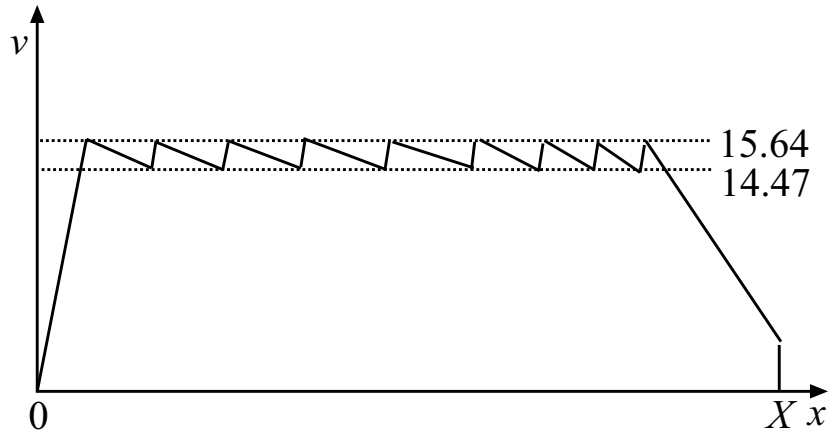


Figure 3.4: Speed profile of the optimal type over a small valley.

### 3.1.4 Discussion

A problem with the optimal control is the selection of the switching points. In Howlett's paper, the optimal switching points were found via a proprietary program, Metromiser. Such selection is dependent on the existing knowledge of the track topology.

It was seen that optimal control is able to provide an optimal control strategy which minimises fuel consumption for the specific switching points. Further development would be required for such implementation on the long-haul train. In-train forces, for example were not included in the model. As the trains are over 2.5km long, the assumption of a single-point mass train cannot hold.

Guidance systems based on optimal control are currently available for long-haul trains. The LEADER system (NYAB, 2003), developed by New York Air Brake, provides a near-optimal suggestion of speed along per-programmed track based on current position. The system does not calculate the optimal strategy based on current status; instead, it calculates the optimal strategy for that particular track using pre-programmed database and the initial conditions of the train. At the end of the trip, one can compare the performance of the driver with the optimal run calculated by the system.

For Coallink it is advisable to employ these techniques to find an optimal speed profile. This profile could then be used as a yardstick for performance evaluation for human drivers as well as autonomous speed controllers.

## 3.2 Braking Profile

### 3.2.1 Introduction

The basic idea of the braking profile method is to calculate the required velocity curve of the train for it to reach the designated speed at the end of the distance. The braking profile methods are implemented mostly as a safety backup in the automatic train protection (ATP) system. Certain scenarios, such as the case that the driver has failed to keep the speed within the safety limit, will result in the activation of the ATP system.

The basic ATP system design will apply the emergency brake until the train has come to a complete stop when activated. The problem with this system is that it will often cause large impact forces and possible wheel damages due to slip. This is because the emergency brake setting exerts the highest pressure on the pneumatic braking system, resulting in tremendous impact forces and energy transfer via the wheels.

A more advanced ATP system used currently by the Japanese trains was described by Watanabe and Takashige (1994). It operates by transmitting the current speed limit on the current track to the train. The controller onboard the train then compares this signal to its current speed. If the later exceeds the limit, brake is applied until the current speed is below the received limit.

In cases where the trains are required to come to a complete stop, many regions of decreased speed limit are specified before the point of complete stop. The speed profile before the point, mostly stations, is step-like.

The disadvantages of such system are:

1. For the train to reach complete stop, the driver is required to repeatedly apply and release the brakes every time the train crosses a region. This occurs as the train will always travel at less than the specified speed limit, and the system will not allow the train to reach complete stop.
2. The block lengths are predetermined by the margin distance and idle running distance of brakes. Once calculated it is fixed. Therefore it is

impossible to increase the traffic density on these sections of the railway later on.

3. Since the braking performances of the trains differ from one to another, the block length is determined by using the worst case to ensure safety. This means some trains will have to stop much earlier than necessary, which result in reduction in traffic density.

Improvement on the ATP system is currently in progress. One example is the automatic speed enforcement system (ASES) used by Amtrak's Northeast Corridor railway (Thelen and Tse, 1990). A similar system is also under development for the Chinese coal railway (Tang and Gao, 1996), as the current ATP system only works for the light freight and passenger trains. These systems, based on the existing ATP system, apply a gradual service brake instead of the emergency brake to reduce the impact experienced by the train.

Another advanced ATP system suggested by Watanabe and Takashige (1994) resolves the above mentioned disadvantages by calculating the speed profile of the train on an individual basis according to the train's current condition and the current environment, *e.g.*, distance to previous train.

The inputs the advanced ATP system requires from the system are:

1. the distance to the preceding train, *i.e.*, the distance between two trains on the same track,
2. the starting point of a speed restriction, *e.g.*, tunnel or a turn, and
3. the block identification number of the current track section.

The information the advanced ATP system stores on the train are:

1. the braking performance of the train,
2. the information about the track,
3. the absolute locations measure from beginning of the railway,

4. the absolute location of curves and gradients, and

5. sizes and locations of every car.

### 3.2.2 Methodology

The system calculates the brake profile via the current speed and the distance to the target area with its designated speed limit. As the brake system of each train differs from each other, some of the parameters vary.

The proposed methods try to improve the algorithm that calculates the speed profile by making it more smoothly and reduce the force required. The following equations and parameters were given for the Chinese coal train by Tang and Gao (1996).

Due to the extra long train length, the pneumatic control signal requires a few seconds to setup and equalise across the whole train. Thus, the braking processing can be divided into two parts: the virtual braking period for the braking signal to reach all the wagons and the effective braking period where the brake starts to reduce the speed of the train to the desired value. Thus, the braking distance can be given as follows,

$$S = S_k + S_e,$$

where S is the total braking distance, $S_k$ is the equivalent virtual braking distance and $S_e$ is the effective braking distance.

During the virtual braking period the speed of the train will not be uniform as the front wagons will start to brake before the end wagons. For simplification, the assumption here is that the speed of the train remains constant throughout this period.

The virtual braking distance can thus be given as

$$S = \frac{1000 V_0 t_k}{60 \times 60} = \frac{V_0 t_k}{3.6},$$

where $V_0$ is the initial speed and the $t_k$ is the equivalent virtual braking time, *i.e.*, the time taken for the brake signal to travel through the whole train. For the Chinese coal train, it is given

$$\begin{aligned} \text{Emergency braking} \quad & t_k = (1.5 + 0.18n)(1 - 0.05i_k), \\ \text{Service braking} \quad & t_k = (2.8 + 0.0014rn)(1 - 0.1i_k), \end{aligned}$$

where $i_k$ is the equivalent gradient in the braking distance, $r$ is the service brake reduction factor and $n$ is the number of wagons in the train. The equivalent gradient is the average gradient for the specific distance.

The effective braking distance is given as

$$S_e = \frac{V_0}{3.6} t_n + \frac{4.17\alpha(V_n^2 - V_{n+1}^2)}{103\beta\theta_h\psi_{hs} + \omega_{0s} + i_j},$$

where $\beta$ is the coefficient for the equivalent train brake rate, $\theta_h$ is the equivalent distance friction coefficient, $\psi_{hs}$ is the equivalent friction coefficient and $\omega_{0s}$ is the train equivalent resistive force. The equivalent parameters are the average values for the specific distance.

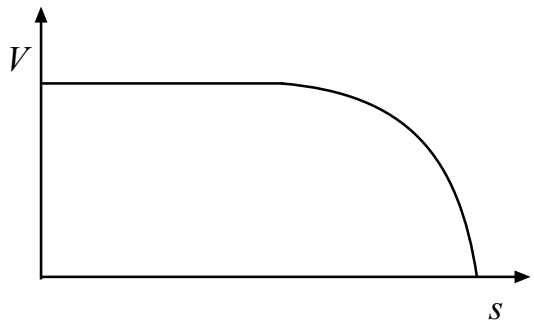


Figure 3.5: The braking profile, *i.e.*, the speed-distance curve.

From these equations, the braking profile curve can be determined, depending on the parameter values. Fig. 3.5 shows the general trend of these curves, with a smooth deceleration as the train approaches its stop.

### 3.2.3 Discussion

In Fig. 3.6 the suppression method refers to the ATP system that utilises emergency brakes while the braking profile is the method that utilises gradual braking settings.

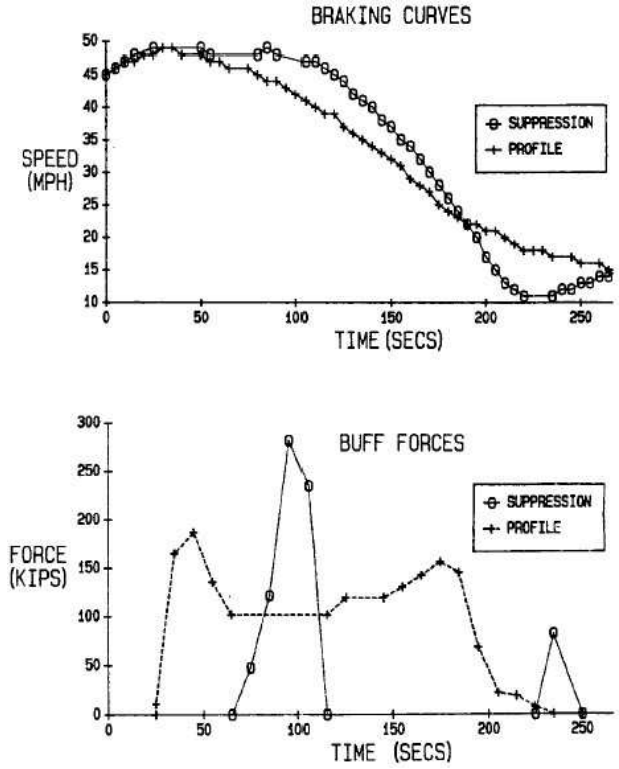


Figure 3.6: Comparison of speed reduction and train force between suppression method and braking profile method (Thelen and Tse, 1990).

It can be seen that the gradual braking method smoothes out the speed curve over the whole distance, as well as the in-train forces experienced by the train. The suppression method, on the other hand, was able to reduce speed at a faster rate. This, however, resulted in two peaks in the in-train forces, one caused by the high braking force and the other by the traction force to compensate for the over-braking.

The brake profile method has the clear advantage of reducing the in-train forces while reducing the speed to the safety limit. This will reduce the wear on the couplers that connect the wagons. When taking into account the large

number of wagons per train and the number of fleets, this method would be able to substantially reduce the running cost of the railway.

For cruise control, this method will be able to reduce the in-train force during large changes in reference speeds. However, since reference speed seldom changes during normal operation, the application situations for brake profile are limited.

## 3.3 Maximum Adhesive Control

### 3.3.1 Introduction

Slip is a phenomenon that occurs when the actual radial velocity of the wheel exceeds the theoretical radial velocity of the given linear velocity of the wagon, *i.e.*, the wheel is spinning faster than it should. Slip or slip velocity is defined as

$$slip = \omega r - v,$$

where $\omega$ is the actual radial velocity, $r$ is the radius of the wheel and $v$ is the linear velocity of the wagon.

Through experiments, it was found that the coefficient of friction is dependent on the slip velocity. An interesting phenomenon is that the coefficient of friction actually increases as slip increases initially, only to decrease after reaching the maximum at some small slip value, as shown in Fig. 3.7.

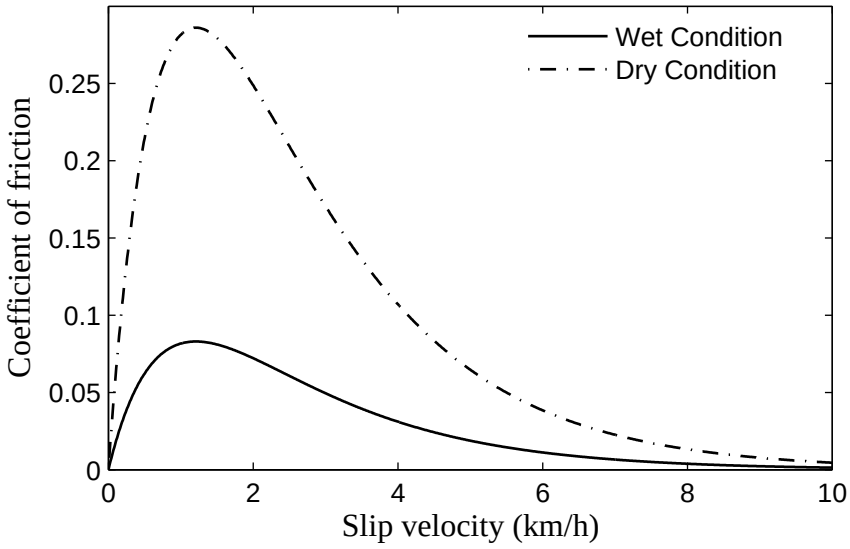


Figure 3.7: Coefficient of friction versus the slip velocity graph.

The challenge is then to keep the slip of the wheel around the point which produces the maximum coefficient of friction, thus results in the maximum adhesive force.

A new method of control was proposed by Ishikawa and Kawamura (1997) to improve the performance such that the slip velocity is kept as closely to the maximum point as possible.

To achieve any type of slip control, accurate reading of the actual wheel radial velocity is required. Normally a speed sensor is installed for this purpose. Watanabe and Yamashita (2001) proposed a novel way of calculating the slip velocity via the inverter currents that feed the traction motors of the locomotive. Although very specific to the particular setup of motors, it provides an alternative to the speed sensor.

### 3.3.2 Methodology

The following model is taken from Ishikawa and Kawamura (1997). First consider a simple one axis train model, shown in Fig. 3.8.

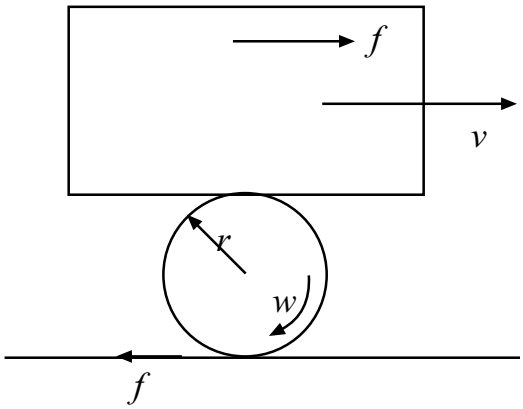


Figure 3.8: One axis train model.

The equations of motion for the model are

$$\frac{dw}{dt} = Te - fr - b\omega,$$
$$W\frac{dv}{dt} = f - cv^2,$$
$$f = \mu W g,$$

where the parameters are given in Table 3.1.

| Symbol | Parameter | Units |
|---|---|---|
| $J$ | Wheel moment | $kg \cdot m$ |
| $Te$ | Input torque | $N \cdot m$ |
| $r$ | Wheel radius | $m$ |
| $b$ | viscosity resistance | $km \cdot m/sec$ |
| $W$ | Train weight | $Kg$ |
| $c$ | Aerodynamic coefficient | $m^3/sec^2$ |
| $g$ | Gravity | $m/sec^2$ |
| $\omega$ | Motor speed | $rad/sec^2$ |
| $f$ | Adhesive force | $N$ |
| $v$ | Train speed | $m/sec$ |

Table 3.1: List of parameters for the differential equations of the wheel in Fig. 3.8.

| | $a$ | $b$ | $c$ | $d$ |
|---|---|---|---|---|
| Wet condition | 0.54 | 1.2 | 0.29 | 0.29 |
| Dry condition | 0.54 | 1.2 | 1.0 | 1.0 |

Table 3.2: Example values for the parameters for the coefficient of friction.

The input torque $Te$ is the input to the system in this case. The measured outputs are the motor speed and the train speed.

The coefficient of friction is assumed to be

$$\mu = c \cdot \exp(-a \cdot slip) - d \cdot \exp(-b \cdot slip), \tag{3.1}$$

where the parameters $a$, $b$, $c$, $d$ depend on the rail condition. An example was provided in Ishikawa and Kawamura (1997). The values are given in Table 3.2. Using these values, the resulted coefficient of friction versus slip velocity graph is plotted in Fig. 3.7.

A straight forward, conventional maximum adhesive force controller is shown Fig. 3.9.

Ishikawa and Kawamura (1997) proposed a PI-based controller. The dynamic equation is given below.

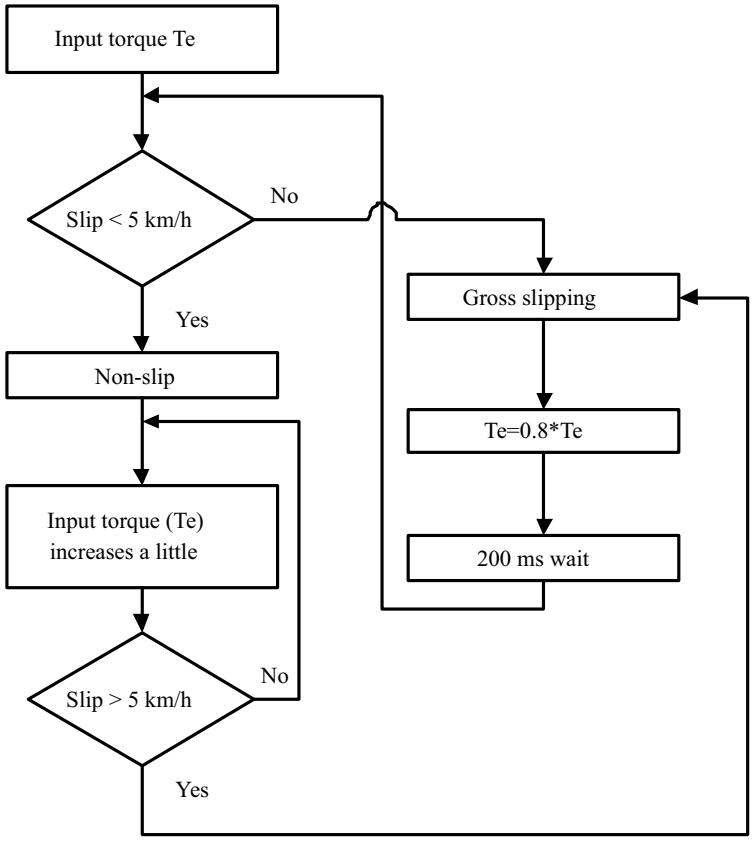


Figure 3.9: Flow chart of a conventional maximum adhesive force control.

$$\frac{d}{dt}\begin{bmatrix}\hat{\omega}\\ \hat{f}\\ \hat{f}'\end{bmatrix} = \begin{bmatrix}\frac{1}{j} & \frac{r}{j} & 0\\ 0 & 0 & 1\\ 0 & 0 & 0\end{bmatrix}\begin{bmatrix}\hat{\omega}\\ \hat{f}\\ \hat{f}'\end{bmatrix} + \begin{bmatrix}\frac{1}{j}\\ 0\\ 0\end{bmatrix} Te + \mathbf{K}(\omega - \hat{\omega}) \tag{3.2}$$

where the gain $K$ is chosen via classic feedback methods such that (3.2) is stable.

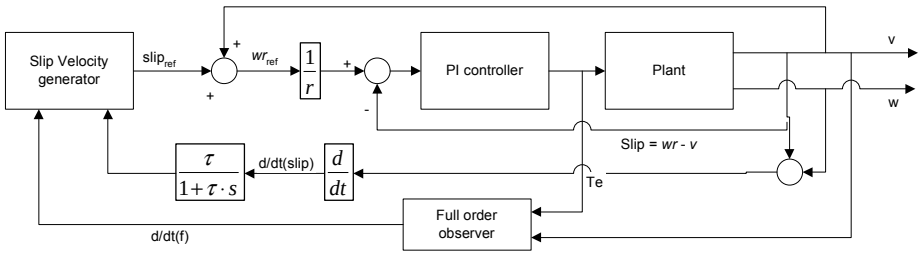


Figure 3.10: PI controller with feedback observer.

The observer calculates the adhesive force and its derivative with the input torque $Te$ and the wheel radial velocity $\omega$. The reference wheel velocity is given as

$$\omega_{ref} = \frac{slip_{ref}}{r} + \frac{v}{r}.$$

The slip velocity generator generates the suitable slip reference for the maximum adhesive force under the current conditions. The algorithm is given as follows.

1. if $\frac{df_k}{dSlip_k} = 0$, the slip reference $slip_{ref}$ is kept the same as the previous sampling period.
2. if $\frac{df_k}{dSlip_k} \neq 0$, then $slip_{ref}^{k+1} = slip_{ref}^{k} + \alpha\frac{df_k}{dslip_k}$
3. return to 1

While Ishikawa and Kawamura (1997) focused on the slip velocity control, Watanabe and Yamashita (2001) proposed an alternative slip velocity detector without speed sensor. As the method is based on careful analysis of the inverter current of the motors, the method will not be discussed in detail

as the resulting controller is very specific to the particular motor behaviour. The general concept is presented below.

Fig. 3.11 is a test result obtained from the configuration whereby a single inverter feeds four motors. The test system has an anti-slip control installed. The rail was sprayed with water so that all four axles would experience slip. It can be seen that the inverter current increases as slip occurred at point A. The slip was then detected and the anti-slip controller initiated at point B. The inverter current reference value drops subsequently.

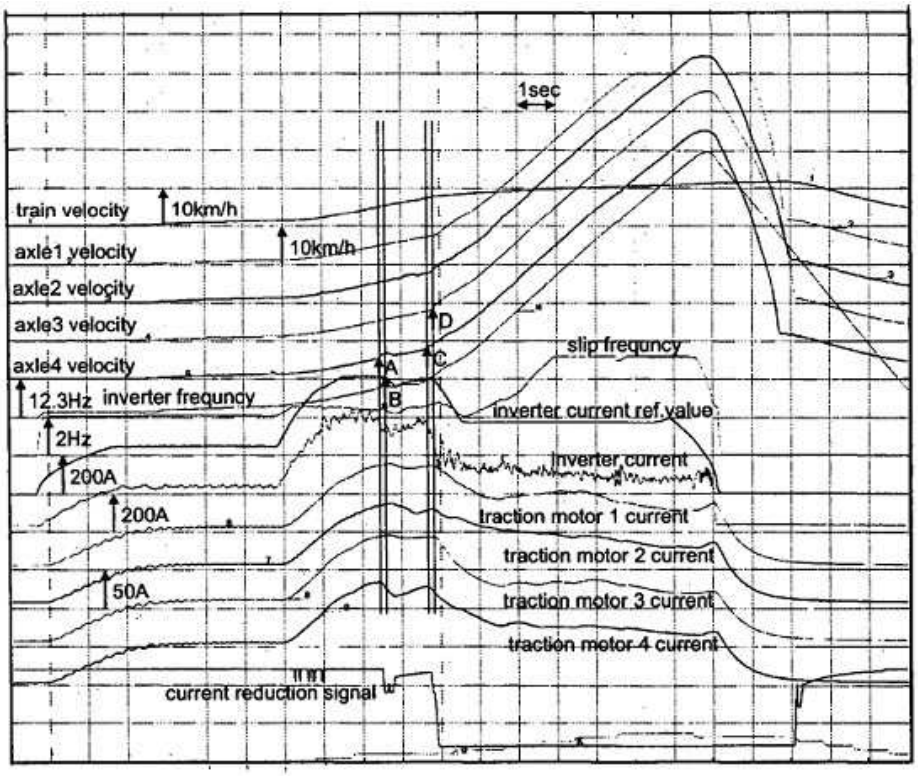


Figure 3.11: The test results from the multiple motor drive (Watanabe and Yamashita, 2001).

The scheme proposed by Watanabe and Yamashita (2001) is a slip detector based on the inverter currents to the individual motors. When slip occurs, a difference will occur between the currents to the motors. The difference could be as a result to the difference of wheel diameter, but this offset would be measured and stored initially. This slip controller would accept other inputs such as the motor torque and rotational acceleration, and will be able to derive the adhesive force at that point.

### 3.3.3 Result

The results from the maximum adhesive control (Ishikawa and Kawamura, 1997) using the PI controller and the conventional criteria-based controller is given in Fig. 3.12 and Fig. 3.13 . It can be clearly seen that the new controller is able to stay much closer to the maximum point, providing the highest adhesive force possible. The conventional controller exhibits oscillatory outputs around the peak slip point, shown in Fig. 3.12. The dashed line in the graph shows the theoretical adhesive force obtained by the model given in (3.1).

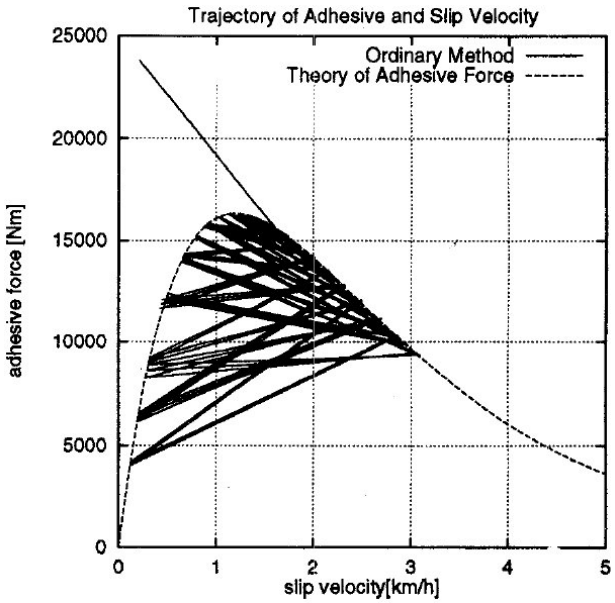


Figure 3.12: Adhesive force versus slip as obtained by the conventional anti-slip control shown in Fig. 3.9 (Ishikawa and Kawamura, 1997).

The slip velocity was then plotted against time, shown in Fig. 3.14. It is clear that the conventional method produced higher peaks with the average slip velocity centred around $1.5km/h$, while the new controller centred around $1km/h$ with subdued oscillations.

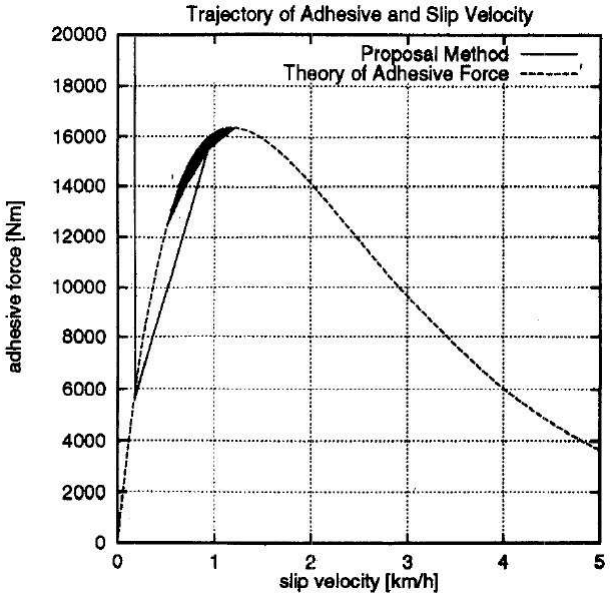


Figure 3.13: Adhesive force versus slip as obtained by the PI controller in Fig. 3.10 (Ishikawa and Kawamura, 1997).

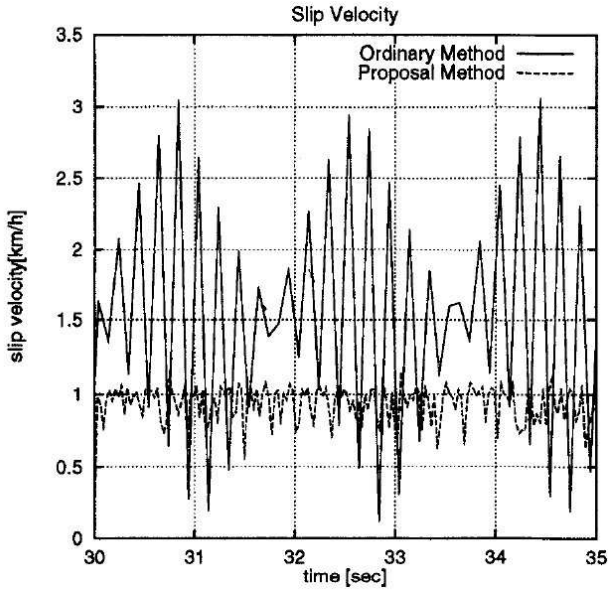


Figure 3.14: Slip velocity versus time (Ishikawa and Kawamura, 1997).

### 3.3.4 Discussion

Adhesive control is an interesting problem at low-level control. For open-loop control, this would affect the efficiency of the traction forces, which will have an effect on energy consumption. Specific parameters of the train are essential for the control method, many of which are not available or uneconomical to obtain. However, in the closed-loop control proposed, such parameter ambiguity will be compensated via the feedback mechanism.

The slip control results shown are purely theoretical. Since numerous external factors affect slip, such as track wetness, performance of such slip control under external disturbances and changing environment remains to be seen.

## 3.4 Mixed $H_2/H_\infty$ Control

### 3.4.1 Introduction

Although originally designed with the new high-speed train (HST) in Taiwan in mind, the close loop controller proposed by Yang and Sun (2001) could be modified to be implemented for the heavy-haul train. The controller, based on the feedback of the states and $H_2$ and $H_\infty$ control, is optimised by linear matrix inequalities (LMI) method (Halder and Kailath, 1999; Scherer *et al.*, 1997). In this paper, the train model used provides more insights into train dynamics and is of more interest than its controller. Thus, in the following section, the model is closely examined.

The model proposed by Yang and Sun (2001) approximates the real train dynamics more closely than the model proposed by Howlett (1996). The few aspects that were ignored by previous studies are incorporated in this model. Firstly, each wagon is considered as an individual entity. The relative displacement and velocities of each wagon forms an important part of the model as it is used to calculate the in-train forces. Secondly, because each wagon is a separate entity, the model is then able to incorporate the coupler forces. As the train length and mass increase, the large coupler forces become inevitable in the design as one of the constraints. It is important that the in-train forces be maintained within the maximum the coupler could withstand to reduce maintenance cost.

The performance of two types of train configuration was also investigated: distributed driving (DD) and pull-push driving (PPD). DD design assumes that all wagons are motorised while in PPD design only the front and the last wagons are powered.

### 3.4.2 Methodology

The couplers in the train are essentially elastic-like connectors. Thus, it can be described by a spring model. Each coupler has free plates that can move one or two centimetres before it starts to pull or push the linkage.

For a spring model, the restoring force is a function of the relative displacement $\xi$, as given below

$$f(\xi) = k\xi,$$

where $k$ is the stiffness coefficient. In Yang and Sun (Yang and Sun, 2001), three types of the spring model are given.

$$k = k_0(1 + \epsilon\xi^2) = \begin{cases} \epsilon = 0 & \text{linear spring,} \\ \epsilon < 0 & \text{softening spring,} \\ \epsilon > 0 & \text{hardening spring,} \end{cases}$$

where $\epsilon$ is the non-linearity factor. As relative displacement $\xi$ increases, a softening spring would results in a smaller stiffness coefficient than the hardening or linear spring. This means that the softening spring is more flexible than the other two and is thus more difficult to control.

The restoring force versus displacement is given in Fig. 3.15. From the graph, it can be seen that the stiffness coefficient is bounded by

$$k^- \leq k \leq k^+,$$

where $k^-$ is the softening spring and $k^+$ is the hardening spring. Since $k^-$ is the most flexible coupler which gives the most severe oscillation, it is reasonable to use $k^-$ in the design for worst case analysis in the case of passenger train, whereby ride quality is highly emphasised.

The resistance experienced by the train is caused by two sources: the rolling resistance and the aerodynamic resistance. The total resistance, or running resistance, is given as

$$R = \underbrace{c_0 + c_v v}_{R^r} + \underbrace{c_a v^2}_{R^a},$$

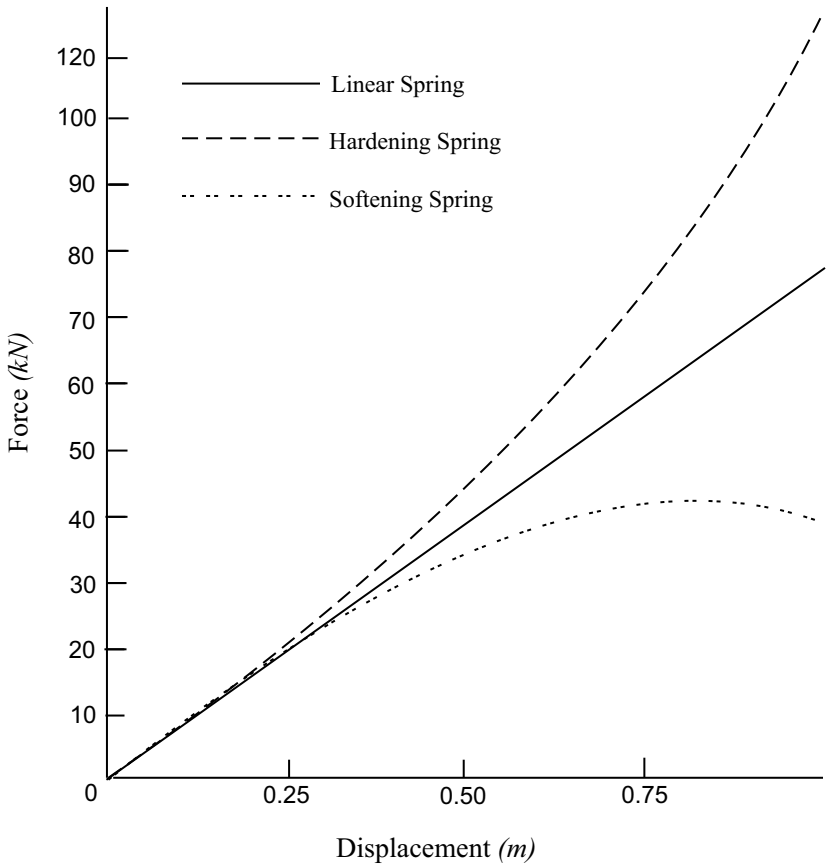


Figure 3.15: Restoring force versus displacement for the different types of spring.

where $v$ is the wagon velocity, the coefficients are determined by wind tunnel tests. $R^r$ and $R^a$ are the rolling resistance and aerodynamic resistance respectively.

Aerodynamic drag is most dominant at high-speed region, mostly experienced by high-speed trains. The rolling resistance, caused by the friction between wheel and rail, is dominant at the low speed range, thus the predominant resistance experienced by freight trains.

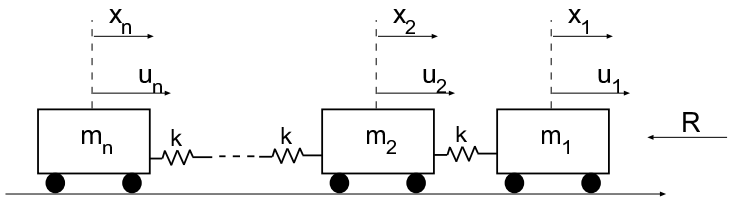


Figure 3.16: Force diagram of the train in longitudinal motion (Yang and Sun, 2001).

Fig. 3.16 is the force diagram of the train model. $x_i$ and $\dot{x}_i$ represent the position and velocity of the $i$th wagon with respect to a static frame on the ground. $u_i$ is the traction of the motorised cars. For DD design all the wagons would have its own traction force, but for PPD $u_i = 0, i = 2 \ldots n-1$ as only the first and the last wagons are powered. The lower bound $k^-$ is used for the stiffness coefficient for worst case analysis.

It is assumed that the aerodynamic drag acts on the first car only. All the wagons experience the rolling resistance. The equations of motion for the wagons are

$$\left.\begin{aligned} m_1\ddot{x}_1 &= u_1 - k^-(x_1 - x_2) - \underbrace{(c_0 + c_v\dot{x}_1)}_{R^r} m_1 - \underbrace{c_a\dot{x}_1^2}_{R^a}(\sum_{i=1}^{n} m_1), \\ m_i\ddot{x}_i &= u_i - k^-(x_i - x_{i-1}) - k^-(x_i - x_{i+1}) - \underbrace{(c_0 + c_v\dot{x}_i)}_{R^r} m_i, \\ & \qquad\qquad i = 2, \ldots, n-1 \\ m_n\ddot{x}_n &= u_n - k^-(x_n - x_{n-1}) - \underbrace{(c_0 + c_v\dot{x}_n)}_{R^r} m_n. \end{aligned}\right\} \quad (3.3)$$

To be able to use linear control theory, the model needs to be linearised first. For the DD design, it is assumed that at the equilibrium state all the

wagons are at a cruising speed $\dot{x}_1^e = \dot{x}_2^e = \cdots = \dot{x}_n^e = v_0$ and zero acceleration $\ddot{x}_1^e = \ddot{x}_2^e = \cdots = \ddot{x}_n^e = 0$. By substituting the previous values into (3.3), the control force and the position can be found as

$$\left.\begin{aligned} u_1^e &= c_0 m_1 + c_v m_1 v_0 + c_a (\sum_{i=1}^{n} m_i) v_0^2 \\ u_i^e &= c_0 m_i + c_v m_i v_0, i = 2, \ldots, n \end{aligned}\right\} \tag{3.4}$$

$$x_1^e = x_2^e = \ldots = x_n^e$$

which means that the relative displacements between the wagons are zero at equilibrium.

Using (3.4) and ignoring higher order terms and substituting $x_i = x_i^e + \delta x_i$ and $u_i = u_i^e + \delta u_i$, the following linearised equations of motion are obtained

$$\left.\begin{aligned} m_1 \delta\ddot{x}_1 &= \delta u_1 - k^-(\delta x_1 - \delta x_2) - (c_0 + c_v \delta\dot{x}_1) m_1 \\ &\quad -2 c_a v_0 \delta\dot{x}_1 \sum_{i=1}^{n} m_1, \\ m_i \delta\ddot{x}_i &= u_i - k^-(\delta x_i - \delta x_{i-1}) - k^-(\delta x_i - \delta x_{i+1}) - (c_0 \\ &\quad + c_v \delta\dot{x}_i) m_i, \qquad i = 2, \ldots, n-1 \\ m_n \delta\ddot{x}_n &= u_n - k^-(\delta x_n - \delta x_{n-1}) - c_v m_n \delta\dot{x}_n. \end{aligned}\right\} \tag{3.5}$$

For the PPD design, (3.4) does not hold due to the lack of enough control inputs to cancel out the rolling resistance in each wagon. However, the approximation is still good enough from the practical point of view since similar control forces are exerted by the locomotives and distributed via couplers. For relatively flat track, it is possible for PPD design to achieve equilibrium operation.

Equation (3.5) can be rewritten in the standard state space form as

$$\dot{x} = Fx + Gu = \begin{bmatrix} 0_{n\times n} & I_{n\times n} \\ F_{21} & F_{22} \end{bmatrix} x + \begin{bmatrix} 0_{n\times l} \\ G_{21} \end{bmatrix} u$$

where $n$ is the number of cars, $l$ is the number of motorised wagons and the state valuables are $x = [\delta x_1 \ \ldots \ x_n \quad \delta\ddot{x}_1 \ \ldots \ \delta\ddot{x}_n]^T$ and $u = [\delta u_1 \ \ldots \ \delta u_l]^T$,

$$G_{21} = \begin{cases} \begin{bmatrix} 1 & 0 \\ 0_{n-2} & 0_{n-2} \\ 0 & 1 \end{bmatrix}, \text{for the PPD type} \\ I_{n\times n}, \text{for the DD type} \end{cases}$$

$$F_{21} = \begin{bmatrix} \frac{-k^-}{m_1} & \frac{k^-}{m_1} & 0 & \dots & \dots & \dots & 0 \\ \frac{k^-}{m_2} & \frac{-2k^-}{m_2} & \frac{k^-}{m_2} & 0 & \dots & \dots & 0 \\ 0 & \frac{k^-}{m_3} & \frac{-2k^-}{m_3} & \frac{k^-}{m_3} & 0 & \dots & 0 \\ \dots & \dots & \dots & \dots & \dots & \dots & \dots \\ 0 & \dots & \dots & \dots & \dots & \dots & 0 \\ 0 & \dots & \dots & 0 & \frac{k^-}{m_{n-1}} & \frac{-2k^-}{m_{n-1}} & \frac{k^-}{m_{n-1}} \\ 0 & \dots & \dots & \dots & 0 & \frac{k^-}{m_n} & \frac{-k^-}{m_n} \end{bmatrix}_{n\times n}$$

$$F_{22} = \begin{bmatrix} -c_v - \frac{2c_a v_0 \left(\sum_{i=1}^{n} m_i\right)}{m_1} & 0 & \dots & \dots & 0 \\ 0 & -c_v & 0 & \dots & 0 \\ \dots & \dots & \dots & \dots & \dots \\ 0 & \dots & 0 & -c_v & 0 \\ 0 & \dots & \dots & \dots & -c_v \end{bmatrix}$$

Assume that all the states can measured, the measured output y is given as

$$y = Cx$$

where $C = I_{2n\times 2n}$. The performance output $z$ is defined as

$$z = Hx$$

where $z$ is required to track the speed command $r(t)$. For PPD design, $z = [\dot{x}_1 \quad \dot{x}_n]^T$ and for DD design, $z = [\dot{x}_1 \quad \dot{x}_2 \quad \dots \quad \dot{x}_n]^T$, therefore

$$H = \begin{cases} \begin{bmatrix} 0_{1\times n} & 1 & 0 & \dots & 0 \\ 0_{1\times n} & 0 & \dots & 0 & 1 \end{bmatrix}_{2\times 2n} & \text{, for the PPD design} \\ [0_{n\times n} \quad I_{n\times n}]_{n\times 2n} & \text{, for the DD design.} \end{cases}$$

### 3.4.3 Results

Two performance comparisons were done by Yang and Sun (2001): between DD and PPD and between mixed $H_2/H_\infty$ and pure $H_2$ and $H_\infty$ control. Their results are shown in Fig. 3.17 and Fig. 3.18. The velocities are assumed to belong to the front locomotive since it is not indicated by Yang and Sun (2001).

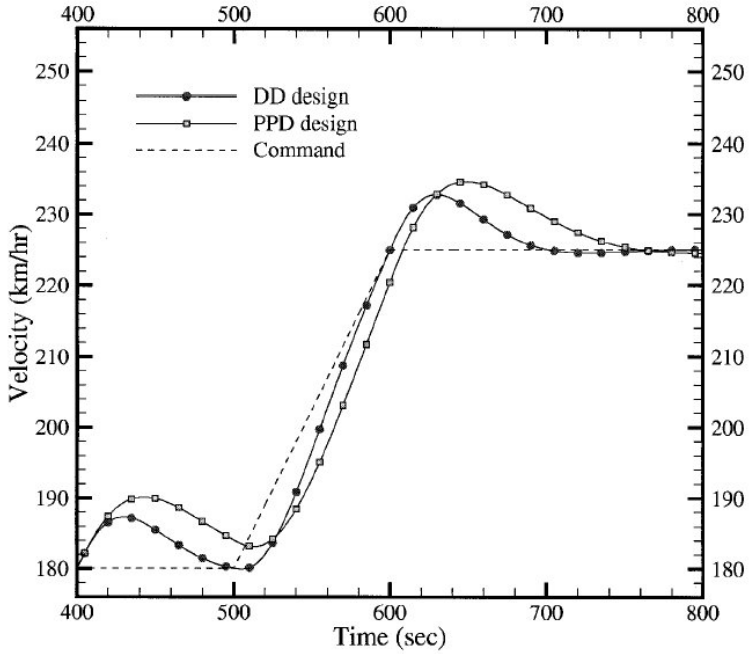


Figure 3.17: The tracking performance of DD and PPD design (Yang and Sun, 2001).

From Fig. 3.17, it is clear that DD design has a smaller overshoot, shorter rise time and faster settling time. Thus for mixed $H_2/H_\infty$ control, DD design has better command tracking performance than PPD design.

The gust attenuation performance of DD and PPD design is given in Fig. 3.18. The trains were subjected to a wind gust of $-20m/s$ at $t = 600s$, an equivalent head-on collision force of around $-20kN$. Again, DD design exhibits smaller velocity fluctuation and faster recovery. This shows that, for mixed $H_2/H_\infty$ control, DD design performs better than PPD design at attenuating wind gust. The one advantage of PPD design, seen from Fig. 3.19, is that it requires less control efforts than DD design, thus reducing energy usage.

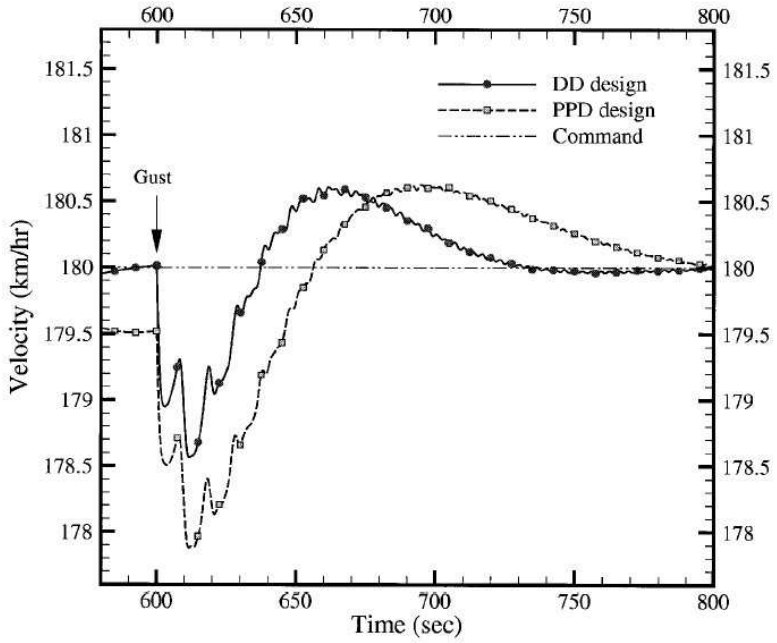


Figure 3.18: The gust attenuation of the DD and PPD design (Yang and Sun, 2001).

It can also be seen that the summed absolute energy usage does not depend on the spring coefficients. Two values of spring coefficients variation $\varepsilon$ are used in this simulation. From the practical side, PPD requires much less maintenance as there are only two motorised cars per train, as opposed to DD design where every car is powered.

The tracking and gust attenuation performance of the different controller is given below. It can be seen that the mixed $H_2/H_\infty$ control perform better than pure $H_2$ control in both aspects, while its settling time is faster than those of $H_\infty$.

From Fig. 3.20, it can be seen that $H_2$ control has the best command tracking performance and $H_\infty$ control has the best gust attenuation. Mixed $H_2/H_\infty$ control shows a good compromise between the two controllers. From Fig. 3.21, it is clear that pure $H_2$ control exhibits excessive oscillation while mixed $H_2/H_\infty$ control was able to perform reasonably well.

It is important to notes that although DD design gave better performance than PPD design in the previous result, the same assumption may not hold for different controller.

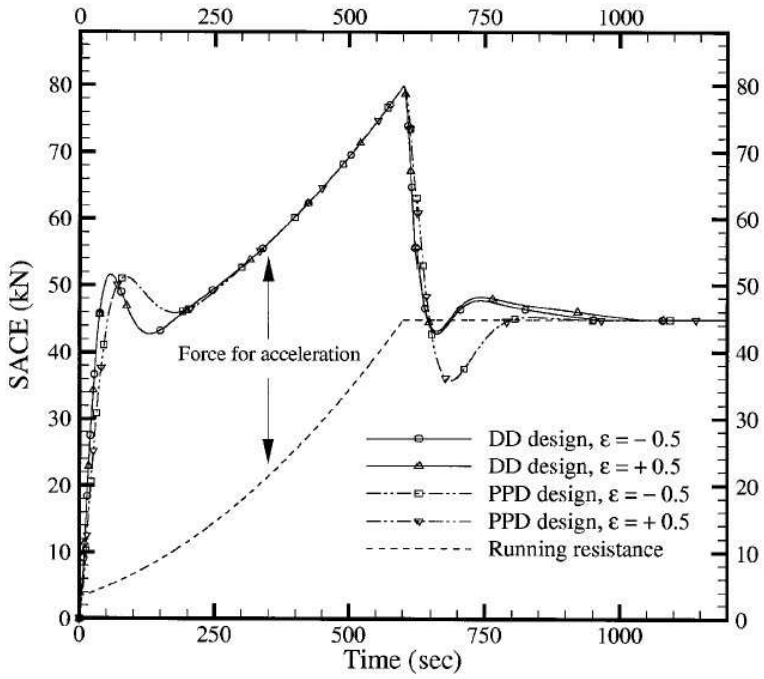


Figure 3.19: Summation of absolute control efforts of DD and PPD design with different spring coefficients (Yang and Sun, 2001).

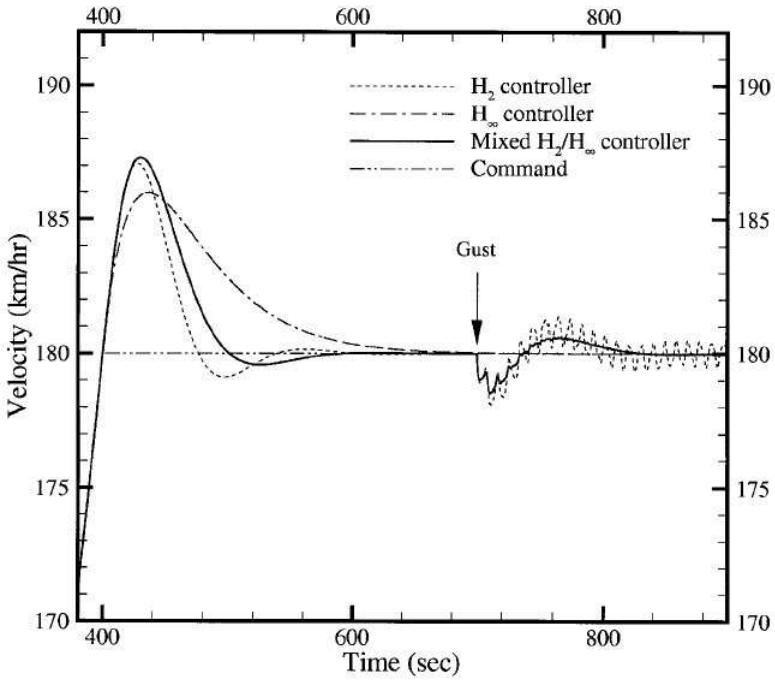


Figure 3.20: The tracking and gust attenuation performance of the $H_2/H_\infty$, pure $H_2$ and $H_\infty$ controllers (Yang and Sun, 2001).

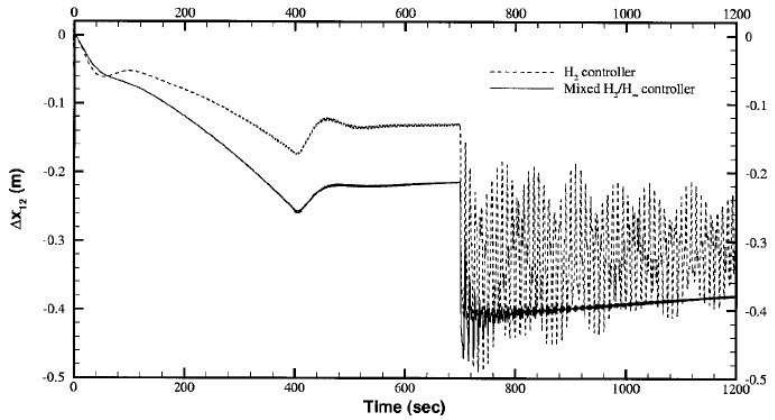


Figure 3.21: Gust attenuation performance of $H_2/H_\infty$ versus pure $H_2$ control (Yang and Sun, 2001).

### 3.4.4 Discussion

The model proposed by Yang and Sun (2001) is a pure theoretical one: the simplifications and modelling methods have not been validated as whether it can sufficiently represent the high-speed train accurately. Further more, such methods are not necessary applicable to ECP/DP trains since the train characteristics such as train length and wagon mass differ substantially.

In this study, the lower value is assumed for worst-case analysis. Although the resultant in-train force are smaller, it produces excessive oscillation which affect the ride quality greatly. This is different from the heavy-haul train, whereby the larger spring coefficient would be considered as the worst-case choice due to the higher in-train force it produces.

The modelling of the external disturbances seems insufficient. Track conditions such as gradient and curvature were not considered. Modelling wind gust as an impulse-like disturbance seems unnatural, as wind gust resistance increases gradually.

In-train force, although modelled, was not a control objective in the controller design. Cruise control results show that it is possible for PPD configuration, similar to certain Coallink train configuration, to be velocity regulated.

## 3.5 Input/Output Decoupling

### 3.5.1 Introduction

In the study by Astolfi and Menini (2002), input/output decoupling of high-speed train is investigated. In a complex multiple inputs multiple outputs (MIMO) system such as the high-speed train, it is highly desirable to be able to control certain particular output without affecting the other outputs. That is, each reference only affects its corresponding output, *e.g.*, changes in reference velocity should have no effects on the in-train force.

### 3.5.2 Methodology

The train model is based on the high-speed train model from Yang and Sun (2001), shown in Fig. 3.16. Rolling resistance coefficients are defined as $c_0$ and $c_v$. Coupler force, called the elastic restoring force $f_e$ here, is defined as a function of the relative displacement $\delta$ between adjacent cars,

$$f_e(\delta) = k_0(1 + \varepsilon\delta^2)\delta, \tag{3.6}$$

where $k_0$ is the spring constant, $\varepsilon$ is the non-linearity factor.

The model shown in Astolfi and Menini (2002) is as follows

$$\begin{aligned} m_1\ddot{x}_1 &= u_1 + f_e(x_2 - x_1) \\ &\quad - (c_0 + c_v\dot{x}_1)m_1 - C_a(\dot{x}_1 - \omega)^2, \\ m_i\ddot{x}_i &= u_i - f_e(x_i - x_{i-1}) + f_e(x_{i+1} - x_i) \\ &\quad - (c_0 + c_v\dot{x}_i)m_i, \quad i = 2, \ldots, n-1, \\ m_n\ddot{x}_n &= u_n - f_e(x_{i-1} - x_i) - (c_0 + c_v\dot{x}_n)m_n. \end{aligned} \tag{3.7}$$

Again, operation around an equilibrium point is considered. In this study, it is assumed that the train is travelling around the desired speed $v_0$, *i.e.*, $x_i^e(t) = v_0, i = 1, \ldots, n$. It is also assumed that the driving forces are constant. $\omega$ is the wind speed.

PPD as well DD operations are considered. Thus, with more than one driving force, the freedom of choice for the constant driving forces will result in

different constant equilibrium distance

$$\delta^e_{i+1} = x^e_{i+1}(t) - x^e_i(t), i = 1, \ldots, n-1.$$

Since the actual position of the train along the railroad is not used in the model, a more logical choice of the state vector would be the equilibrium distance and the train velocity error, *i.e.*,

$$\begin{aligned} x(t) &= [\delta_{2,1} \ \ldots \ \delta_{n,n-1} \ \delta\dot{x}_i \ \ldots \ \delta\dot{x}_n], \\ \delta_{i+1,i} &= x_{i+1}(t) - x_i(t) - \delta^e_{i+1}, \\ \delta\dot{x}_i &= \dot{x}_i - v_0, \end{aligned}$$

where $v_0$ is the desired velocity and $\delta_{i+1,i}$ is the relative displacement, which is the distance offset from the equilibrium distance.

Let $c_\tau = c_0 + c_v v_0$ and assume equilibrium state, from (3.7), the following $n$ non-linear equations can be found:

$$\begin{aligned} 0 &= u^e_1 + f_e(\delta^e_{2,1}) - c_\tau m_1 - C_a v_0^2, \\ 0 &= -f_e(\delta^e_{i,i-1}) + f_e(\delta^e_{i+1,i}) - c_\tau m_i, i = 2, \ldots, n-1, \\ 0 &= u^e_n - f_e(\delta^e_{n,n-1}) - c_\tau m_n, \end{aligned} \tag{3.8}$$

with $n+1$ unknowns $\delta^e_{i,i-1}$, $u^e_1$ and $u^e_n$. To determine the operating point, another equation has to be added to (3.8). The choices suggested by Astolfi and Menini (2002) are

- $\delta^e_{k+1,k} = 0$ for a given $k \in \{1, \ldots, n-1\}$, *i.e.*, one of the equilibrium distance equals to zero, or
- $u^e_1 = u^e_n$, both constant driving forces equal.

In that paper, the first option with $k = 2$ was chosen, *i.e.*, $\delta^e_{3,2} = 0$, for solving the operating point. The PPD case $n = 5$ was considered. The resulting state space model with input

$$u(t) = \begin{bmatrix} \delta u_1 \\ \delta u_5 \end{bmatrix} := \begin{bmatrix} u_1 - u^e_1 \\ u_5 - u^e_5 \end{bmatrix} \tag{3.9}$$

and disturbance (wind disturbance) $\omega$ can be written as:

$$\begin{aligned}
\dot{\delta}_{i+1,i} &= \delta\dot{x}_{i+1} - \delta\dot{x}_i, i = 1, \ldots, 4, && (3.10)\\
m_1\delta\ddot{x}_1 &= \Delta f_e(\delta^e_{2,1} + \delta_{2,1}, \delta^e_{2,1}) - C_a\delta\dot{x}_1^2 - (c_v m_1 + 2C_a v_0)\delta\dot{x}_1 \\
&\quad +\delta u_1 + Ca(2v_0\omega - C_a\omega^2) + 2C_a\delta\dot{x}_1\omega, && (3.11)\\
m_2\delta\ddot{x}_2 &= f_e(\delta_{3,2}) - \Delta f_e(\delta^e_{2,1} + \delta_{2,1}, \delta^e_{2,1}) - m_2 c_v\delta\dot{x}_2 && (3.12)\\
m_3\delta\ddot{x}_3 &= \Delta f_e(\delta^e_{4,3} + \delta_{4,3}, \delta^e_{4,3}) - f_e(\delta_{3,2}) - m_3 c_v\delta\dot{x}_3 && (3.13)\\
m_4\delta\ddot{x}_4 &= \Delta f_e(\delta^e_{5,4} + \delta_{5,4}, \delta^e_{5,4}) - \Delta f_e(\delta^e_{4,3} + \delta_{4,3}, \delta^e_{4,3}) - m_4 c_v\delta\dot{x}_4 && (3.14)\\
m_5\delta\ddot{x}_5 &= -\Delta f_e(\delta^e_{5,4} + \delta_{5,4}, \delta^e_{5,4}) - m_5 c_v\delta\dot{x}_5 + \delta u_5, && (3.15)
\end{aligned}$$

where $\delta\ddot{x}_i = \frac{d}{dt}(\delta\dot{x}_i)$, $f_e(.)$ is given by (3.6) and $\Delta f_e(\delta_1, \delta_2) := f_e(\delta_1) - f_e(\delta_2)$.

### 3.5.3 Results

In that paper, it made the following observations for stability: when rolling resistance is considered in the high-speed train model, despite its slow decay rate, the oscillation of the open-loop system is asymptotically stable. Thus for the closed-loop system, the rate of the exponential decay of the modes of the linearised model can be fixed by the designer, as long as it is faster than the one of the open-loop systems.

In the scenarios proposed by Astolfi and Menini (2002), the following problems need to be satisfied for the closed-loop system with input $r(t) \in \mathbb{R}^2$ and output $y = h(x)$:

- It is (locally) non-interactive between the input $r$ and the output y,
- It is asymptotically stable in the first approximation, with all the eigenvalues of its approximate linearised model having real part smaller than $-c_v/2$, and
- It is such that, for initial conditions sufficiently close to this equilibrium, for small constant reference signals $r$ and for small constant disturbance $\omega$, one has

$$\lim_{t\to+\infty}(r - y(t)) = 0.$$

With the problem defined, various choices of the output $y$ were explored whereby the second output would be the relative displacement of various section of the train.

**The case** $y_2 = \delta_{2,1}$

It is assumed that the output is

$$y = \begin{bmatrix} h_1(x) \\ h_2(x) \end{bmatrix} = \begin{bmatrix} \delta\dot{x}_1 \\ \delta_{2,1} \end{bmatrix}, \tag{3.16}$$

*i.e.*, the first output is the velocity of the first car and the second output is the relative distance between the first and the second car, *i.e.*, the first coupler.

It is found that with (3.9), (3.10) to (3.15) and (3.16) the input-output decoupling problem can be solved with standard steps.

**The case** $y_2 = \delta_{5,4}$

It is assumed that the output is

$$y = \begin{bmatrix} h_1(x) \\ h_2(x) \end{bmatrix} = \begin{bmatrix} \delta\dot{x}_1 \\ \delta_{5,4} \end{bmatrix}, \tag{3.17}$$

*i.e.*, the first output is the velocity of the first car and the second output is the relative distance between the fourth and the fifth car, *i.e.*, the last coupler.

It is found that in this case the problem is not solvable by using (3.9), (3.10) to (3.15) and (3.17).

However, the paper found that with an additional input the problem can be solved. The driving force is then

$$u(t) = \begin{bmatrix} \delta u_1 \\ \delta u_4 \\ \delta u_5 \end{bmatrix} := \begin{bmatrix} u_1 - u_1^e \\ u_4 - u_4^e \\ u_5 - u_5^e \end{bmatrix}. \tag{3.18}$$

The operating point so that $\delta^2_{3,2} = 0$ and $\delta^2_{5,4} = 0$ is determined. Consequently, the state space equations of the system become (3.10) to (3.13) and

$$\begin{aligned} m_4\delta\ddot{x}_4 &= f_e(\delta^e_{5,4}) - \Delta f_e(\delta^e_{4,3} + \delta_{4,3}, \delta^e_{4,3}) - m_4 c_v \delta\dot{x}_4 + \delta u_4 \\ m_5\delta\ddot{x}_5 &= -\Delta f_e(\delta^e_{5,4} - m_5 c_v \delta\dot{x}_5 + \delta u_5, \end{aligned}$$

which replace (3.14) and (3.15).

**The case** $y_2 = \delta_{4,3}$

It is assumed that the output is

$$y = \begin{bmatrix} h_1(x) \\ h_2(x) \end{bmatrix} = \begin{bmatrix} \delta\dot{x}_1 \\ \delta_{4,3} \end{bmatrix}, \tag{3.19}$$

*i.e.*, the first output is the velocity of the first car and the second output is the relative distance between the third and the fourth car, *i.e.*, the second coupler from the rear.

In this case, the additional third driving force is again required to satisfy the problem statement. Thus the input is now

$$u(t) = \begin{bmatrix} \delta u_1 \\ \delta u_3 \\ \delta u_5 \end{bmatrix} := \begin{bmatrix} u_1 - u^e_1 \\ u_3 - u^e_3 \\ u_5 - u^e_5 \end{bmatrix}. \tag{3.20}$$

The operating point so that $\delta^2_{3,2} = 0$ and $\delta^2_{4,3} = 0$ is determined. Consequently, the state space equations of the system become (3.10) to (3.12), (3.15) and

$$\begin{aligned} m_3\delta\ddot{x}_3 &= (f_e(\delta^e_{4,3}) - f_e(\delta^e_{3,2})) - m_3 c_v \delta\dot{x}_3 + \delta u_3 \\ m_4\delta\ddot{x}_4 &= \Delta f_e(\delta^e_{5,4} + \delta_{5,4}, \delta^e_{5,4}) - f_e(\delta_{4,3}) - m_4 c_v \delta\dot{x}_4, \end{aligned}$$

which replace (3.13) and (3.14).

In this paper, simulated results showed that input/output decoupling can be achieved along with strengthened stability. The second property meant the system converges quickly, since the eigenvalues of the linearisation of the closed-loop system were placed well to the left of the axis $\mathrm{Re}(\lambda) = -c_v/2$.

An interesting second simulation was also performed with the parameter perturbed. The masses of the cars were changed without the controller being modified. This is to simulate the real-life situation where the passenger from one car would move to the other cars. In this case, the strengthened stability remains, however, the decoupling property is lost.

When the reference velocity is changed, in the perturbed case, the second output, in this case the relative displacement, is also affected. Although the first output, the velocity of the first car, still follows the reference, the decoupling property no longer holds.

However, if the second reference, the relative displacement changes, the first output is not affect and the decoupling property partially holds in this case. In the paper, it is stated that this holds for all parameter variations except for $k_0$ and $\varepsilon_1$. The explanation is that the elastic force is properly compensated by the inner state feedback used in the design.

The perturbed simulation also showed more oscillations than the original model, although asymptotic stability and asymptotic regulation are preserved even under these conditions.

### 3.5.4 Discussion

This paper gives interesting insight to the behaviour of the model proposed by Yang and Sun (2001) as well as train behaviour for different control situation.

This paper shows that for a PPD configuration, like those found in Coallink trains, the problem of input/output decoupling with strengthened stability is not solvable unless a third input is added. The only exception is that if the second output is the relative displacement between the first two cars, which is solvable in PPD.

Relating this finding to Coallink trains, this would mean that it is impossible to control the coupler forces within the wagons without affecting the speed regulation performance. The force will be controllable, but will affect other train performances during the process.

If the decoupling property criteria can be met, then the paper also shows

that asymptotic set point regulation could be obtained even under a constant disturbance.

However, the study proposed in the paper remains theoretical. Both the model and the controller have not been validated.

In the case of Coallink trains, in-train force optimisation is not possible with this method. First, in extra long trains, the output number exceeds the input number tremendously. With too few inputs, input-output decoupling is not possible, as stated in the paper. Secondly, the decoupling property is very sensitive toward parameter changes. In practice, wagon mass differs within a train, as well as differs from train to train. From the above reasons, it can be concluded that application of this type of control will need further investigation.

## 3.6 Suboptimal Control Strategies for Multi-locomotive Powered Trains

### 3.6.1 Introduction

The paper by Gruber and Bayoumi (1982) is unique in the sense that it was written long before the ECP/DP system was even studied by AAR in 1992, whom finally defined the first draft of the standard in 2002. The vision of the authors deserves respect, for they proposed a control system on a brake system that was not even named yet. In the paper, the term "electropneumatic brakes" was used to define an electronically controlled pneumatic brake system that had no signal delays, essentially what the modern day ECP system represents.

A list of train control problems were discussed in the paper. Some of the methods were simple linear interpolations. The paper proposed a global controller as well as a lower-level cruise controller.

### 3.6.2 Methodology

The paper was divided into two different sections: one part deals with off-line schedules, achieving trajectory optimisation, while the second part deals with the regulation control. The two use different models during the design process.

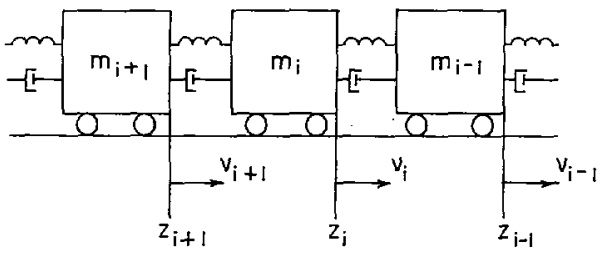


Figure 3.22: The train model (Gruber and Bayoumi, 1982).

In the model used by the regulation controller, the train configuration was chosen symmetric with a locomotive at each end as well as one in the middle

of the train. The couplers were modelled as spring force with spring constant $k$ and damping coefficients $c_c$ and $c_l$, for wagon and locomotive respectively.

The actual velocity vector $\mathbf{v}$ and input vector $\mathbf{u}$ that consist of traction and brake force were used together with the nominal values $\mathbf{v}^n$ and $\mathbf{u}^n$ to define the deviation values

$$\begin{aligned} \delta\mathbf{v} &= \mathbf{v} - \mathbf{v}^n, \\ \delta\mathbf{u} &= \mathbf{u} - \mathbf{u}^n. \end{aligned}$$

The nominal velocity $\mathbf{v}^n$ is maintained by the nominal input $\mathbf{u}^n$ that equals the resistance and gravitational force.

The linearised model is given as

$$\begin{aligned} m_i\delta\dot{v}_i(t) &= k\{\Delta_i(t) - \Delta_{i+1}(t)\} \\ &\quad +c_i\{\delta v_{i-1}(t) - 2\delta v_i(t) + \delta v_{i+1}(t)\} \\ &\quad +\delta u_i(t) + \delta d_i(t), i = 1, \ldots, n, \qquad (3.21) \\ \dot{\Delta}_i(t) &= \delta v_{i-1}(t) - \delta v_i(t), i = 2, \ldots, n, \qquad (3.22) \end{aligned}$$

where $\Delta_i$ is the displacement from the nominal force position of the cars, $m_i$ is the mass of the car, $c_i$ is the damping coefficient. For locomotives, $m_i = m_l$ and $c_i = c_l$, while for wagons $m_i = m_c$ and $c_i = c_c$. $d_i$ are the disturbances, namely the track grades and the curves.

In this model the linearised drag term was neglected as it is much smaller than the damping forces. Input vector $\mathbf{u}$ represent brake forces, or traction forces for the case $i = 1, m, n$. $m, n$ are the middle and end car of the train respectively.

Note that the model only takes into account the damping interaction between cars. For spring forces, only the rear coupler of each car was considered. This differs from the approaches taken by Yang and Sun (2001) and Astolfi and Menini (2002). By only considering the rear coupler, the complexity of the model was reduced. Since there was not explanation given in the paper, it could only be assumed that this selection was justified by its calculation simplicity.

The state space equations are

$$\begin{aligned}
\delta\dot{\mathbf{x}}(t) &= \mathbf{A}\delta\mathbf{x}(t) + \mathbf{B}\delta\bar{\mathbf{u}}(t), \\
\delta\mathbf{x}'(t) &= [\delta v_1, \ldots, \delta v_n, \Delta_2, \ldots, \Delta_n], \\
\delta\mathbf{u}'(t) &= [\delta\bar{\mathbf{u}}_1, \ldots, \delta\bar{\mathbf{u}}_n], \\
\delta\bar{u}_i &= \frac{\delta u_i}{m_i},
\end{aligned}$$

and A is given as

$$A = \left[\begin{array}{c|c} H & G \\ \hline F & 0 \end{array}\right],$$

with

$$H = \begin{bmatrix}
-\bar{c}_L & \bar{c}_L & & & & & \\
\bar{c}_c & -2\bar{c}_c & \bar{c}_c & & & \bigcirc & \\
 & \ddots & \ddots & \ddots & & & \\
 & & \bar{c}_L & -2\bar{c}_L & \bar{c}_L & & \\
 & & & \bar{c}_c & -2\bar{c}_c & \bar{c}_c & \\
 & \bigcirc & & & \ddots & \ddots & \ddots \\
 & & & & & \bar{c}_L & -\bar{c}_L
\end{bmatrix}_{n,n},$$

$$F = \begin{bmatrix}
1 & -1 & & & & \\
 & 1 & -1 & \bigcirc & & \\
 & \bigcirc & \ddots & \ddots & & \\
 & & & 1 & -1
\end{bmatrix}_{n-1,n},$$

$$G = \begin{bmatrix}
\bar{k}_L & & & & & \\
-\bar{k}_c & \bar{k}_c & & & & \\
 & \ddots & \ddots & & \bigcirc & \\
 & & \bar{k}_L & -\bar{k}_L & & \\
 & & & \bar{k}_c & -\bar{k}_c & \\
 & \bigcirc & & & \ddots & \ddots \\
 & & & & & \bar{k}_c & -\bar{k}_c \\
 & & & & & & \bar{k}_L
\end{bmatrix}_{n,n-1},$$

with per unit mass coefficients $\bar{k_c} = \frac{k}{m_c}$, $\bar{k_L} = \frac{k}{m_L}$, $\bar{c_c} = \frac{c_c}{c_c}$ and $\bar{k_L} = \frac{k_L}{m_L}$.

Matrix $B$ is given as

$$B = \left[\begin{array}{ccccc} 1 & & & & \\ & 1 & & \bigcirc & \\ & & 1 & & \\ & \bigcirc & & \ddots & \\ & & & & 1 \\ \hline & & \bigcirc_{n-1,n} & & \end{array}\right]_{2n-1,n} \tag{3.23}$$

The controller is designed to minimise the coupler forces and velocity deviations, *i.e.*,

$$\delta v_1^2 + \sum_{i=2}^{n} [\delta v_i^2 + \Delta_i^2] = minimum.$$

For the rest of that paper, the train configuration consists of 3 locomotives, 9 wagons.

For off-line scheduling, some assumptions were made. The first was that the schedule was chosen such that the reference velocity was maintained, without contributing to additional accelerations and decelerations of the train. It was assumed that the closed-loop controller would handle this. Secondly, the input variations were assumed continuous and there were no power limits.

For the implementation of the off-line scheduling, the time instants at which the appropriate inputs should be applied need to be determined on-line. The inputs are nonlinear functions of the scheduling parameters $p$, *e.g.*, grades and velocity profiles and train data, as well as travelled distances $z$ of the train:

$$\mathbf{u}^n = \mathbf{f^n}(\mathbf{z}, \mathbf{p}).$$

In the paper, the function was chosen as illustrated in Fig 3.23. Step functions with variable amplitudes were used to approximate the inputs. This was justified since real traction is quantised. Large changes were approximated by a sequence of several small steps, since traction can be varied one step at a time only. Time instants $\tau_{ji}$ were determined on-line.

The scheduling function $\mathbf{u}^n$ for Fig. 3.23 can be written as

$$\begin{aligned} u_j^n(t) &= A_1(\epsilon(t) - \epsilon(t - \tau_{j2})) + A_2\epsilon(t - \tau_{j2}), \qquad j = 1, 4, 6 \quad \text{throttling} \\ u_j^n(t) &= A_2\epsilon(t - \tau_{j2}), \qquad j = 2, 3, 5 \quad \text{braking,} \end{aligned}$$

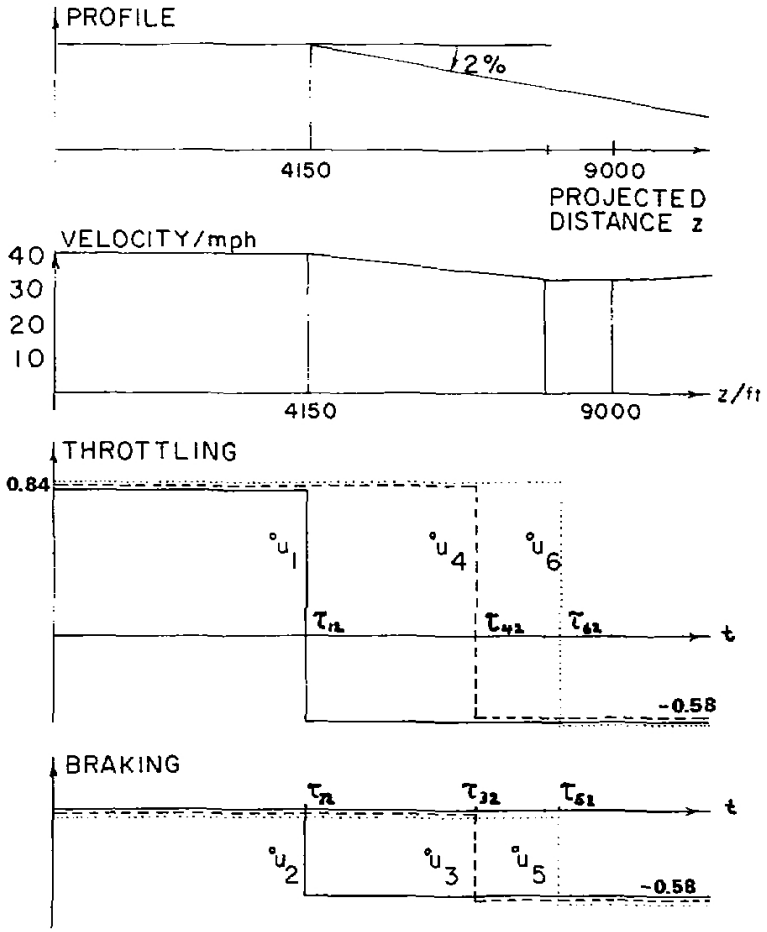


Figure 3.23: Profiles and off-line schedule for flat-downhill simulation (Gruber and Bayoumi, 1982).

where $\epsilon(t)$ is step function and

$$\begin{aligned} \tau_{ji} &= f_\tau(z), \\ A_i &= f_a(\mathbf{p}). \end{aligned}$$

The times $\tau_{ji}$ can be chosen according to some plan. In the paper, the $\tau_{ji}$ were as follows:

- $\tau_{1j} = \tau_{2i}$, $\tau_{12}$ = time if $z_1 = 4150$ ft,
- $\tau_{4j} = \tau_{3i}$, $\tau_{42}$ = time if $z_{2n/3} = 4150$ ft,
- $\tau_{6j} = \tau_{5i}$, $\tau_{62}$ = time if $z_n = 4150$ ft,

where n is assumed to be multiple of t. $A_i$ is chosen such as to maintain the constant reference velocity. The time instants $\tau_{j2}, j = 1, 4, 6$ correspond to the times when the first locomotive, $\frac{2}{3}$ of the train and the last locomotive reach the slope given in Fig. 3.23.

In comparison to the simple scheme proposed by Gruber and Bayoumi (1982), an optimised scheduling which takes in-train forces into consideration has been recently proposed by (Zhuan and Xia, 2005).

Due to the complexity of the control problem, five simplification steps were taken in order to find the suboptimal control strategies, to tackle the five challenges proposed in the paper:

1. large number of inputs,
2. constraints on the states,
3. constraints on the inputs,
4. large number of states, and
5. not all the states are measurable.

The first simplification step was to reduce the number of inputs. For the propose train of 60 cars in the paper, 60 individual brake inputs would be

required, in additional to the three locomotives. The paper propose that the wagon brake inputs be separated into three inputs, each acting on a third of the train. Uniform brake was used at most cases, only when there is zero crossing of the steady-state coupler forces will two different brake inputs be applied. The brake inputs are now $u_i, i = 2, 3, 5$ while the locomotive inputs are $u_i, i = 1, 4, 6$.

The second step was to ignore displacement constraints in the design.

The third simplification stage has to deal with the constraints of the inputs. The input constraints refer to the fact that wagons can only have negative inputs, thus bringing nonlinearity into the model. In order to reduce the different combinations possible and thus the nonlinearity, the paper proposes a two case scenario:

- when throttle is applied, no wagon brake will be applied $u_i^n = 0, i = 2, 3, 5$, feedback is limited to the locomotives only $\delta^1\mathbf{u} = K_1\delta x(t)$,
- when brake is applied, all locomotives and wagons will only brake $u_i^n \neq 0, i = 2, 3, 5$, although not necessary of the same magnitude, feedback for all 6 inputs $\delta^2\mathbf{u} = K_2\delta x(t)$.

The controller chooses either input depending on whether the inputs values are positive or negative, *i.e.*, traction or braking. In this setup, inputs freedom was limited to these two cases.

The fourth simplification deals with the large number of states. To evaluate the feedback matrices, the Riccati equation needs to be easily solvable. The paper does this by first simplifying the model, then applying the obtained results to the the large scale system.

The two methods proposed in the paper were small scale system containing a limited number of cars with original weight and a reduced order model of the long train, with reduced number of cars with increased masses to match the original train mass.

The objective function to find the optimal solutions is

$$J_j = \int_0^\infty (\delta\mathbf{x}'Q\delta\mathbf{x} + \delta^j\mathbf{u}'R_j\delta^j\mathbf{u})dt, j = 1, 2. \tag{3.24}$$

Two feedback systems are then

$$\delta^j \mathbf{u}(t) = K_j \delta \mathbf{x}(t), j = 1, 2.$$

Once the feedback matrices are obtained, they need to be adapted to the long train. For the small scale system, the key point is that the traction and braking force per unit mass should be invariant, *they should remain constant after the small scale system has been scaled to the full model*. Since the braking input of each car influences the same mass, the weigh pattern will not change. For traction, the weighing pattern will be increased by a factor that depends on the number of additional cars. For the increased mass model, the weight is simply multiplied by the ratio of the increased mass to the original car mass.

The last challenge was that not all the states are measurable. The paper claimed that displacement feedback were negligible, based on the simulated results. For the velocities, it proposes a simple static approximation:

$$\begin{aligned} v_i &= v_1, & i &= 2, \ldots, n/3, n = \text{multiple of } 3, \\ v_i &= v_m, & i &= n/3+1, \ldots, m-1, m+1, \ldots, 2n/3, \\ v_i &= v_n, & i &= 2n/3+1, \ldots, n-1, \end{aligned}$$

where again $m$ and $n$ are the middle and last car of the train, both locomotives in the proposed configuration.

The paper provides two justifications for such crude approximation:

1. the velocity changes slowly along the train, and
2. the velocity variations decrease with increasing distances from the locomotives,

which means that the velocities at or near the locomotives are most important. It is also at these positions where maximal steady-state coupler forces are expected. The paper states that the error of this approximation was difficult to estimate.

### 3.6.3 Results

The simulated model apparently considers aerodynamic drag and rolling friction, as well as coupler dead zones, although they were not defined by Gruber and Bayoumi (1982). However, the results provided were given without the dead zones. The paper states that dead zones degrade the performance as the dead zones widens. Input nonlinearities in terms of throttle quantisation were not considered, *continuous control input range is used*.

The 62 car train was simulated under two situations: a flat-downhill and a flat-uphill section with 2 percent slope. Fig. 3.23 shows the schedule for the downhill case. A similar schedule was used for the uphill case.

The obtained results are given in Table 3.6.3.

| | energy $(J)$ | $\Delta_{max}$ $(ft)$ | position $(\Delta_{max})$ | time $(s)$ | $\delta v_{max}$ $(ft/sec)$ |
|---|---|---|---|---|---|
| Small scale model controller | | | | | |
| Uphill | 9141 | 0.273 | $\Delta_2$ | 87.9 | 1.01 |
| Downhill | 9389 | 0.136 | $\Delta_{39}$ | 75.6 | 1.20 |
| Increased mass model controller | | | | | |
| Uphill | 9248 | 0.269 | $\Delta_2$ | 88.0 | 0.96 |
| Downhill | 9367 | 0.133 | $\Delta_{39}$ | 70.7 | 0.82 |

Table 3.3: Comparison of the performance of the two controllers.

The performances were good, with speed variation kept under 3 percent. In comparison, the open-loop deviation went up to 20 percent. In addition, stronger oscillation occurred throughout the train due to the eigenvalues locations.

It should be noted that the input power limitations were not applied in the model, so the required inputs could exceed the maximum values. The flat-downhill case is shown in Fig. 3.24.

From the graphs, the brake application of the second third of the trains at $t =$ 50 s can be clearly seen. A second jump can be observed where the controller switches from the 3 input control law (traction only) to the 6 input case ($t \simeq$ 80 s). This coincides with switching on of the third braking input $u_5^n$.

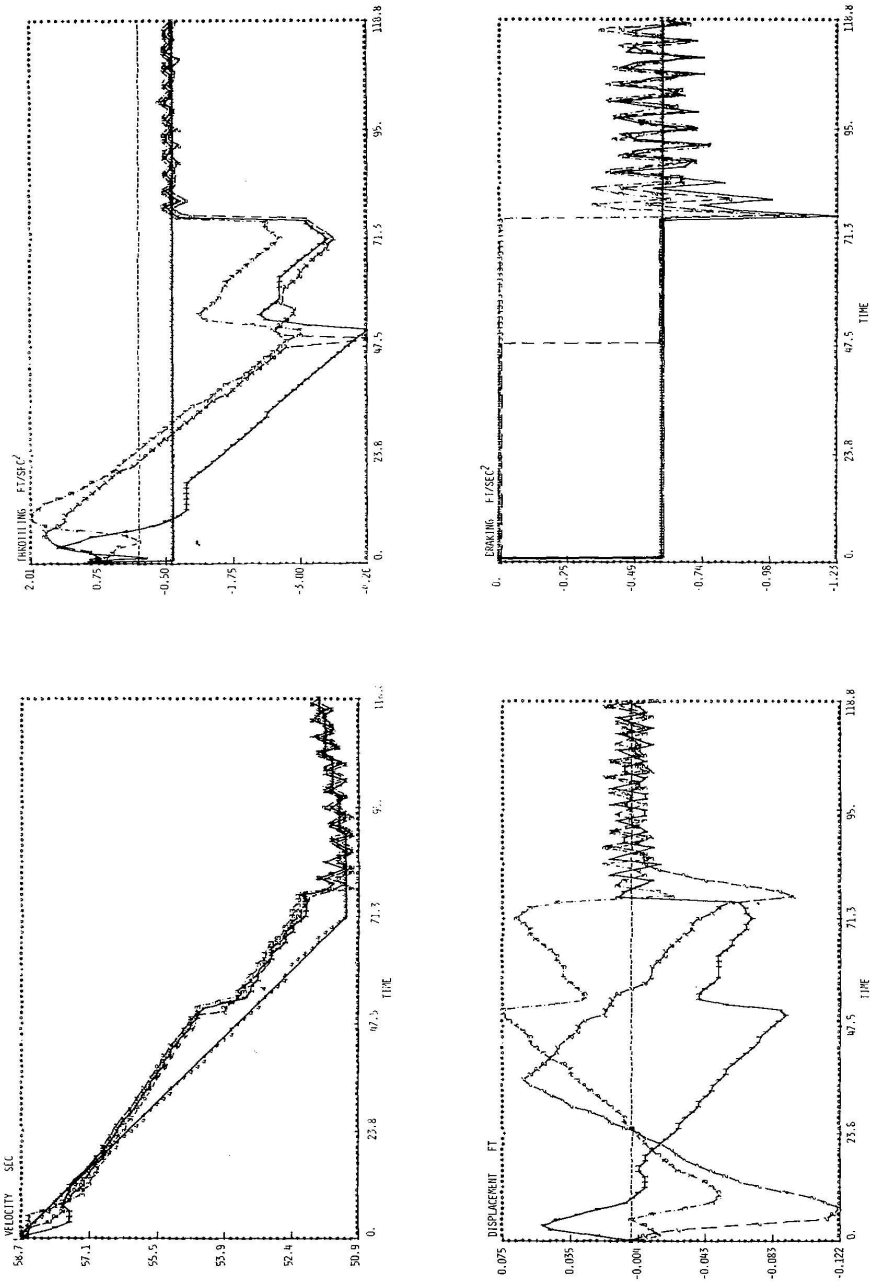


Figure 3.24: Simulation result for the closed-loop system with the small scale model controller implemented; flat-downhill simulation (Gruber and Bayoumi, 1982).

### 3.6.4 Discussion

The paper by Gruber and Bayoumi (1982) provides a study on the theoretical behaviours and possible control strategies of a train with electropneumatic braking.

The train model used in the paper neglected the rear coupler spring force. With no justification provided and no verification on the results, the model can only provide pure theoretical results.

The limited computational power in 1982 forced numerous simplifications to be made. The reduction of train length was necessary for the simulation to be completed within reasonable time with the limited computing power available. This reduces the amounts of train dynamics considered for extra long trains such as Coallink trains. Since large in-train forces occurs within the long wagon groups, excessive reduced model will act as a low pass filter and only exhibit smoothed out reduced in-train force dynamics.

However, the track topology was taken as disturbances in the dynamics of the train model. In modern technology, the track information is accurately provided by GPS/GIS equipment installed at the locomotives. This extra information will facilitate better handling of trains.

Scheduling only considered track grade for track condition. Other condition such as curvature resistance was ignored. Moreover, the scheduling signals overlooked in-train forces and coupler dynamics.

Input-conversion from forces to locomotive notches and the corresponding quantisation problems such as jittering were neglected.

Overall, the controller by Gruber and Bayoumi (1982) provides a theoretical investigation for multi-locomotive trains. With considerable simplification and assumptions, the controller has not been verified to work with extra long heavy-haul trains.

# Chapter 4

# Train Modelling

To design a feedback controller, a mathematical model of the train is required. Most of the existing literatures on heavy-haul train control considers the train as a single body mass, such as the optimal control study by Howlett (1996). The main reason behind such approximation is that nearly all existing freight trains only have one control setting for traction and braking for the whole train, *i.e.*, all the locomotive have the same traction power level and all the wagons have the same brake level. The other reason is that in-train force is not an issue in short trains. With the new ECP train, this approach is no longer sufficient.

Another approach to train dynamics modelling is the full analysis of all forces experienced by a car. These forces include lateral, vertical, longitudinal movements and pitch, roll and yaw rotations, as well as the movements of the wheels. The resulting model of this analysis is a differential equation of very high order. In the case of the train, such tradeoffs become more evident. In Garg and Dukkipati (1984), one wagon has shown up to 27 degrees of freedom. Clearly to consider all these variables for a 200 wagon train in modelling is impractical and a full model of this model is unnecessary in this study, as most of these factors affect the other motions such as vertical movement along the track.

In this study, the focus is on the longitudinal motion of the train. The main factors that affect the longitudinal motion of a wagon are in-train force, resistance forces and traction or braking forces.

For this study, each car is considered as an individual mass connected by elastic couplers. This allows individual states of the cars to be analysed, which is required for in-train forces calculations. Simplified versions of the model were used in the passenger train study of Yang and Sun (2001) and Gruber and Bayoumi (1982).

## 4.1 Coupler System

The cars are connected either via knuckle-like couplers or solid draw bars. These end-of-car links are connected to the draft gears, which then connect to the undercarriage of the cars. As the draft gear experiences compression forces from the couplers, its overall length changes up to the maximum displacement. Draft gears consist of rigid supporting frames as well as cushioning devices that provide damping. Once the draft gear travel reaches the maximum, the draft gear becomes solid and the impact forces are directly transmitted to the car body.

For example, the structure and the mechanism of the coupler used in the Spoornet Coallink wagons is shown in Fig 4.1. Each coupler has free plates that can move one or two centimetres before it starts to pull or push the linkage.

The draft gear, together with the coupler or draw gear, forms the coupler system, shown in Fig. 4.2. Slacks in the knuckle-like couplers result in dead band in the force displacement response. Below the maximum displacement the draft gear behaves elastic-like. The force displacement response of the coupler system is shown in Fig. 4.3.

To simplify the calculations of over hundreds of coupler system found in a heavy-haul train, the coupler system is taken as a spring force with damping, as suggested by Garg and Dukkipati (1984),

$$F_c = k_i(x_i - x_{i+1}) + d_i(\dot{x}_i - \dot{x}_{i+1}),$$

where $k_i$ is the spring constant, the gradient of the curve in Fig. 4.3, $x_i, x_{i+1}$ and $\dot{x}_i, \dot{x}_{i+1}$ are the displacements and velocities of the $i^{th}$ and $(i+1)^{th}$ wagons

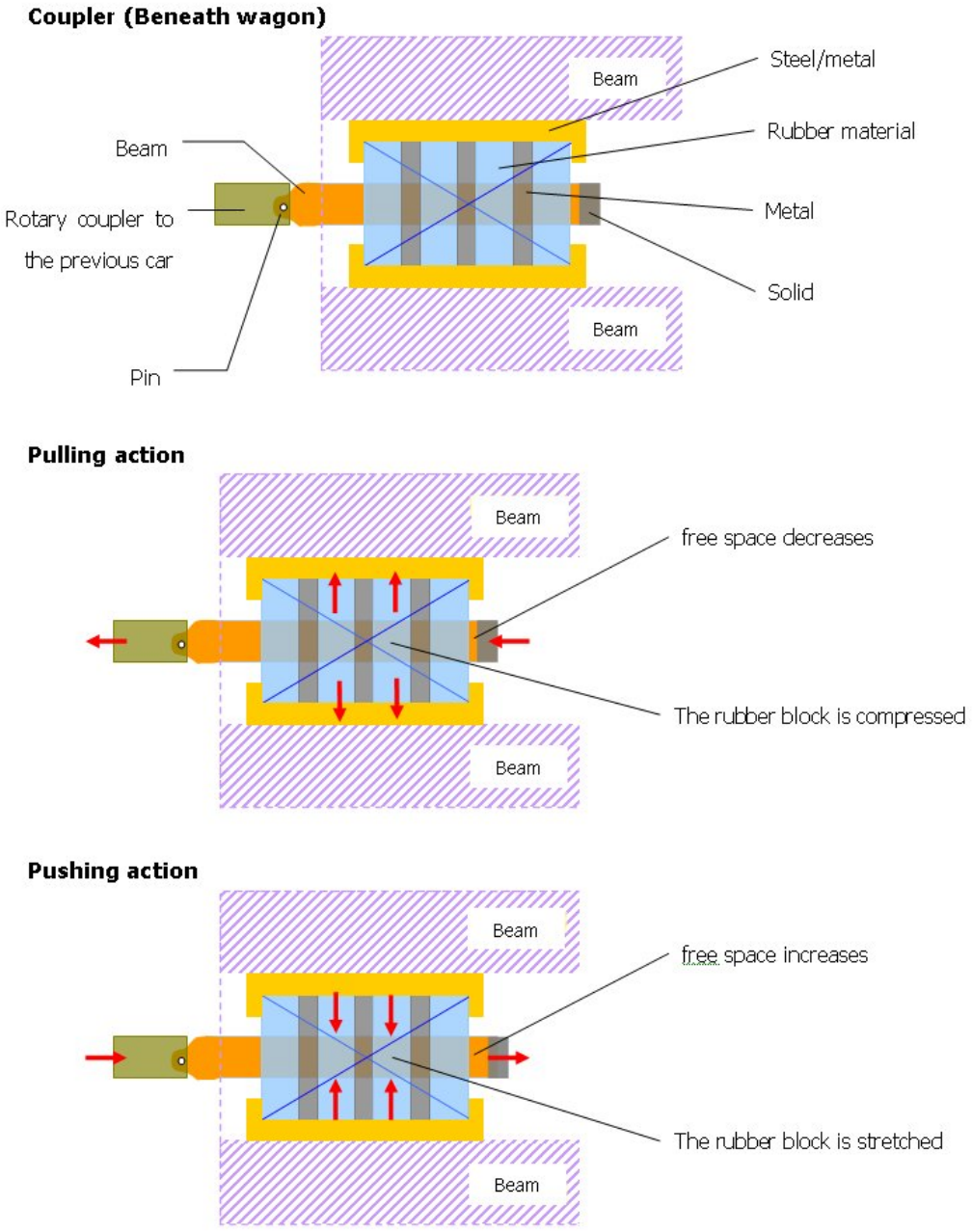


Figure 4.1: F-type coupler used to link wagons in excess of 100 tones used in Coallink trains.

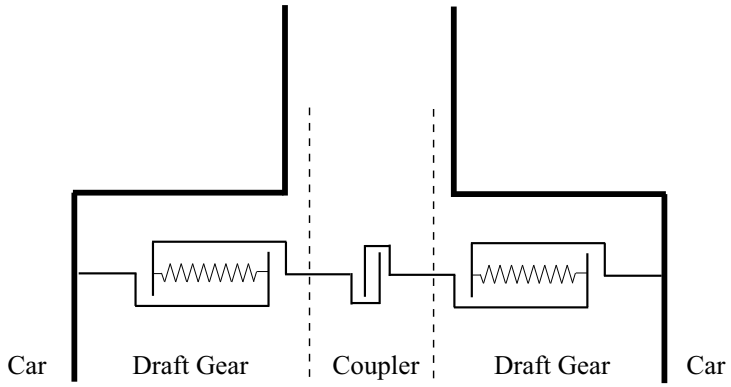


Figure 4.2: Simplified schematic representation of the coupler system setup.

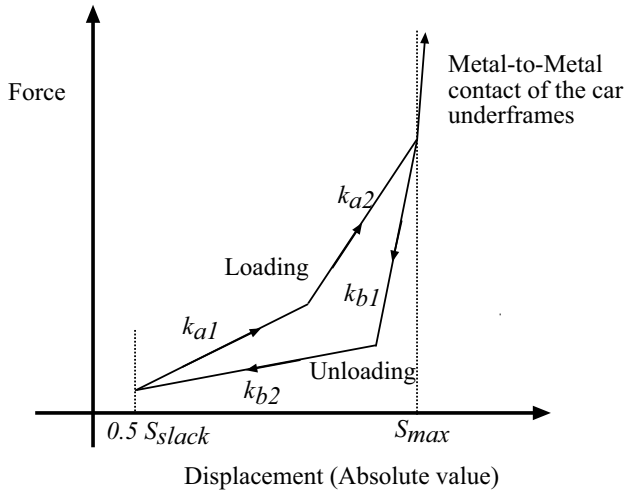


Figure 4.3: Force displacement characteristic of the coupler system.

respectively. Damping constant $d_i$ is taken as $1 \times 10^{-2} k_i$ since actual data are not available. Data from other studies (Gruber and Bayoumi, 1982) shows that damping constants could be as high as $\frac{1}{34}$ of the spring constant. By taking smaller damping constants, which results in more oscillations and slower decay rate, the worst case analysis approach is used.

The spring force approximation holds well when draft gear travel is less than the maximum. Once it reaches the maximum, the coupler force becomes internal forces, which results in a non-linear system.

In this study, this non-linearity is approximated closely by using a linear system together with dynamic spring constants and hard displacement limiters which add non-linear behaviours to the system. For displacements below the maximum travel but greater than half coupler slack $s_{slack}$, a single spring constant is used to calculate the coupler force, shown in Fig. 4.4 . This constant $k_1$ is chosen to be larger than the actual constants $k_{ai}, k_{bi}, i = 1, 2$ in Fig. 4.3. In this estimation, any slight changes in the displacement will result in a greater disturbance in the coupler force, stronger oscillations and thus the worst case study.

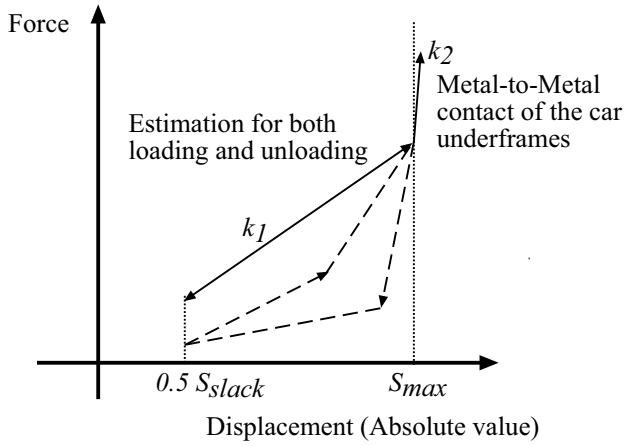


Figure 4.4: Worst case estimation of the force displacement characteristic of the coupler system

The coupler force is now given as:

$$F_c(x_i, x_{i+1}, \dot{x}_i, \dot{x}_{i+1}) = \begin{cases} k_{1i}(x_i - x_{i+1}) + d_i(\dot{x}_i - \dot{x}_{i+1}), & if |x_i - x_{i+1}| \geq \frac{1}{2} s_{slack}, \\ 0, & if |x_i - x_{i+1}| < \frac{1}{2} s_{slack}, \\ k_{2i}(x_i - x_{i+1}) + d_i(\dot{x}_i - \dot{x}_{i+1}), & if |x_i - x_{i+1}| \geq \frac{1}{2} s_{max}, \end{cases} \tag{4.1}$$

where $k_{1i}$ is the worst case spring coefficient and $S_{max}$ is the maximum static travel for the coupler system. $k_{2i}(x_i - x_{i+1})$ is an estimate for internal forces for test purposes. In reality couplers will be damaged once the maximum travel has been reached for a prolong period of time.

## 4.2 Force Model

Force model is used in the controller design and simulation. Each car is considered individually and is interconnected with spring-like couplers. Taking into consideration of the rake configurations whereby four wagons are coupled via rigid bars, in this study, these rakes are considered as a single entity with four times the mass and length of a single wagon. This is similar to the increased mass model (Gruber and Bayoumi, 1982) although in this case the grouping is done so to better describe the actual wagon grouping in real-life.

The two major resistances experienced by a train are rolling resistance and aerodynamic drag. While the former is experienced by each car, the aerodynamic drag is only considered for the first car, often a locomotive. The general resistance is given as

$$R = \underbrace{c_0 + c_v v}_{R^r} + \underbrace{c_a v^2}_{R^a},$$

where $v$ is the velocity of the car, $R^r$ is the rolling resistance, $R^a$ is the aerodynamic drag and the coefficients $c_0, c_v, c_a$ are obtained experimentally.

Aerodynamic drag only becomes dominant during high speed operation, thus at the low speed that heavy-haul trains operate in, rolling resistance is the more significant factor. Many previous studies simply ignore aerodynamic drag for this reason (Astolfi and Menini, 2002).

The model is given in Fig. 4.5.

In Fig. 4.5 $n$ is the number of units, *i.e.*, rakes and locomotives. The equations of motion of the train are

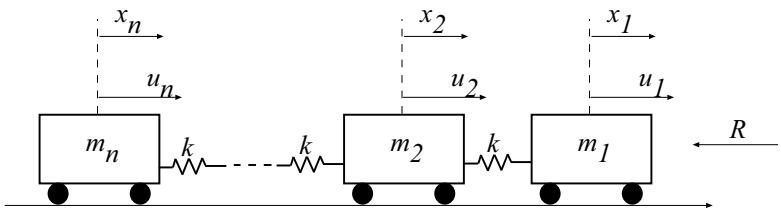


Figure 4.5: Force diagram of the train.

$$
\begin{aligned}
m_1\ddot{x}_1 &= u_1 - k_1(x_1 - x_2) - d_1(\dot{x}_1 - \dot{x}_2) - \underbrace{(c_0 + c_v\dot{x}_1)m_1}_{R^r} \\
&\quad \underbrace{- c_a\dot{x}_1^2(\sum_{i=1}^{n} m_i)}_{R^a} - 9.98\sin\theta_1 m_1 - 0.004D_1 m_1, \\
m_i\ddot{x}_i &= u_i - k_i(x_i - x_{i+1}) - k_{i-1}(x_i - x_{i-1}) \\
&\quad + d_{i-1}(\dot{x}_{i-1} - \dot{x}_i) - d_i(\dot{x}_i - \dot{x}_{i+1}) \\
&\quad - (c_0 + c_v\dot{x}_i)m_i - 9.98\sin\theta_i m_i - 0.004D_i m_i, \quad i = 2, \ldots, n-1, \\
m_n\ddot{x}_n &= u_n - k_{n-1}(x_n - x_{n-1}) - d_{n-1}(\dot{x}_n - \dot{x}_{n-1}) - (c_0 + c_v\dot{x}_n)m_n \\
&\quad - 9.98\sin\theta_n m_n - 0.004D_n m_n, \qquad (4.2)
\end{aligned}
$$

where

- $\dot{x}_i$ and $x_i$ are the velocity and the displacement of the car with respect to a static frame on the ground;
- $k_i$ and $d_i$ are the spring and damping constants of the coupler system;
- $m_i$ and $u_i$ are the mass and traction force of the $i^{th}$ unit (locomotive or rake) respectively;
- $R^a$ and $R^r$ are the aerodynamic and rolling resistances respectively;
- $\theta_i$ is the slope angle while degree of curvature is calculated as $D_i = 0.5d_{wheelbase}/R$ (Garg and Dukkipati (1984)), $R$ is the curve radius, as shown in Fig. 4.6;

- the gravitational and curvature resistance forces experienced by the car are $9.98m_i \sin(\theta_i)$ and $0.004m_i D_i$ respectively (Garg and Dukkipati (1984)).

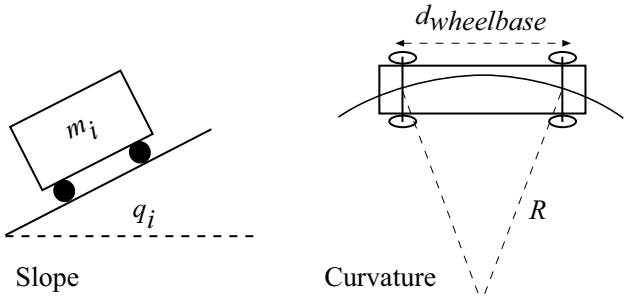


Figure 4.6: Slope and curve angles.

The model in (4.2) is used for controller design, actual simulated model imposes additional non-linearities:

- Inputs $u_i \leq 0$ if the $i^{th}$ unit is a rake. This is due to the fact that although the wagons are not powered in a heavy-haul train, they are still able to exert a braking force.
- Input constraints such as power limitation and slew rate is applied. The details are described in section 4.3.
- The model ignores dead band in the coupler slack. In the actual model, this non-linearity is taken into account by calculating coupler forces by using (4.1).

Note for this study, all states are assumed to be available, either through an observer or an online train simulator such as the LEADER package by New York Air Brake (NYAB, 2003).

## 4.3 Control Constraints

In control system, a fast actuator helps to improve system response time. However, in real life, instantaneous control is not possible. In the case of

the Coallink train, the limitations are the traction and brake system of the locomotive and the ECP brake system.

Both traction and dynamic brake efforts, or regenerative brake, of the locomotive are governed by the current velocity and the current gear setting, or notch. The traction and dynamic effort versus velocity graph for the 7E1 locomotive used in the Coallink train are shown in figures 4.7 and 4.8.

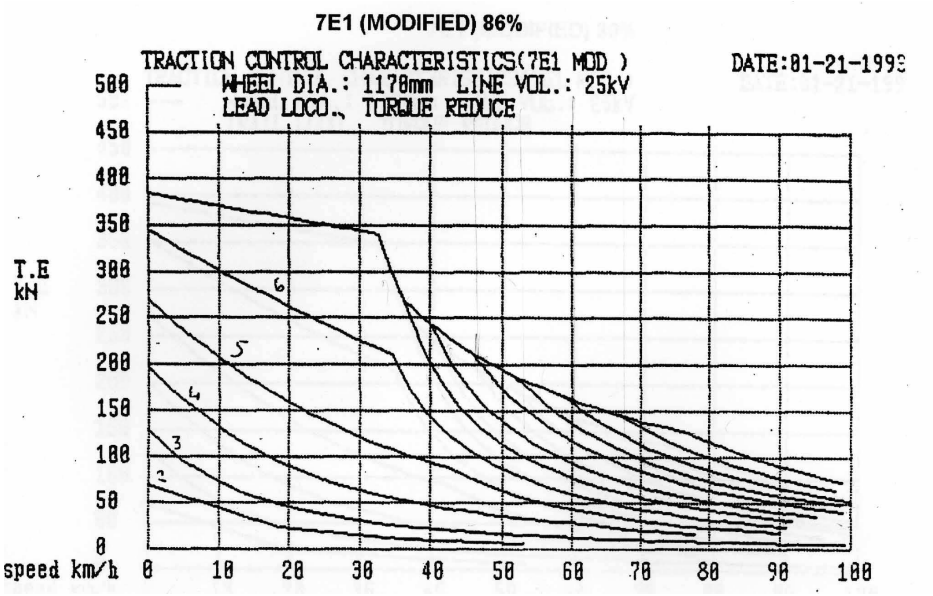


Figure 4.7: Traction effort versus velocity graph for 7E1 AC locomotive (Spoornet, 2002).

In practice, any notch changes requires up to 10 seconds delay for the field change in the AC motor. Going from traction to regenerative braking and vice versa will result in even greater delays due to the reversal of field. The reason for this is that the same sets of motors are used for both traction and regenerative braking. Any sudden change in notch settings is undesirable as this introduces abrupt increase in traction or braking forces, which results in large spikes in in-train forces. Without closed-loop control, such spike will travel down the train, resulting in further damage to the coupler system.

In the model, notch inputs are used for locomotives, which are then translated into force via a lookup table, shown in Fig. 4.9. 10 sec delay is imposed for any notch changes of the same type, while changing from traction to braking requires 20 sec delay.

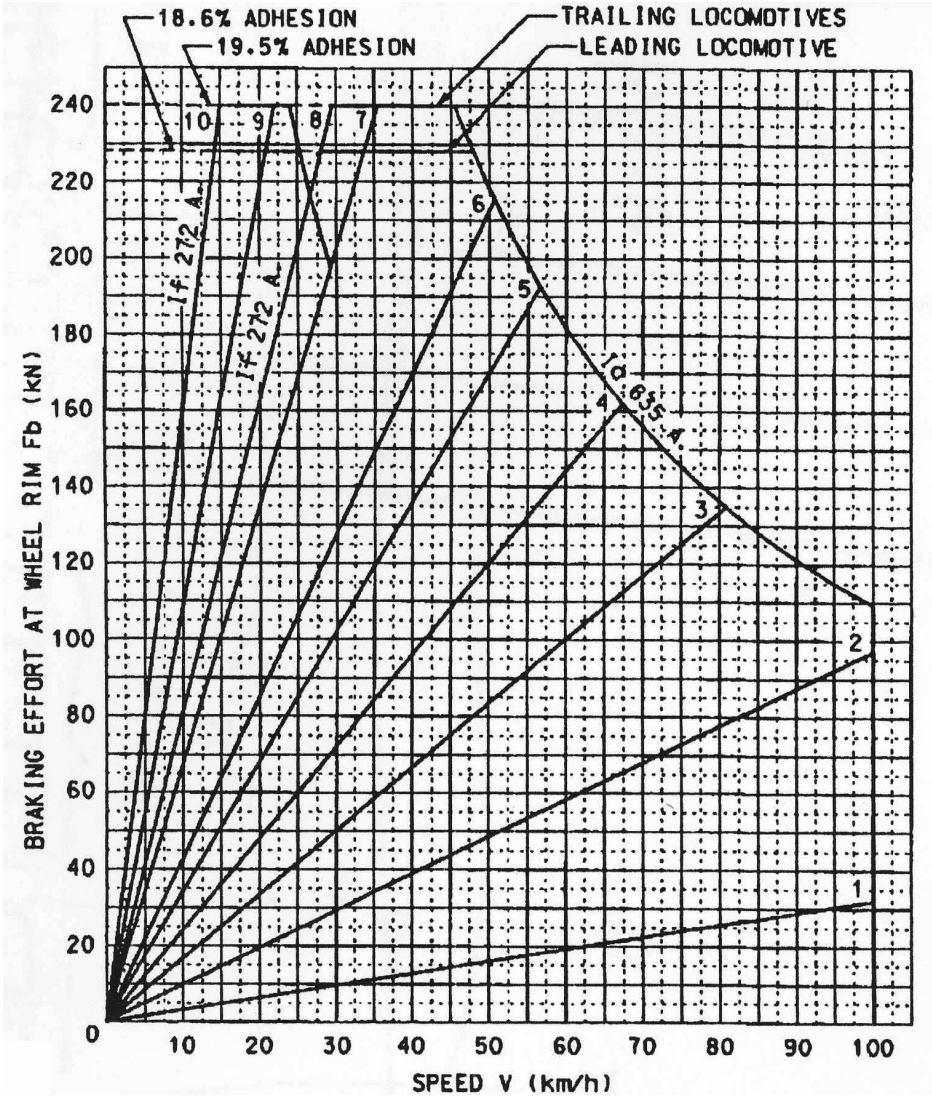


Figure 4.8: Dynamic brake effort versus velocity graph for 7E1 AC locomotive (Spoornet, 2002).

For wagons, brake force is not dependent on the current velocity, thus a magnitude and a rate of change limit are imposed. For ECP system, the build-up time for pressures is around 10 sec. In comparison, the pneumatic system can take up to 175 sec. During the delay period for both the locomotive and the wagon inputs, the current force is gradually build up to the new force, *i.e.*,

$$F_d(t) = U_0 + \frac{(U_n - U_0)}{t_d} t, \quad t \in [0, t_d]$$

where $F_d$ is the traction/brake force during the delay period, $U_0$ and $U_d$ are the original and new input force, and $t_d$ is the delay period.

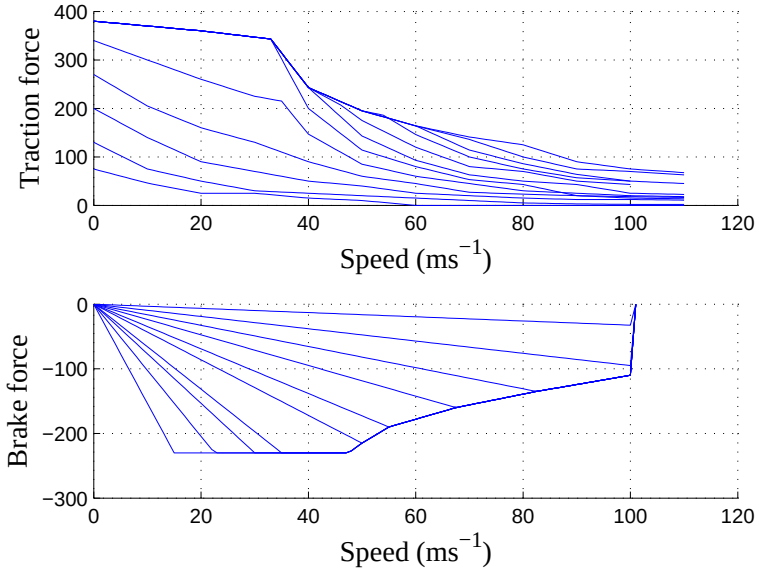


Figure 4.9: Lookup table for traction and brake force for 7E1 AC locomotive.

The magnitude and the rate of change for wagon brake forces are hard-limited in the model. All locomotive traction and brake outputs are obtained via lookup tables. The results are very close to the actual locomotive nonlinear behaviours.

# Chapter 5

# Model Validation

From an analytic point of view, the non-linear model described in Section 4.2 seems to represent the dynamics of a train sufficiently. However, the question remains whether it will be able to act as a train simulator for the Coallink train.

The train model requires a list of parameters of the train, of which some are not available while others are only estimates of the varying value in real life. The initial conditions also affect train behaviour under the same inputs.

To further increase the difficulty, only partial electronically recorded input/output data sets are available. Although the output velocity and in-train forces were recorded electronically, the corresponding inputs data were handwritten. The accuracy of these inputs data are affected by the human factor.

Thus to validates the model, a good set of input/output data need to be compiled. The following sections describe the procedures that were used to combine four different sets of data into one correlated data set that in the end helped to validates the model.

## 5.1 Parameters

The parameters used in the simulation are given in table 5.1. The values are based on the Coallink trains operating in South Africa by Spoornet.

| Parameter | Value | Unit |
|---|---|---|
| No. of wagons | 200 | |
| No. of locos | 6 | |
| | *Locomotive* | |
| mass (7E1) | 126000 | $kg$ |
| $c_0$ | $7.6658 \times 10^{-3}$ | $Nkg^{-1}$ |
| $c_v$ | $1.08 \times 10^{-4}$ | $Ns(mkg)^{-1}$ |
| $c_a$ | $2.06 \times 10{-}5$ | $Ns^2(m^2kg)^{-1}$ |
| $k$ | $78 \sim 121 \times 10^6$ | $Nm^{-1}$ |
| Length | 20.47 | $m$ |
| Max coupler slack | $39.87 \times 10^{-3}$ | $m$ |
| Max traction | 380 | $kN$ |
| Max brake | 230 | $kN$ |
| | *Wagon* | |
| Loaded mass | 104250 | $kg$ |
| $c_0$ | $6.3625 \times 10^{-3}$ | $Nkg^{-1}$ |
| $c_v$ | $1.08 \times 10^{-4}$ | $Ns(mkg)^{-1}$ |
| $c_a$ | $1.4918 \times 10{-}5$ | $Ns^2(m^2kg)^{-1}$ |
| $k$ | $29.29 \sim 49 \times 10^6$ | $Nm^{-1}$ |
| Length | 12.07 | $m$ |
| Max coupler slack | $77.5 \times 10^{-3}$ | $m$ |
| Max brake | 100 | $kN$ |
| wheelbase dist. | 8.310 | $m$ |
| | *Track* | |
| Slope $\theta$ | $-0.015 \sim 0.015$ | $rad$ |
| Min curve radius | 300 | $m$ |

Table 5.1: Heavy-haul train parameters.

The connector behaviour is influenced mostly by the spring coefficient $k$: a large spring coefficient results in a more rigid behaviour while a smaller spring coefficient causes more severe oscillation, although larger spring coefficient results in larger in-train forces. In this study, this value varies proportionally to the displacement difference between adjacent cars, as shown in Fig. 4.4.

## 5.2 Available Data

With the roll out of ECP and DP equipped trains, Spoornet initialised trial runs to test the various aspect of the upgrade. In particular, three ECP trial runs took place on the $11^{th}$, $18^{th}$, and $24^{th}$ November 2003. The train configuration from front to the rear of the train is as follows:

**Week 3** : 20842 tons, 3 locos - 100 wagons - 3 locos - 100 wagons

**Week 4** : 20974 tons, 4 locos - 200 wagons - 2 locos

**Week 5** : 20846 tons, 6 locos - 200 wagons

where the first column are the overall train mass, locos stand for locomotives, in this case 7E1 AC locomotives, and the wagons all ECP-equipped. The wagons were grouped in number of four into a rake.

Data from these trail runs were used for internal Spoornet evaluation on the performance of the different train configurations. All three runs were operated by human drivers. Three test coaches were connected between the first locomotive group and the wagons. The test coaches carried equipments for the data measurements and rest area for personnel.

Train parameters are gathered as much as possible from the various data sheets and experiment obtained values that Spoornet engineers provided. While most of the data are available, some of the parameters were simply unavailable.

For some of these parameters, the worst case estimation are made, *e.g.*, coupler damping coefficients. Other parameters like the efficiency rate of the wagon brake were different from trial run to trial run. In this case, the

| Kilometre point | Longitude | Latitude | Altitude |
|---|---|---|---|
| 0.178 | -26.572 | 30.021 | 5586.014 |
| 0.176 | -26.572 | 30.021 | 5585.942 |
| 0.174 | -26.572 | 30.021 | 5585.871 |
| 0.172 | -26.572 | 30.021 | 5585.799 |
| 0.170 | -26.572 | 30.021 | 5585.734 |
| 0.168 | -26.572 | 30.021 | 5585.689 |
| 0.166 | -26.572 | 30.021 | 5585.654 |
| 0.164 | -26.572 | 30.021 | 5585.619 |

Table 5.2: Sample of the GPS data for Coallink line.

value was adjusted by trial-and-error until the simulation results match the recorded values.

Once the train parameters have been identified, the next stage is to validate the model with input/output data.

Four different data sets were received from Spoornet:

- GPS data of the track,
- GIS data of the track,
- handwritten input data for the three trial runs, and
- electronically recorded output data for the three trial runs.

### 5.2.1 GPS Data

GPS data contain the GPS data from an onboard GPS receiver and altitude values measured from a barometer with respect to kilometre points along the track. The data were gathered on another independent trial run beyond the three trial runs. A sample of the data is given in Table 5.2. The latitude and longitude data are given in degrees. The altitude values were labelled in metres while in fact it was in feet. Another interesting note is that the data was given in reverse order, from Richard's Bay to Ermelo. In comparison, all the other data started at Ermelo.

Plotting the data reveals that the barometer often missed data points, with the altitude remaining the same for few metres and then suddenly dropping hundred metres within the next metre or two.

Values in this data are very precise, up to three decimal places. Although the GPS data accuracy is guaranteed by its technology, the accuracy of the altitude value is not consistent and requires validation via other sources.

### 5.2.2 GIS Data

Geographical Information System (GIS) data consist of track curvature, slope as well as other information such as station name and other features like tunnels. A sample of the data are given in Table 5.3, where the types of feature are given as

- 1 = Beginning of slope (distance per metre vertical)
- 2 = Beginning of curve (curve radius given in column 2 in metre)
- 3 = End of curve
- 4 = Beginning of stop test (Initial speed give in column 2 in km/h)
- 5 = End of stop test
- 8 = Name of the location

Note that the GIS data do not give the altitude of the points. Instead the slope grade per metre vertical is given, *e.g.*, the maximum uphill grade is 1/160, *i.e.*, 160 metre for 1 metre climb.

These data are sparse, but correspond very closely to the GPS slope data once the kilometre offset between the two data sets has been compensated for. The track grade values in the GIS data are more accurate than the altitude values in the GPS data in providing track grade ruling information. However, the given grade values were rounded off, thus not as precise as the altitude values.

| Kilometre point | Magnitude of feature | Type of feature |
|---|---|---|
| 84.746 | 1600 | 2 |
| 84.893 | -1917 | 1 |
| 85.15 | KMP 120 | 8 |
| 85.226 | 1600 | 3 |
| 85.45 | Neutral Section | 8 |
| 85.555 | -406 | 1 |
| 85.638 | -1600 | 2 |
| 86.2 | KMP 140 | 8 |
| 86.45 | KMP 162* | 8 |
| 86.64 | 150 | 1 |
| 86.329 | -1600 | 3 |
| 87.15 | KMP 240 | 8 |

Table 5.3: Sample of the GIS data for Coallink line.

GIS data were chosen as the track simulation for two reasons; firstly, its track grade values are more accurate than the GPS altitude values, although not as precise. Since the GPS altitude values were measured onboard a moving train, the barometer values could be affected by atmospherical changes as well train vibration. Since track modulations are slow and gentle, GIS track data provide a low-pass filtered version of the actual track characteristics. Secondly, it is a more complete set of track information, including curvature as well as where stop tests were conducted.

### 5.2.3 Handwritten Inputs Notes

During the trial runs, a railway engineer sits in the first locomotive and record the current traction notches, brake level as well as current speed on a GIS data printout for the track. He notes the current position by reading off the passed-by moss poles, a sample of the recorded values are shown in Table 5.4.

The handwritten notes are imprecise and sparse. Precision is not a problem for the control settings, since it is defined in discrete notches. For kilometre points and current velocity values, the handwritten values raises the question of both precision and accuracy.

The first problem is the accuracy of the instance when the railroad engineer

| Kilometre | moss pole | Traction 1 (notch) | Traction 2 (notch) | Brake | Armature Current | Current Speed |
|---|---|---|---|---|---|---|
| 6 | 1 | 14 | 0 | 0 | 600 | 64 |
| 8 | 1 | 0 | 0 | 0 | 0 | 52 |
| 10 | 1 | STOP | | | | |
| 12 | 1 | -1 | 6 | 0 | 120 | 38 |
| 14 | 5 | -10 | 3 | 0 | 570 | 46 |
| 15 | 12 | -10 | -10 | 0 | 600 | 54 |
| 18 | 5 | 5 | 0 | 0 | 110 | 79 |
| 20 | 8 | 0 | 0 | 0 | 0 | 58 |
| 22 | 1 | -10 | -10 | 0.25 | 600 | 52 |

Table 5.4: Sample of the input data.

notes the current inputs. It is possible that input changes are only noted later. It is also possible that some input changes were not noted at all.

Secondly, the moss poles along the track are not placed at a fixed interval. On average, there are 18 to 24 moss poles per kilometre. Thus, it is impossible to determine the exact location for the input record. Interestingly, the distance between successive kilometre point moss poles are not strictly one kilometre apart, but could increase or decrease to allow joining tracks to meet at the same kilometre points.

During the course of the trip, the train often slows down or even stop due to traffic signals and other reasons, as recorded in the written notes. However, it is unclear when the driver started to respond to the signal.

Another problem is that there are no control records as how the driver stops and starts off the train again. Driver often speed up the train using different combination of traction notch settings depending on the current track condition. Thus, it is difficult to reproduce the train behaviour before and after these stops.

From simulation, it can be observed that input offsets affect the results greatly; even an offset of 100 metres can result in substantially different outputs.

| Date | Time | Distance (km) | Speed (km/h) | CouplerA Load (kN) |
|---|---|---|---|---|
| 2003/11/24 | 17:0:37.14 | 26.777054E-3 | 0.000 | 268.945312 |
| 2003/11/24 | 17:0:38.13 | 26.777054E-3 | 0.000 | 268.872070 |
| 2003/11/24 | 17:0:39.12 | 26.777054E-3 | 0.000 | 268.395996 |
| 2003/11/24 | 17:0:40.11 | 26.777054E-3 | 0.000 | 268.615723 |
| 2003/11/24 | 17:0:41.15 | 26.777054E-3 | 0.000 | 268.249512 |
| 2003/11/24 | 17:0:42.14 | 26.777054E-3 | 0.000 | 268.615723 |
| 2003/11/24 | 17:0:43.13 | 26.777054E-3 | 0.000 | 268.579102 |
| 2003/11/24 | 17:0:44.17 | 26.777054E-3 | 0.000 | 267.553711 |
| 2003/11/24 | 17:0:45.11 | 26.777054E-3 | 0.000 | 267.077637 |
| Date | Time | Brake Pipe (kPa) | Brake Cylinder (kPa) | Wagon1Bar (kN) |
| 2003/11/24 | 17:0:37.14 | 536.000977 | 0.029297 | 323.876953 |
| 2003/11/24 | 17:0:38.13 | 535.986328 | 0.073242 | 324.267578 |
| 2003/11/24 | 17:0:39.12 | 536.147461 | 0.058594 | 323.144531 |
| 2003/11/24 | 17:0:40.11 | 536.030273 | -0.102539 | 323.828125 |
| 2003/11/24 | 17:0:41.15 | 536.162109 | 0.190430 | 323.388672 |
| 2003/11/24 | 17:0:42.14 | 536.088867 | 0.000000 | 323.242187 |
| 2003/11/24 | 17:0:43.13 | 536.250000 | -0.073242 | 322.998047 |
| 2003/11/24 | 17:0:44.17 | 536.030273 | 0.102539 | 318.701172 |
| 2003/11/24 | 17:0:45.11 | 536.220703 | -0.029297 | 317.968750 |

Table 5.5: Sample of the output data for Coallink line during trial runs.

### 5.2.4 Electronically Recorded Output Data

During trial runs, test coaches with measurement instruments were connected at the front of the train. Velocity of the train was electronically measured as well as in-train force(s) at coupler(s). Certain trial runs recorded only one in-train force, while others recorded two. A sample of the data are given in Table 5.5.

## 5.3 Methodology

The first challenge for model validation is the offset compensation of the handwritten inputs notes to the electronically recorded output data to gen-

erate a complete input/output data. It is assumed there is no offset between the GIS data and the input data set, since the later was written on a printout of the former.

### 5.3.1 Offset between Input and Output Data

The input data and the output data have one common set of values, *i.e.*, the velocity of the train. Both sets were plotted against kilometre points, so that the offset could be viewed graphically. Interestingly, all three trial run data sets showed the same offset of 2.9 km between their hand written input note and electronically recorded data.

In Fig. 5.1, data from handwritten input notes are plotted on the top figures, while the measured output data are plotted on the lower two. The middle velocity graph acts as a offset indicator for the two sets of data. Week 4 data were used, shown in Table 5.6.

### 5.3.2 Offset within Input Data

However, sometimes there are offsets within the input data set itself. Because of the moss pole impreciseness and human factor, the control inputs could be misaligned as well.

While velocity pattern changes drastically, the in-train force pattern is less affected by the offset error in the track condition. Rather, it follows the input patterns closely. Thus by comparing the in-train force pattern of the simulated and recorded set graphically, the input offset could be determined.

In Fig. 5.2, a sample in-train force data from week 3 and week 4 are plotted against the corresponding input data, with week 3 data shown in Table 5.7. From the top figure in Fig. 5.2, it is clear that while in-train force from week 3 correlated very well with its input, week 4 data had a distinct offset in between them.

Simulations are performed on a section of track where the initial conditions are relatively stable, with no input offset adjustment. The simulated output velocity and in-train force are then compared to the recorded set graphically.

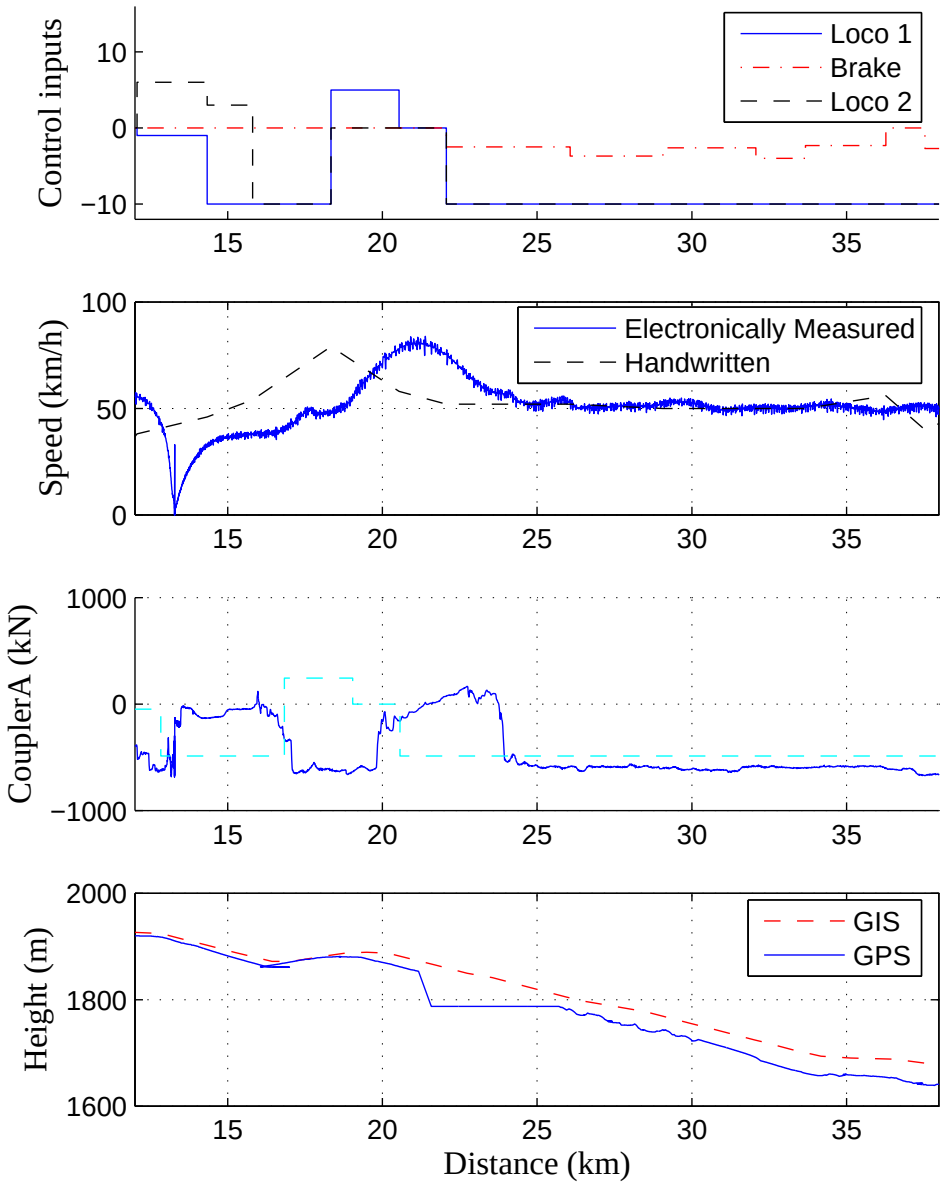


Figure 5.1: Input/Output data without offset compensation.

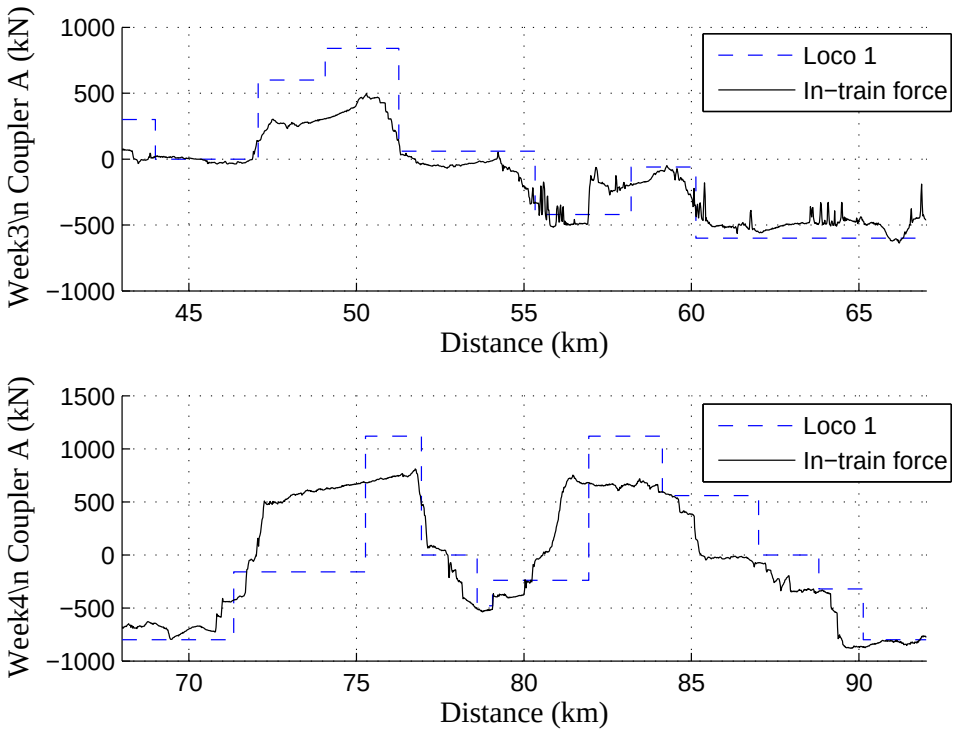


Figure 5.2: Week 3 and Week 4 in-train forces and control inputs.

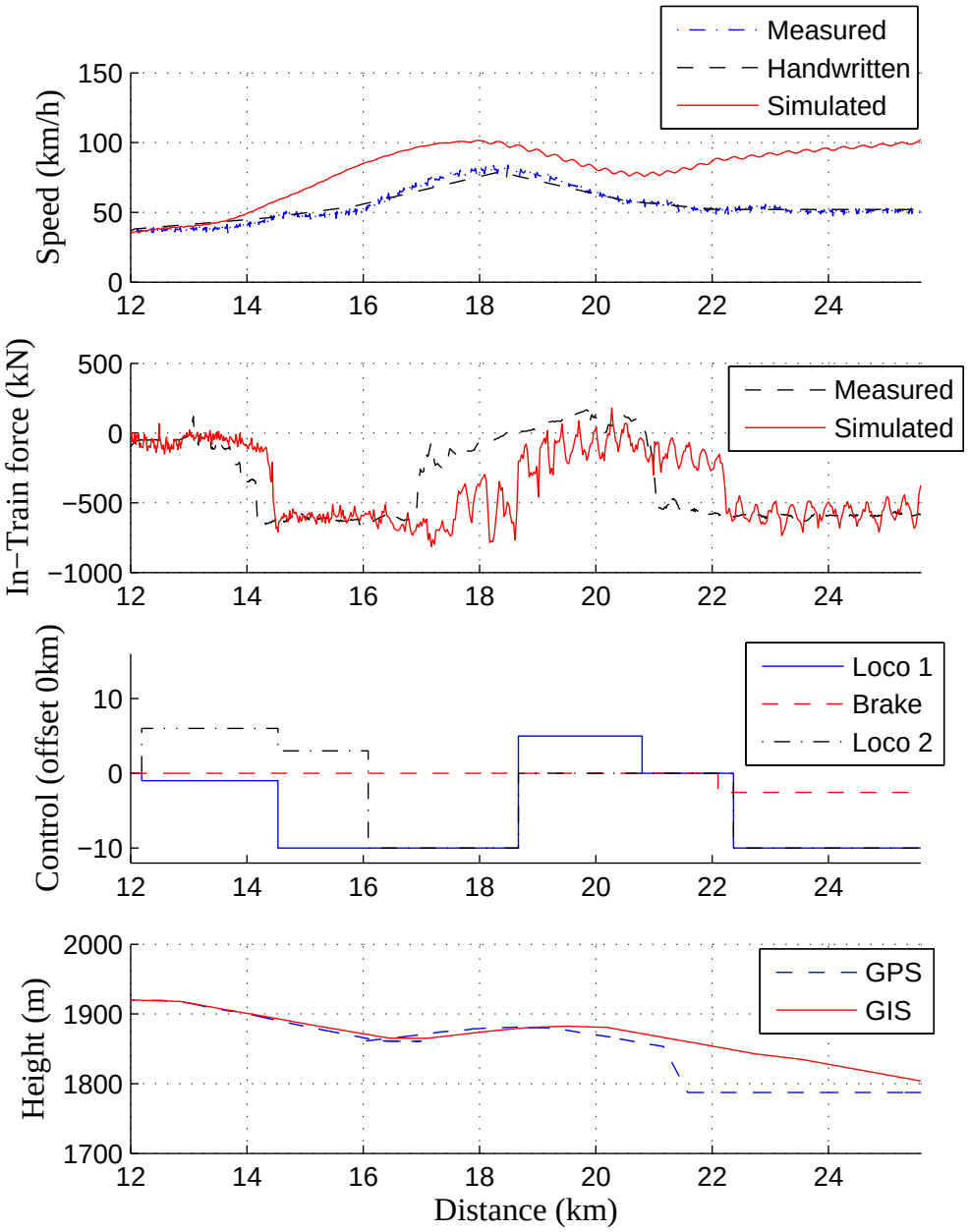


Figure 5.3: Simulated result with no input offset compensation.

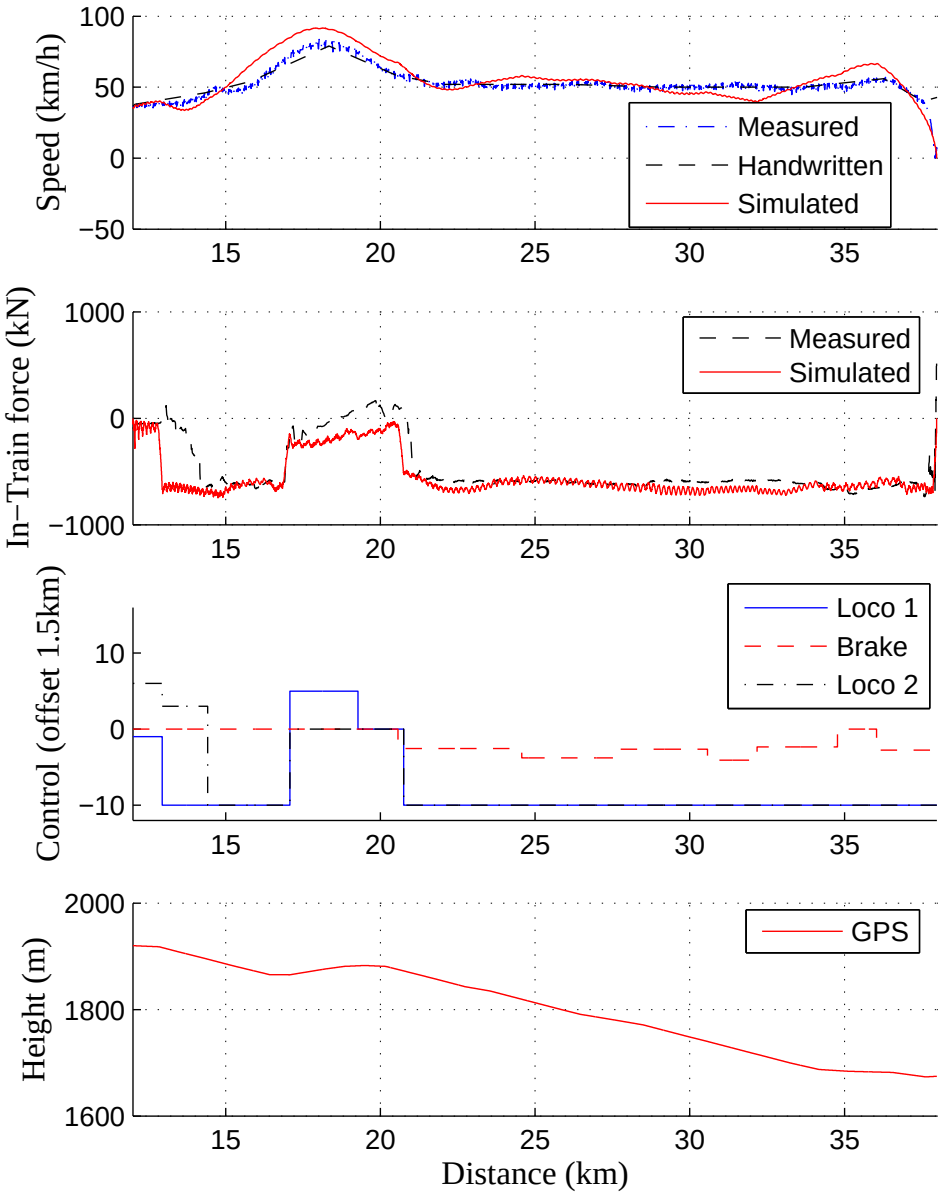


Figure 5.4: Input offset compensated simulated result.

In Fig. 5.3, the week 4 trial run simulation assumed no input offset. From the graph, it is clear that the two velocities do not match up. Although the in-train force shows very similar patterns, a clear offset is present.

In Fig. 5.4, the input offset was compensated. From the graph, it is clear now that both velocity and in-train outputs match closely. The slight discrepancy in the velocity output is the result from parameter inaccuracies as well as the sparse GIS data. .

## 5.4 Results

In the following results, parameters from Table 5.1 are used. Some of the parameters are modified according to the actual conditions provided.

### 5.4.1 Sampling Time

Once the different data sets have been aligned, the first test is to see the effect of the sampling time has on the simulation output.

The use of fine simulation time poses the question of practicality. Since train dynamics are not fast, nor are the external disturbances such as track modulation, finer simulation time does not guarantee more accurate results.

From experiment, it is clear that simulation time is approximately inversely proportional to sampling time. By increasing the sampling time by factor of ten, a hour of simulation time could be reduce to less than ten minutes. It will be interesting to see if the results would remain consistent. Week 4 data were chosen for this experiment.

From Fig. 5.5 to Fig. 5.8, it is clear that as sampling time increases, in-train forces exhibit more jittering. Velocity performance seems to be independent of sampling time. From the results, sampling time of 0.5 second gives the best trade-off between accurate results and simulation time.

Note that during the trial run, one of the front locomotives was faulty. This was specified in the simulation setup. From the results, it can be seen that

| | | |
|---|---|---|
| Week | 4 | |
| Simulation time | 2000 | sec |
| Sampling time | 0.1-10 | sec |
| | | |
| Faulty locomotive | 4 | |
| Wagon mass | 101 090 | kg |
| Input offset | -1.5 | km |
| Initial position | 12 | km |
| Initial velocity | 10 | $ms^{-1}$ |
| Initial altitude | 1920 | m |

Table 5.6: Modified parameters for simulation for week 4.

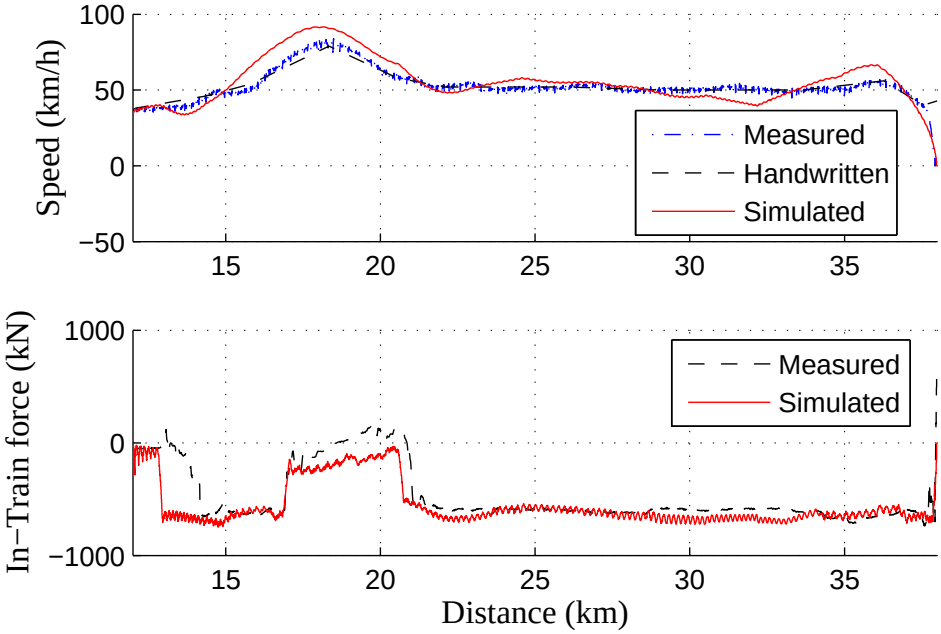


Figure 5.5: Week 4 with 0.1 seconds sampling time.

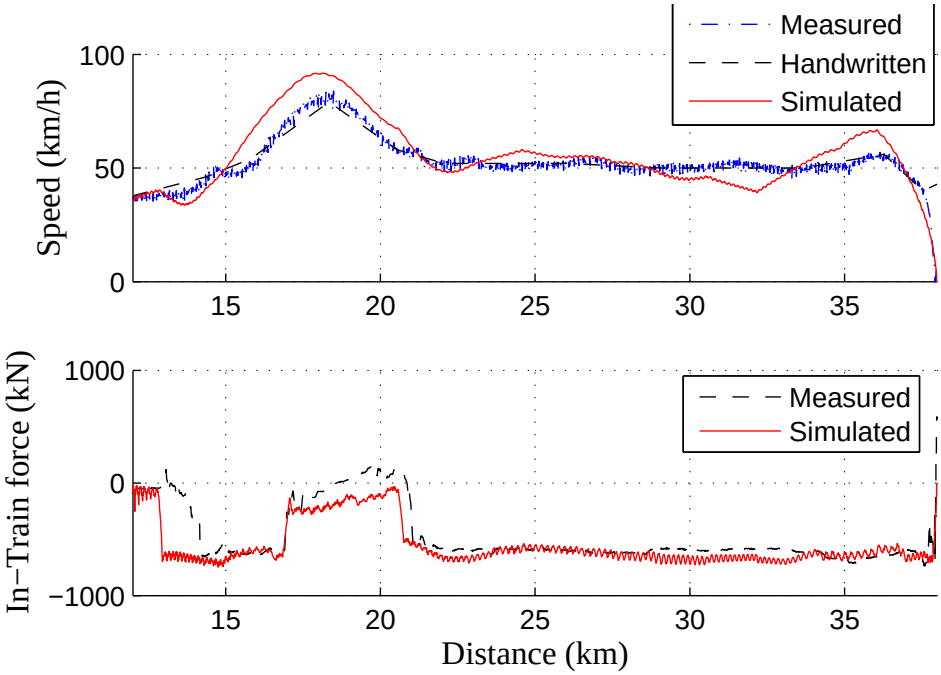


Figure 5.6: Week 4 with 0.5 seconds sampling time.

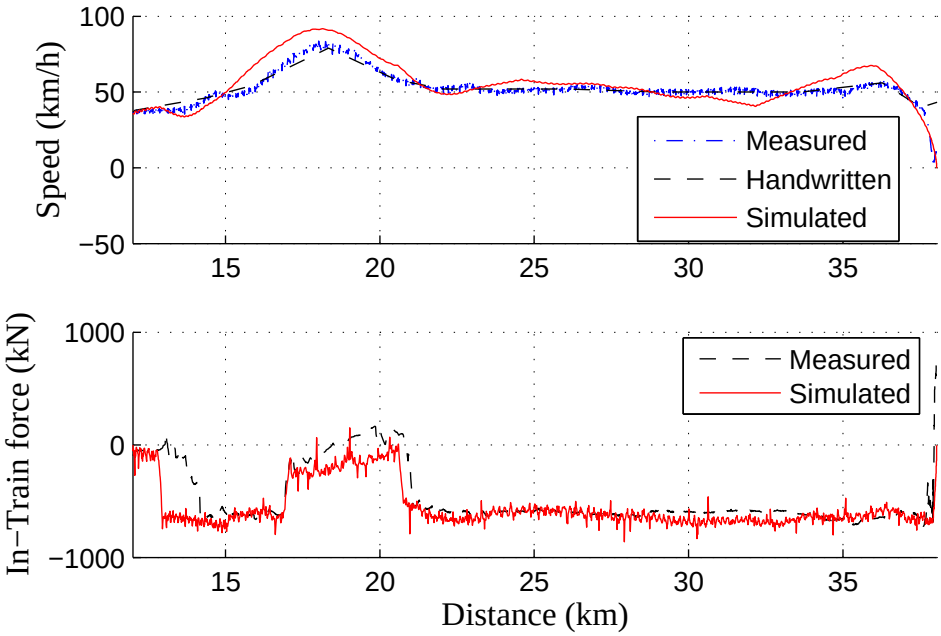


Figure 5.7: Week 4 with 1 second sampling time.

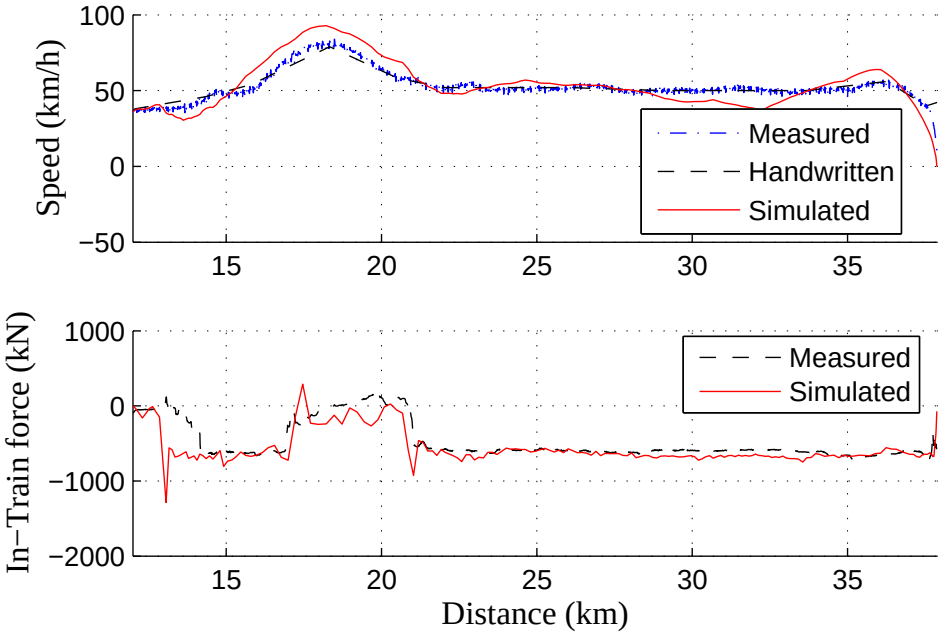


Figure 5.8: Week 4 with 10 seconds sampling time.

the model is able to simulate such changes accurately.

### 5.4.2 Slack Simulation

In section 4.1 coupler slack was discussed. However, it is also one of the parameters that is not available. It will be interesting to investigate whether dead band modelling in the coupler model would have a profound effect on the results.

A section of the track with constant inputs is chosen from week 3. This allows a direct comparison on the effect track modulation has on deadband. There is only one notch change at the beginning of the section around 141 km with no further notch changes or brakes for the rest of the section.

From Fig. 5.9 and Fig. 5.10 it is clear that deadband modelling results in constant small oscillations. However, the same oscillations only occur at few instances on the recorded data.

| | | |
|---|---|---|
| Week | 3 | |
| Simulation time | 2000 | sec |
| Sampling time | 0.5 | sec |
| | | |
| Wagon mass | 100 685 | kg |
| Input offset | -1.5 | km |
| Initial position | 140 | km |
| Initial velocity | 75 | $ms^{-1}$ |
| Initial altitude | 1134.3 | m |

Table 5.7: Modified parameters for simulation for week 3.

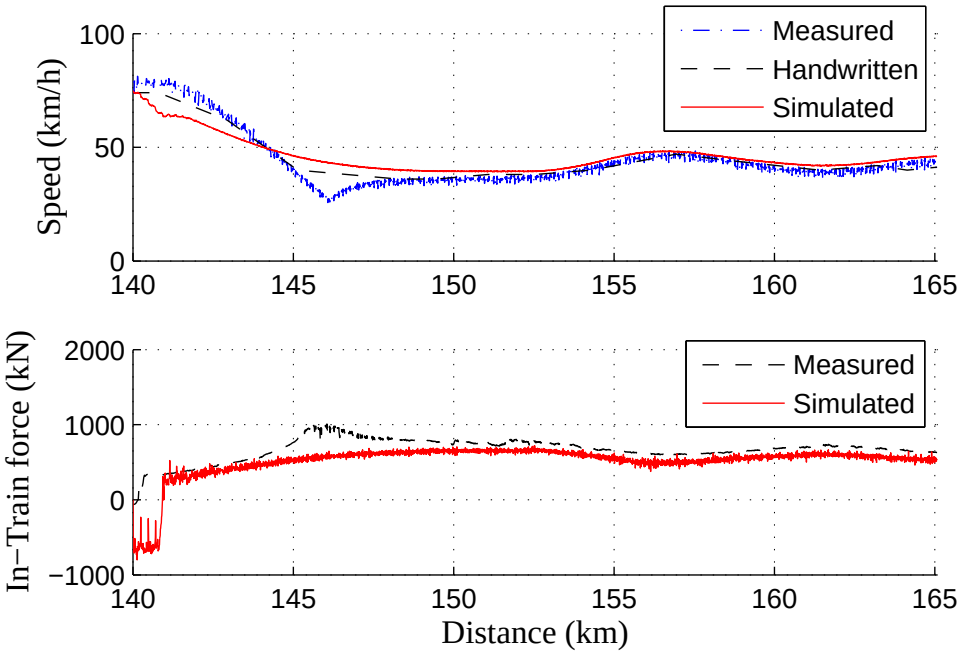


Figure 5.9: Week 3 with coupler slack simulated.

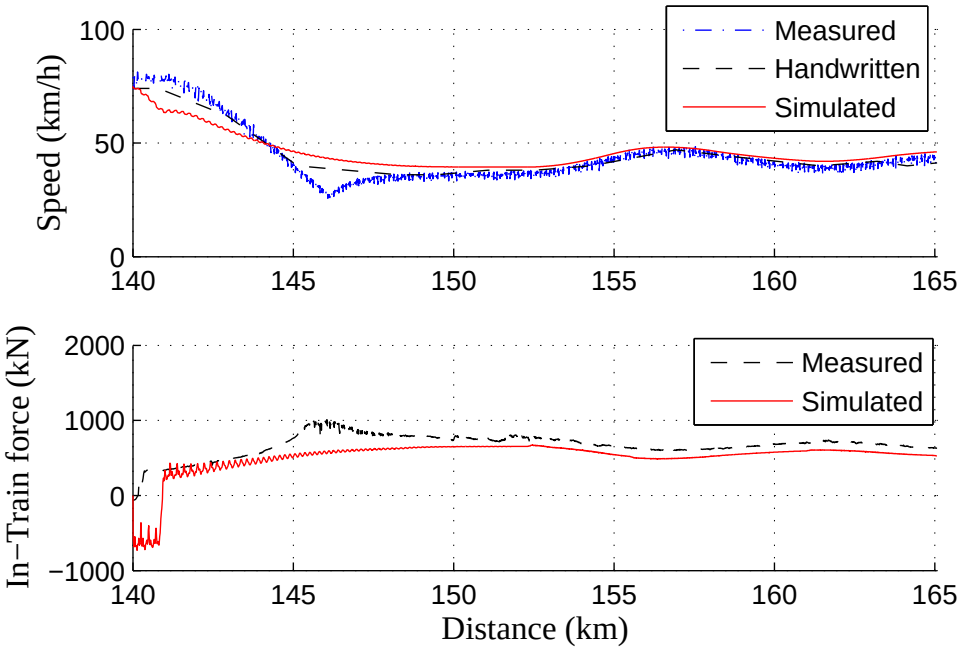


Figure 5.10: Week 3 without coupler slack simulated.

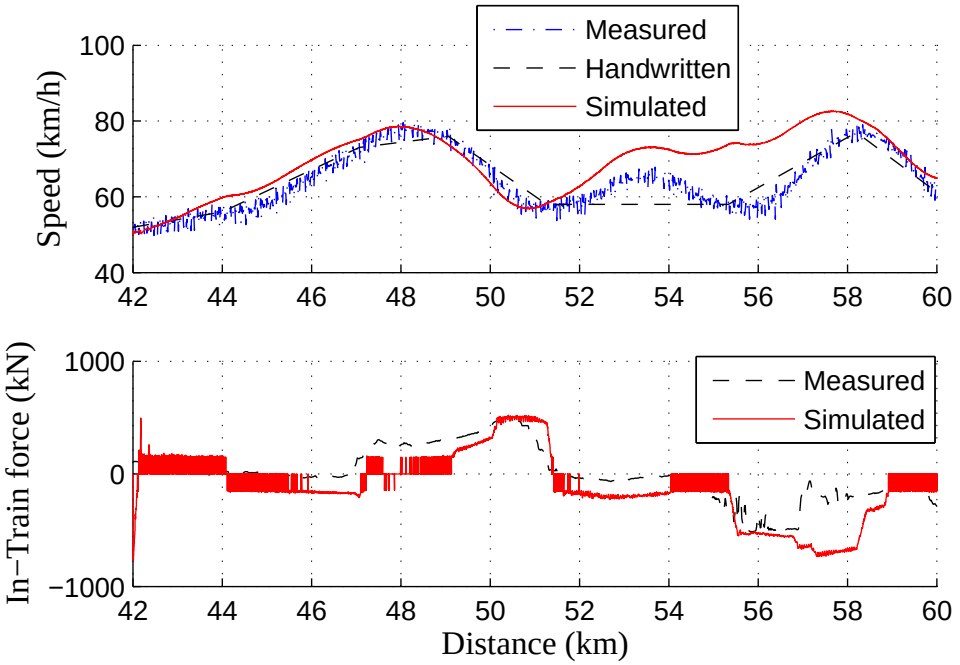


Figure 5.11: Second section from Week 3 with coupler slack simulated.

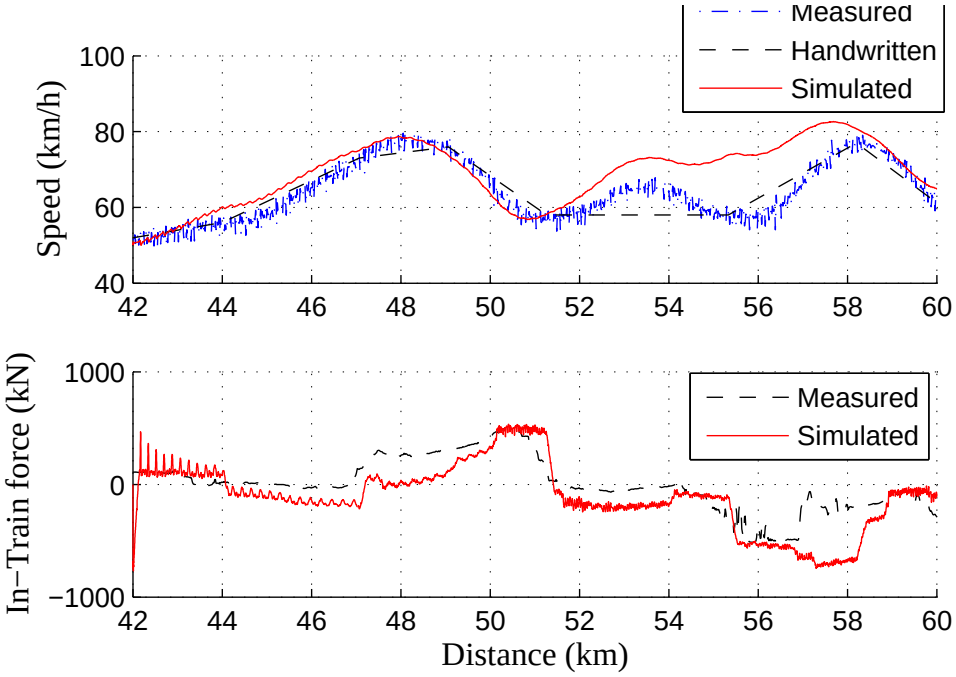


Figure 5.12: Second section from Week 3 without coupler slack simulated.

Next, another section of track from week 3 trial run was simulated. In this section, frequent control changes occurred. From Fig. 5.11 and Fig. 5.12, it is evident that deadband modelling again resulted in oscillations that did not occur in the recorded data. Thus, it is clear that deadband modelling does not provide more accurate results.

### 5.4.3 Damping coefficient

From the draft gears' data sheets, the spring coefficients can be determined from the force-displacement characteristic curves. However, the damping coefficients are not available. For the simulation, a fraction of the spring coefficient is used.

Fig. 5.13 compares the simulated velocity and in-train force outputs with zero damping coefficients. The damping coefficients are then increased progressively from $0.0001k_i$, $0.01k_i$ and finally $k_i$, with $k_i$ being the spring coefficients. Similar figures of these results are shown in shown in Fig. 5.14, Fig. 5.15 and Fig. 5.16. Train setup and recorded data from week 3 are used, of

which a different section of track was used.

From the simulation, it is very clear that in-train force is greatly influenced if the damping coefficients are set too small. With damping coefficients above $0.01k_i$, the simulation results correspond most closely to the recorded data, in terms of transient jittering and the steady-state behaviours. This shows that there exists some robustness of the damping coefficients in a reasonable range.

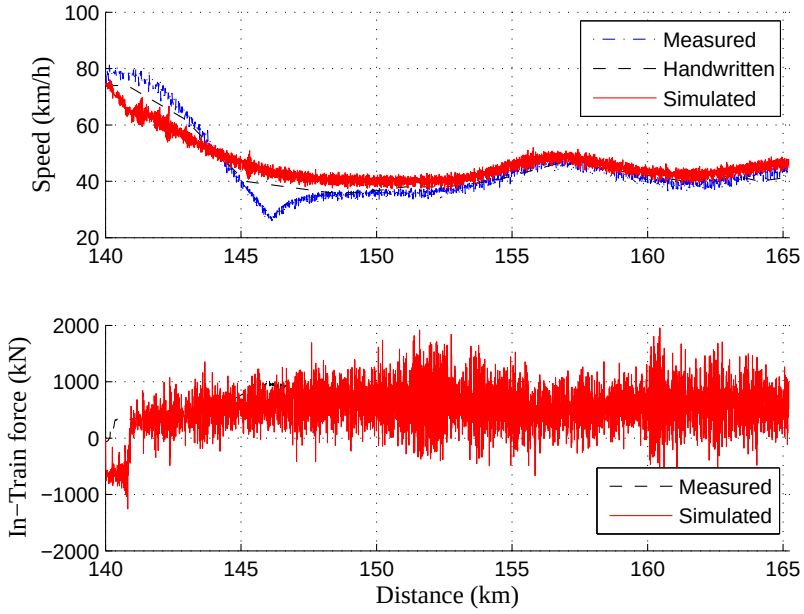


Figure 5.13: Simulated result with zero damping coefficient.

## 5.5 Discussion

From the results, it is clear that the model is able to reproduce the output data, using offset-compensated handwritten input data. Both the velocity output and the in-train forces outputs match closely to the recorded values. Even with faulty locomotives, the model is still able to produce accurate results. This is exceptional given that many parameters were only estimates or not even unavailable.

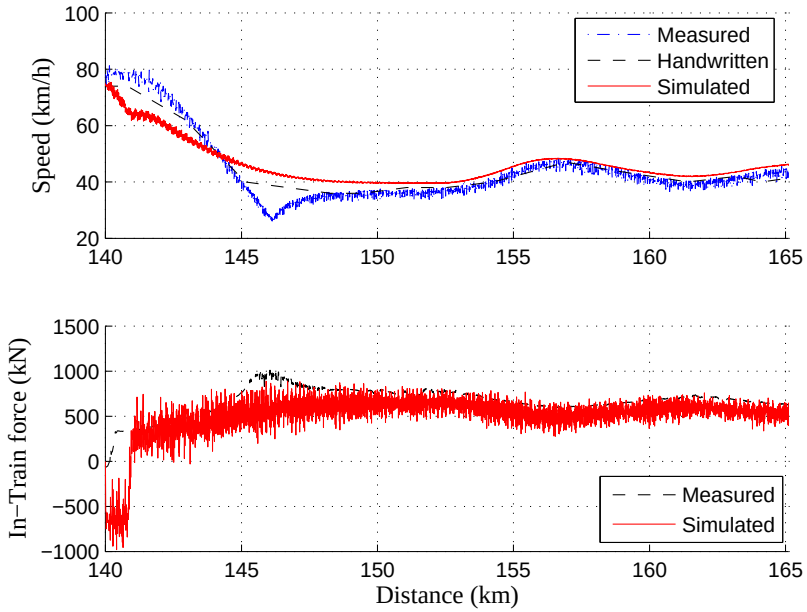


Figure 5.14: Simulated result with damping coefficient of 0.0001 times the spring coefficient.

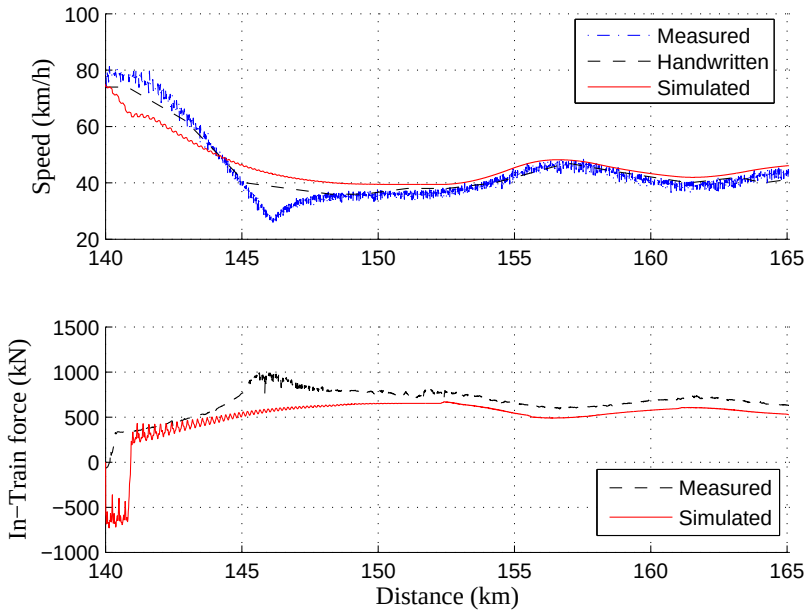


Figure 5.15: Simulated result with damping coefficient of 0.01 times the spring coefficient.

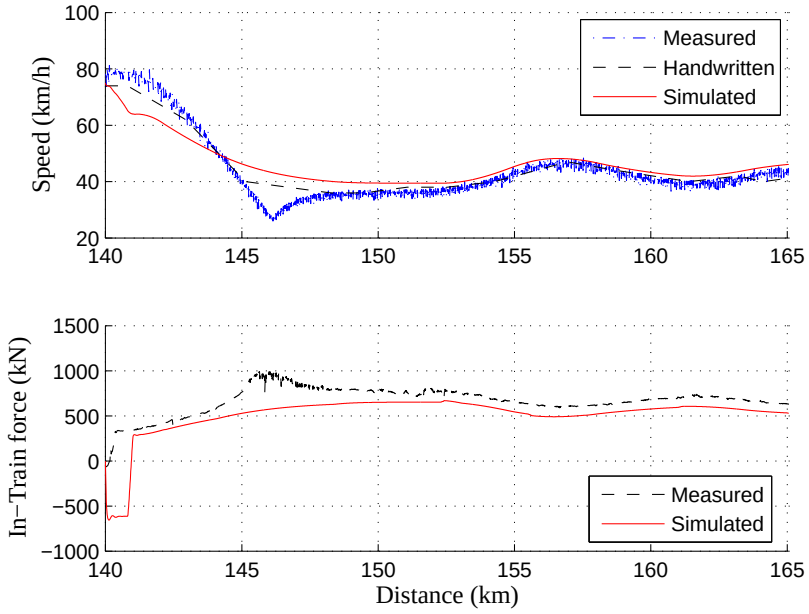


Figure 5.16: Simulated result with damping coefficient equal to the spring coefficient.

There are deviations in some of the results. This can be attributed to parameter uncertainties. One of the most influential is the wagon brake force. Unlike locomotive, there are no look-up tables for ECP wagon brakes. The model assumes a linear relationship between ECP input and the output brake force. The result shows that this assumption is sufficient for most cases. However, extremely worn brake blocks could reduce the efficiency of the wagon brakes. Such conditions are not recorded and could cause deviation in the simulation.

Another important parameter is the initial condition of the train. This includes the initial velocity as well as the relative distance of each car. This is obviously unavailable and impractical to measure. By choosing a starting point whereby the in-train force are close to zero, the simulated result was able to match the recorded data very closely.

The weather condition also affects the efficiency of the train. Heavy rains and strong wind could reduce adhesion unpredictably. Such disturbances are difficult to reproduce and will result in deviations in simulation results in terms of traction/brake efficiencies.

## 5.6 Conclusion

From the validation process, sampling time of 0.5 sec seems to be the best combination of simulation accuracy and simulation time. Another finding is that deadband modelling of coupler slack does not bring additional accuracy to the results.

Some insights into the dynamics of the train model can be observed: velocity output is heavily dependent on the control input and track condition, while in-train force is dependent on the control input and less affected by track modulations. It can be concluded that for velocity regulation, the track topology needs to be examined closely to determine the reference velocity. A well-chosen control input, on the other hand, would be able to counter most of the in-train forces introduced by track modulations.

Coupler characteristics such as damping and spring constants affect the jittering oscillation and magnitude of the coupler forces respectively. Large damping reduces excessive oscillations while larger spring constant resulted in larger in-train forces.

Overall, the model has been proved accurate as a train simulator, provided it has adequate and accurate key parameter values. Some of the key parameters include the mass of the locomotives and wagons, as well as the initial speed of the train. Other values, such as brake efficiency, can be tuned via trial-and-error.

# Chapter 6

# Controller design

The controller design is split into two: the open-loop controller and the closed-loop controller. Open-loop control provides a rough estimate for the required control efforts while the closed-loop controller fine-tunes the control inputs according to the desired optimising goals.

## 6.1 Open-loop Control

### 6.1.1 Introduction

Generally speaking, all open-loop controllers try to estimate the best control inputs to achieve the given goals. A good example is a golfer, whose aim is to try to get the ball as close to the hole as possible. The difference between a good player and a beginner is that the good player will base his judgement on existing knowledge, such as the available club size, his own strength. He may also make a few estimations, such as the distance to the hole, the wind speed.

It is obvious that the more accurate knowledge available the larger the chance of a hole-in-one. The challenge in real life situations is that most things are not measurable or unknown. In the case of golf, the wind speed could change abruptly. In addition, it is not practical to carry an anemometer and use it

every time a golfer wishes to play. Thus, a tradeoff has to be made between practicality and detailed knowledge.

Another argument in the case of the good and amateur golfer is that even with the same knowledge, a good golfer is able to control his/her strength more precisely. An amateur, who may be stronger physically, may still play disappointedly if he/she is unable to swing with the right force.

Similarly, in the case of train handling, the ECP system provides an accurate, precise mean to brake control. Traction control, however, is limited by notch behaviours discussed in section 4.3. Such limitation affects the open-loop controller performance notably. Closed-loop controller compensates such limitations via the feedback mechanism.

The complete open-loop controller consists of the open-loop control for maintaining equilibrium speed and transient control for speed changes. The structure is given in Fig. 6.1.

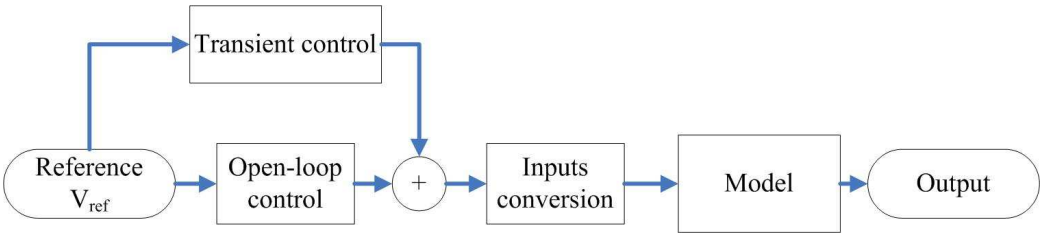


Figure 6.1: Open-loop control.

### 6.1.2 Open-loop Controller

In the operation of a train, the objective is to try keep the train around the desired speed while staying within the constraints. Some of the constraints include the available traction and brake efforts.

The open-loop controller is required to calculate the forces required for the train to maintain the desired speed under current conditions. Using the force equations used in section 4.2, the following results are obtained by assuming

zero acceleration and constant and uniform travelling speed:

$$\left.\begin{aligned} u_1 &= k_1(x_1 - x_2) + (c_0 + c_v v_d)m_1 \\ &\quad + c_a v_d^2 M + 9.98 \sin\theta_1 m_1 + 0.004 D_1 m_1, \\ u_i &= k_i(x_i - x_{i+1}) - k_{i-1}(x_{i-1} - x_i) + (c_0 + c_v v_d)m_i \\ &\quad + 9.98 \sin\theta_i m_i + 0.004 D_i m_i, \quad i = 2, \ldots, n-1, \\ u_n &= -k_{n-1}(x_{n-1} - x_n) + (c_0 + c_v v_d)m_n \\ &\quad + 9.98 \sin\theta_n m_n + 0.004 D_n m_n, \end{aligned}\right\} \tag{6.1}$$

where $M = \sum_{i=1}^{n} m_i$, $v_d$ is the desired velocity.

For a given train consisting of $n$ cars, $n$ equations are available. However, there are $2n$ unknown variables, $u_1, \ldots, u_n, x_1, \ldots, x_n$. Thus the system in (6.1) is under-determined.

There are two approaches to solving this problem. The one approach is to assume $x_{i+1} - x_i = 0, \quad i = 1, \ldots, n-1$ are zero, *i.e.*, there are no in-train force present during the equilibrium state. All velocities are also assumed to equal to a constant velocity, *i.e.*, $\dot{x}_i = v_d, \quad i = 1, \ldots, n$. In this case, the forces are reduced to

$$\left.\begin{aligned} u_1 &= (c_0 + c_v v_d)m_1 + c_a v_d^2 M + 9.98 \sin\theta_1 m_1 + 0.004 D_1 m_1, \\ u_i &= (c_0 + c_v v_d)m_i + 9.98 \sin\theta_i m_i + 0.004 D_i m_i, \quad i = 2, \ldots, n-1, \\ u_n &= (c_0 + c_v v_d)m_n + 9.98 \sin\theta_n m_n + 0.004 D_n m_n. \end{aligned}\right\} \tag{6.2}$$

While such solution may be viable in a theoretical setup, it is impossible in the heavy-haul train setup where the wagons are not powered. In actual fact, an equilibrium in-train force $k_i(x_{i+1} - x_i)$ would be required in most cases to overcome the other resistance forces. The only exception would be the case where only braking force is required, of which (6.2) would hold. For all other scenarios where traction is required, the following steps would have to be considered.

One may be tempted to only consider the case whereby all wagon control force $u_i$ are assumed to be zero to greatly reduce the number of unknowns.

There are two problems to this scenario. The first one is that this is only true for traction, since wagons have individual brake with the ECP system, thus have negative control forces. Secondly, even with the reduction, there are still $n + l$, $l$ is the number of locomotives, unknowns. With only $n$ equation, the system is still under-determined.

The second approach to the problem is to consider the train as a single unit. In this case, by summing the equilibrium forces in (6.1), the total effective force is

$$\begin{aligned} u_T &= u_1 + u_2 + \cdots + u_n \\ &= \sum_{i=1}^{n} m_i(c_a v_d^2 + c_0 + c_v v_d + 9.98 \sin\theta_i + 0.004 D_i). \end{aligned} \tag{6.3}$$

In practice, it is impossible to determine the exact states of $x_i, i = 1, \ldots, n$ due to the large number of sensors and the related costs. Thus there is no unique way of solving the system in (6.1).

In this study this equilibrium force is spread equally throughout the locomotives, *i.e.*,

$$\begin{aligned} u^e_{loco} &= \begin{cases} \dfrac{u_T}{l}, & u_T > 0 \\ \dfrac{u_T}{n}, & u_T \leq 0 \end{cases} \\ u^e_{wagon} &= \begin{cases} 0, & u_T > 0 \\ \dfrac{u_T}{n}, & u_T \leq 0 \end{cases} \end{aligned} \tag{6.4}$$

$l$ is the number of locomotives and $n$ is the number of cars in the train.

Such approach is the same as the current control setup found in the Coallink trains. Although there are two consists, *i.e.*, consecutively connected locomotive groups, one at the front and the other at the rear, the rear consist follows the command of the first consist, while all the locomotives within the consist receive the same control command.

For this study, such an open-loop control is sufficient. It is also proven to be safe as this type of open-loop control mimics human driver behaviour. The

controller shown in (6.4) determines the necessary traction force required to sustain the desired speed.

It is clear that an optimised distribution of the equilibrium force exists for each section of track. To calculate this optimised distribution, one would need to consider the car position, topology information. Optimised distribution would have to be recalculated as the train travels down the track. Optimised distribution calculation is unnecessary in this study as the closed-loop controller will provide a similar or even better optimal results. For an optimal open-loop design, a paper was recently proposed by Zhuan and Xia (2005).

### 6.1.3 Transient Control

With the controller described in section 6.1.2, a certain degree of steady-state error is unavoidable, especially during reference speed changes. To minimise this steady state error, thus improving the open-loop controller performance, an additional force is applied to accelerate or decelerate the train to the new reference.

To calculate the required additional force, we must go back to (6.3), since

$$F = m \times a,$$

by adding the additional term $a_d$, (6.3) becomes

$$u_T = \sum_{i=1}^{n} m_i(a_d + c_a v_d^2 + c_0 + c_v v_d + 9.98 \sin\theta_i + 0.004 D_i),$$

where $a_d$ is the acceleration term, defined for a certain acceleration time period $t_a$.

Constant acceleration time can be used to determine $a_d$ by taking the difference between the two reference speed and divide them by a predefined acceleration time,

$$a_d = \frac{v_d(i+1) - v_d(i)}{t_a}, \tag{6.5}$$

where $v_d(i+1)$ is the new reference speed, $v_d(i)$ the previous reference speed and $t_a$ the predefined acceleration time.

In practice, the locomotive is limited by acceleration rate. Given the acceleration rate, the additional force can be easily calculated. The required acceleration time can be determined by simple manipulation of (6.5)

$$t_a = \frac{v_d(i+1) - v_d(i)}{a_d}.$$

The purpose of this transient control is to assist the open-loop controller in reaching the desired speed faster by only analysing the changes in reference speed. It is disabled when closed-loop controller is available as the two perform similar functions.

## 6.2 Closed-loop Controller

The complete closed-loop controller consist of the open-loop control for maintaining equilibrium speed and closed-loop control for deviation feedbacks. The structure is given in Fig. 6.2.

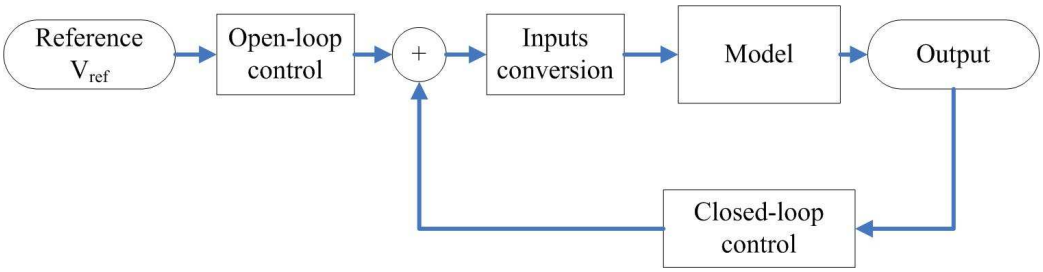


Figure 6.2: Closed-loop control.

### 6.2.1 Linearisation

Following the linearisation method described in Goodwin *et al.* (2001), assume the train is in the steady-state. There are no acceleration and all the units of the train are travelling at the same speed, *i.e.*, an equilibrium state

stated by

$$\left.\begin{array}{rcl} x_i &=& x_i^e + \delta x_i, \\ \dot{x}_i &=& v_d + \delta \dot{x}_i, \\ \ddot{x}_i &=& 0, \\ u_i &=& u_i^e + \delta u_i, \end{array}\right\} \tag{6.6}$$

where $v_d$ is the equilibrium speed, $u_i^e$ is the open-loop force described in section 6.1.2. Subsequently, it follows that the equilibrium displacements $x_i^e, x_{i+1}^e$ is such that

$$k_i(x_i^e - x_{i+1}^e) = \sum_{a=1}^{i} u_a^e - \sum_{a=i+1}^{n} u_a^e, \quad i = 1, \ldots, n-1, \tag{6.7}$$

since not all cars are powered.

The state variable $\mathbf{x}$ is chosen as

$$\delta \mathbf{x^1} \;=\; [\delta x_1 \;\ldots\; \delta x_n \quad \delta \dot{x}_1 \;\ldots\; \delta \dot{x}_n],$$

where $\delta \mathbf{x^1}$ is a $2n$ vector. For closed-loop design, the exact position of the train on the track, or the real displacement $s_i$ of each car, and the relative displacement difference $\delta x_i - \delta x_{i+1}$ are required.

The positions are required for finding the current track condition from the GIS data, as well as updating the reference speed. The relative displacement difference is required for the model.

To calculate the current position $s_i(t)$,

$$\begin{array}{rcl} s_i(t) &=& x_i(t) + s_i(t_0), \\ x_i &=& x_i^e + \delta x_i, \end{array}$$

where $s_i(t_0)$ is the initial position for the $i$th car.

To find $\delta x_i - \delta x_{i+1}$, $\delta x_1$ is assumed to be zero, together with (6.7),

$$\begin{array}{rcl} x_{i+1}^e &=& x_i^e - \dfrac{1}{k_i}\left(\displaystyle\sum_{a=1}^{i} u_a^e - \sum_{a=i}^{n} u_a^e\right), \\ \delta x_{i+1} &=& x_{i+1} - x_{i+1}^e. \end{array}$$

By first calculating $\delta x_2, x_2^e$, the other relative displacement differences can by found successively by repeating the calculation.

The summation (6.7) needs to be repeated for every coupler force, but direct evaluation of car position is possible.

Substituting (6.6) into the model (4.2) and defining the state variables

$$\begin{aligned}\delta\mathbf{x}' &= [\delta x_1 \ \ldots \ \delta x_n \quad \delta\dot{x}_1 \ \ldots \ \delta\dot{x}_n],\\ \delta\mathbf{u}' &= [\delta u_1 \ \ldots \ \delta u_n],\end{aligned}$$

the following state space model can be found:

$$\delta\dot{\mathbf{x}} = \begin{bmatrix}\mathbf{0}_{n\times n} & \mathbf{A}_{12}\\ \mathbf{A}_{21} & \mathbf{A}_{22}\end{bmatrix}\delta\mathbf{x} + \begin{bmatrix}\mathbf{0}_{n\times n}\\ \mathbf{B}_{21}\end{bmatrix}\delta\mathbf{u},$$

where

$$\mathbf{A}_{12} = \begin{bmatrix}1 & 0 & 0 & \ldots & 0\\ 0 & 1 & 0 & \ldots & 0\\ \ldots & \ldots & \ldots & \ldots & \ldots\\ 0 & \ldots & \ldots & 0 & 1\end{bmatrix}_{n\times n},$$

$$\mathbf{A}_{21} = \begin{bmatrix}-\frac{k_1}{m_1} & \frac{k_1}{m_1} & 0 & \ldots & 0 & 0 & 0\\ \frac{k_1}{m_2} & -\frac{k_1+k_2}{m_2} & \frac{k_2}{m_2} & \ldots & 0 & 0 & 0\\ \vdots & \vdots & \vdots & \ddots & \vdots & \vdots & \vdots\\ 0 & 0 & 0 & \ldots & \frac{k_{n-2}}{m_{n-1}} & -\frac{k_{n-2}+k_{n-1}}{m_{n-1}} & \frac{k_{n-1}}{m_{n-1}}\\ 0 & 0 & 0 & \ldots & 0 & \frac{k_{n-1}}{m_n} & \frac{-k_{n-1}}{m_n}\end{bmatrix}_{n\times n},$$

$$\mathbf{A}_{22} = \begin{bmatrix}-c_v - \frac{2c_a v_0 M}{m_1} & 0 & \ldots & 0\\ 0 & -c_v & \ldots & 0\\ \vdots & \vdots & \ddots & \vdots\\ 0 & \ldots & \ldots & -c_v\end{bmatrix}_{n\times n}.$$

Matrix $\mathbf{B}_{21}$ is more complicated than the rest of the matrices, since it depends on train configuration. The possible configurations for traction and brake inputs are:

- unified, where one setting is used of all pulling locomotives, and one setting for all braking wagons, as currently used by Spoornet,
- distributed, where more than one inputs are used for groups of cars, which will be discussed in introduction of the fencing concept and

- individual inputs for every single car.

With three options for traction and braking, there are nine difference combinations of inputs. The matrices $\mathbf{B}_{21}$ for two extremes are given as follows: for one inputs for all locomotives and one brake for all the wagons,

$$\mathbf{B}_{21} = \begin{bmatrix} \mathbf{1}_{l\times 1} & \mathbf{0}_{l\times 1} \\ \mathbf{0}_{n-l\times 1} & \mathbf{1}_{n-l\times 1} \end{bmatrix},$$

where $l$ is the number of locomotives, and for individual inputs

$$\mathbf{B}_{21} = \mathbf{I}_{n\times n}. \tag{6.8}$$

### 6.2.2 Fencing

In the previous section, (6.8) assumes ideal individual control is assumed. However, availability of control signal bandwidth prohibits this.

Because of the ECP channel limitation of 32, as described by AAR specifications, it is not possible to have individual control. To provide a solution to this problem, the idea of fencing is proposed.

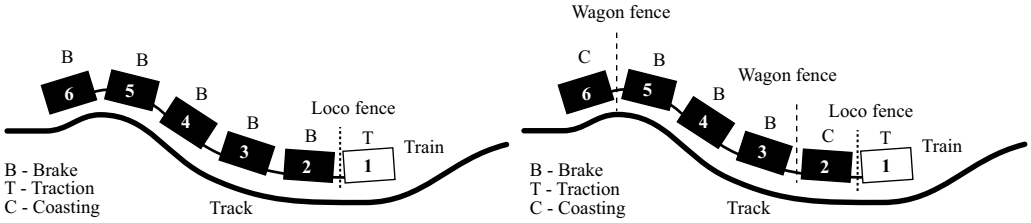


Figure 6.3: Comparison between with and without adaptive fencing.

In the left of Fig. 6.3, car 6, although climbing uphill, has to apply its brake since the train only has one control signal for all the wagons. With adaptive wagon fencing, showing on the right of Fig. 6.3, wagon with similar track conditions are grouped and controlled together. The term fence refers to the separation of control signals.

The adaptive wagon fencing controller automatically calculates new fences for the train as it travels down the track.

$$F = [f_1, f_2, \ldots, f_j],$$

where $f_i$ are the first car of the group. The number of fences $j$ and $\mathbf{B_{21}}$ will vary with the complexity of the track modulation. Define the number of car within a fence group as $g(i) = f_{i+1} - f_i,\ i = 0, \ldots, j$ with $f_0 = 1$, the matrix $\mathbf{B}_{21}$ can be written as

$$\mathbf{B_{21}} = \begin{bmatrix} \mathbf{1}_{g(1)\times 1} & \mathbf{0}_{g(1)\times 1} & \ldots & \mathbf{0} & \mathbf{0} \\ & \mathbf{1}_{g(2)\times 1} & \ldots & & \\ & & \ldots & \mathbf{1}_{g(j-1)\times 1} & \\ \mathbf{0} & \mathbf{0} & \ldots & \mathbf{0}_{g(j)\times 1} & \mathbf{1}_{g(j)\times 1} \end{bmatrix}.$$

The concept of adaptive fencing is well related to interests in the control community of reconfigurable/switching control systems Wu (1995) and Slotine and Li (1991).

To evaluate whether a new set of fences is required, the controller calculates the median of the slope angles and the track curvature the train experiences at each sampling time $t_s$. If either exceeds the previous value by a predefined threshold $f_{th}$, a new set of fences will be calculated.

From the leading car, the controller will add a fence between the current and the next unit under the following conditions:

(i) The unit type differs, *e.g.*, rake following a locomotive

(ii) The slope experienced by the next unit exceeds the slope experienced by the previous fenced unit by a predefined threshold $f_{seg}$.

(iii) The above condition occurs for the track curvature.

### 6.2.3 LQR Control

Based on the LQR optimisation method described in Goodwin *et al.* (2001), the cost function is defined as

$$J = \int \delta\mathbf{x}'\mathbf{Q}\delta\mathbf{x} + \delta\mathbf{u}'\mathbf{R}\delta\mathbf{u}, \tag{6.9}$$

where $\mathbf{Q}$ and $\mathbf{R}$ are the weights.

To use LQR method, the running costs: in-train force, energy consumption and travelling time need to be quantified. Energy consumption is directly related to the matrix $\mathbf{R}$, while the matrix $\mathbf{Q}$ determines the weights for in-train force and velocity tracking. By improving velocity tracking, in essence one improves the travelling time.

Individual weights are given to the cars. For example, one could have a stronger emphasis on the in-train force of the middle wagon, or less emphasis on the brake usage across the wagons. Such parameter flexibility allows the controller to be adaptive to different conditions.

The weighting matrix $Q$ is chosen such that

$$\begin{aligned}\delta\mathbf{x}'\mathbf{Q}\delta\mathbf{x} &= \sum_{i=1}^{n-1} q_{1i}k_i^2(\delta x_i - \delta x_{i+1})^2 + q_{1i}d_i^2(\delta\dot{x}_i - \delta\dot{x}_{i+1})^2 \\ &\quad + \sum_{i=1}^{n} q_{2i}(\delta\dot{x}_i - v_d)^2,\end{aligned}$$

in which all the $q$'s are positive. The term $q_{1i}$ is to penalise the in-train forces experienced by the couplers, and the term $q_{2i}$ is to penalise the travelling speed tracking of the whole train.

The matrix $R$ is chosen to be diagonal and will determine the fuel consumption as well as brake usage, *i.e.*,

$$\mathbf{R} = \begin{bmatrix} r_1 & 0 & \dots & 0 \\ 0 & r_2 & \dots & 0 \\ \dots & \dots & \ddots & \dots \\ 0 & 0 & \dots & r_n \end{bmatrix},$$

where $r_i, i = 1, \dots, n$ are the weighting coefficients for the traction and brake force on each car. When adaptive fencing occurs, the size $n$ will change accordingly. For unified operation, only two weights will be used, one for traction and one for wagon brake.

Once the feedback gain $K$ has been obtained by solving the objective function (6.9), the complete controller becomes

$$\mathbf{u} = \mathbf{u}^e + K\delta\mathbf{x},$$

where $\mathbf{u}^e$ is the open-loop control described in Section 6.1.2.

The weights are first chosen through the given train parameters, such as coupler type, brake system type. Further simulation runs determine the range for the weights. There is no one optimised parameter set; instead, parameters can be tuned during operation to fit the current need at the time.

For example, consider a scenario where the controller would focus on velocity tracking for most of the trip. When difficult terrains are encountered, more emphasis would be placed on the in-train force weights to ensure coupler strain are not exceeded. On a smooth downhill section, emphasis could be shifted to energy consumption, allowing the train speed to drift slightly away from the reference speed.

Although the closed-loop controller will not be able to optimise the travelling time and fuel efficiency at the global level, through cost coefficients $q_{2i}$ and $r_i$ travelling time and fuel consumption can be optimised locally, *i.e.*, at the current track position.

It is possible that the closed-loop LQR controller issues traction inputs to the wagons. Other undesired inputs include high frequency jittering. Such out-of-bounds inputs will be adjusted by the input limiters, as as specified by section 4.3. Both rate of change and maximum and minimum values are limited. Essentially, these input limiters act as low-pass filters, filtering unwanted high frequency jittering and abrupt changes in the control inputs that could result in undesired behaviours such as excessive high in-train forces. The result is improved stability by maintaining control inputs within acceptable range.

## 6.3 Input Chattering

Both the open-loop and closed-loop control are designed around force models. Thus, the control inputs are in forces. However, since the locomotives and wagons accept notches and brake levels as inputs, conversions are required.

The first step is to converts locomotive inputs via look-up tables, shown in Fig. 4.9, while brake inputs will be converted linearly using the maximum brake.

In application, problem arises with locomotive notches. Since locomotive notches are quantised inputs, it is difficult to obtain the desired force out of the locomotives. The unfiltered inputs will result in excessive switching between notches, causing chattering effects on the input signals, as shown in Fig. 6.4. This will cause corresponding chattering on the in-train forces.

By specifying a threshold boundary around quantised levels, the excessive switching will be minimised. This essentially filters the inputs through a low pass filter around each notch level. In Fig. 6.5, the quantised input is smoothened out.

Similar methods are used in sliding mode control, as described by Slotine and Li (1991). By smoothening out the discontinuous control law, an optimal trade-off between control bandwidth and tracking precision is made. In addition, robustness is achieved for high frequency dynamics.

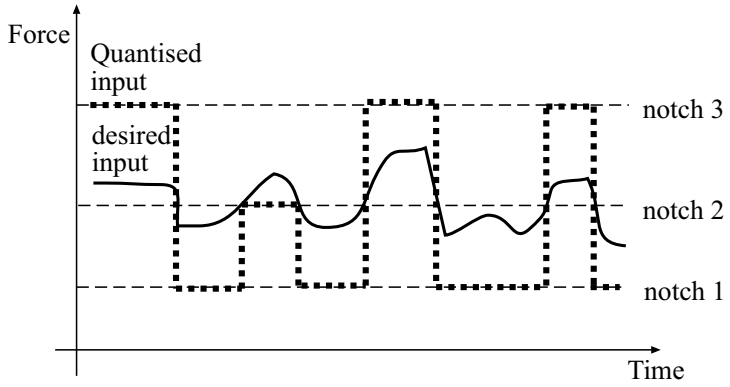


Figure 6.4: Excessive input switching due to quantisation.

Defining the required force $f_t$ and lookup table output as $g(n, v)$ where $n$ is the notch and $v$ is the current velocity, the output force $F_l$ for the $l$th locomotive can be defined as:

$$\begin{aligned} F_l(f_t, v) &= g(n, v),\ if\ G(n-1, v) \leq f_t < G(n, v), \\ G(n, v) &= g(n, v) + \alpha\big(g(n+1, v) - g(n, v)\big), \end{aligned}$$

where $G(n, v)$ is the upper boundary value for current notch level $n$, while $G(n-1, v)$ is the lower boundary value. $\alpha$ is the ratio of the separation for the boundary. Thus, any notch changes will only occur if the required force $f_t$ is greater than the current upper boundary $G(n, v)$, or becomes less than the upper boundary of the notch below $G(n-1, v)$.

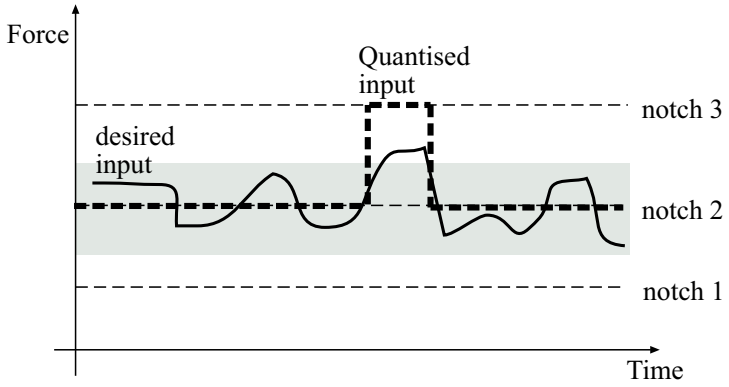


Figure 6.5: Excessive input switching minimised by specifying a boundary layer.

The other areas that discontinuous control inputs exist are the switching between traction and braking. Both the locomotive and wagon inputs are affected. Recall open-loop control (6.4):

$$u^e_{loco} = \begin{cases} \dfrac{u_T}{l}, & u_T > 0 \\ \dfrac{u_T}{n}, & u_T \leq 0 \end{cases}$$

$$u^e_{wagon} = \begin{cases} 0, & u_T > 0 \\ \dfrac{u_T}{n}, & u_T \leq 0 \end{cases}$$

During braking, the demanded brake force is spread across the whole train, in the case of Coallink train, with 200 wagons and 6 locomotives. When traction is required, the demanded traction force is only spread around locomotives, only 6 in Coallink trains. Thus when the train moves from brake to traction, a sudden surge of traction demand is sent to the locomotives. The reverse does not occur because brake force is spread out.

To reduce chattering during brake to traction transitions, a conditional one-way threshold boundary is set for locomotive input switching: during one-way brake to traction transitions, if the demanded acceleration is smaller than $a_{th}$, then the locomotive will only power at a fraction of the demanded level. This avoids the sudden peak of in-train force from occurring during the transition.

# Chapter 7

# Simulation Result

In this section, the two main focuses are the effects of train configuration, which includes level of individual control and fencing, and closed-loop controller performance based on parameter tuning for different objectives.

Using the Coallink GIS data, the section of track starting at 63 km is chosen. This section contains a very challenging section of ruling grade where the train is momentarily powered to 80 km/h to be able to climb over the uphill climb of 1/76 grade using momentum. The grade specification for uphill is 1/160.

Parameters from Table 5.1 and Table 5.6 are used with any modifications specified otherwise. For input chattering parameters, the threshold $a_{th}$ is set to 0.1 $ms^{-1}$ while locomotive notch boundary ratio $\alpha$ is set to 0.3.

Throughout the results, the recorded velocity and in-train force data from week 4 are plotted to allow comparison between simulated results and recorded data.

## 7.1 Open-loop Controller

The simulation has the same setup as the actual trial run for week 4: Two consists with four locomotives at the front and two locomotives at the rear,

the simulated train consists of 200 wagons modelled as 50 rakes. Unified ECP is used for all the wagons. The comparison here is between the recorded human driver and the open-loop controller.

The two results in Fig. 7.1 and Fig. 7.2 are open-loop controller without and with the transient controls.

Fig. 7.1 shows that the open-loop controller is sufficient in maintaining the velocity of the train, but is unable to bring the train to the new reference speed. Although the train velocity $v_{sim}$ deviates from the reference $v_{ref}$ after the change at 70km point, the in-train force pattern is very close to those of the recorded, suggesting that the reference speed pattern is approximately the same as the actual driver control pattern.

Fig. 7.2 is a mixture of the advantages and disadvantages of open-loop transient control. At the 70km point, transient control is able increase the train speed to 80 km/h, based only on the reference speed differences. At 76 km point, it initialises deceleration of the train in hope to bring the velocity down from 80 km/h to 60 km/h. However, the controller is unaware of the velocity was already around 60 km/h due to the difficult track that exceeded the maximum specified grade. Without any feedback, the train slows down to a even lower speed.

From the results, it shows that the open-loop control can closely mimic the driving pattern of the human driver given the same reference speed signals. Transient control proves to be operational on normal tracks within specified grade, but can deviate the train further on difficult tracks.

## 7.2 Closed-loop Controller

As expected, the previous section shows that the open-loop controller is unable to counter disturbances such as difficult track, although it functions very well if the track is within normal specifications, *i.e*, section before 76 km point. To further improve on the controller, in this section, the closed-loop controller is added onto the open-loop controller.

On all of the results, the recorded velocity and in-train force are provided as a reference. Even though some of the results are based on different reference

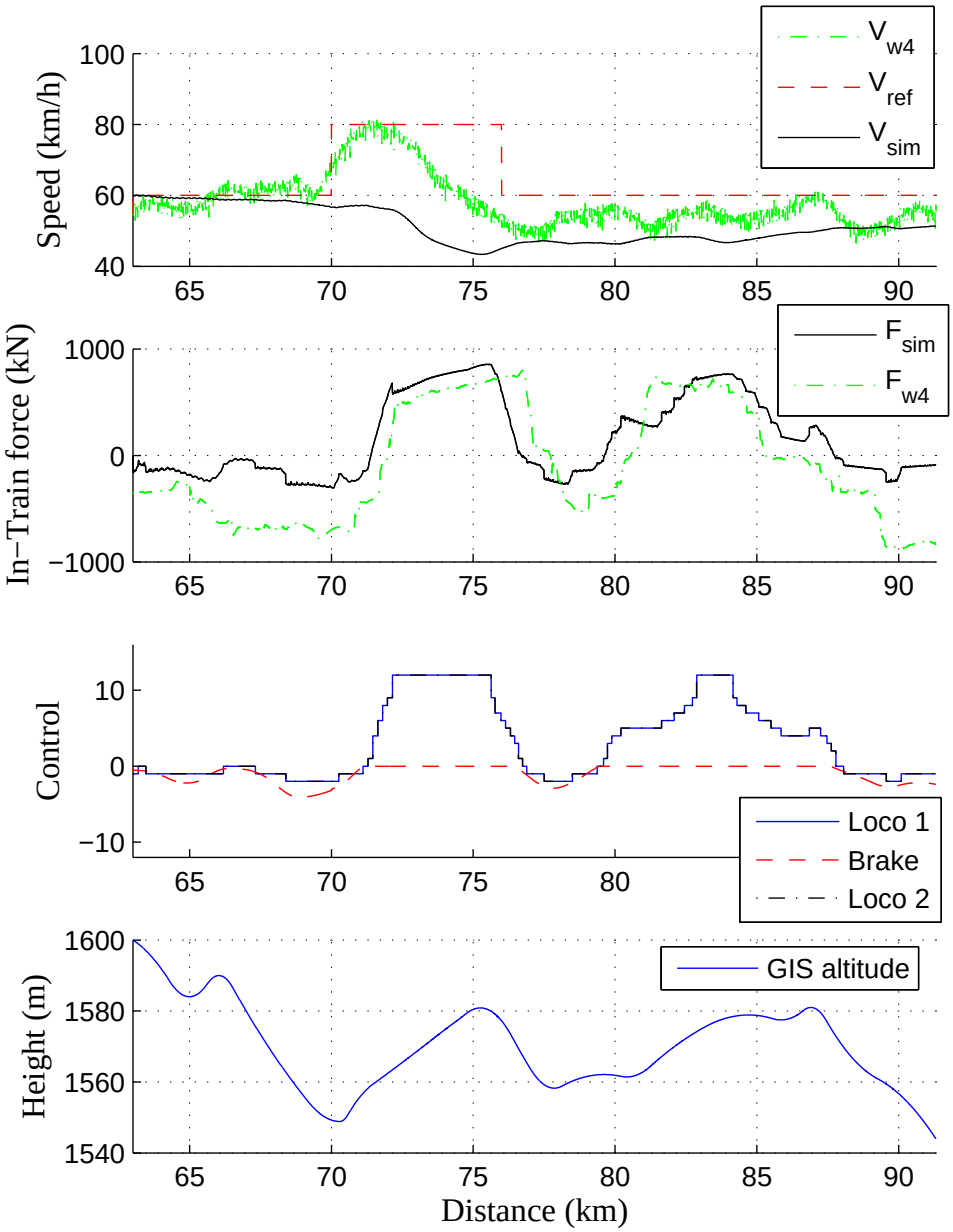


Figure 7.1: Open-loop controller without transient control.

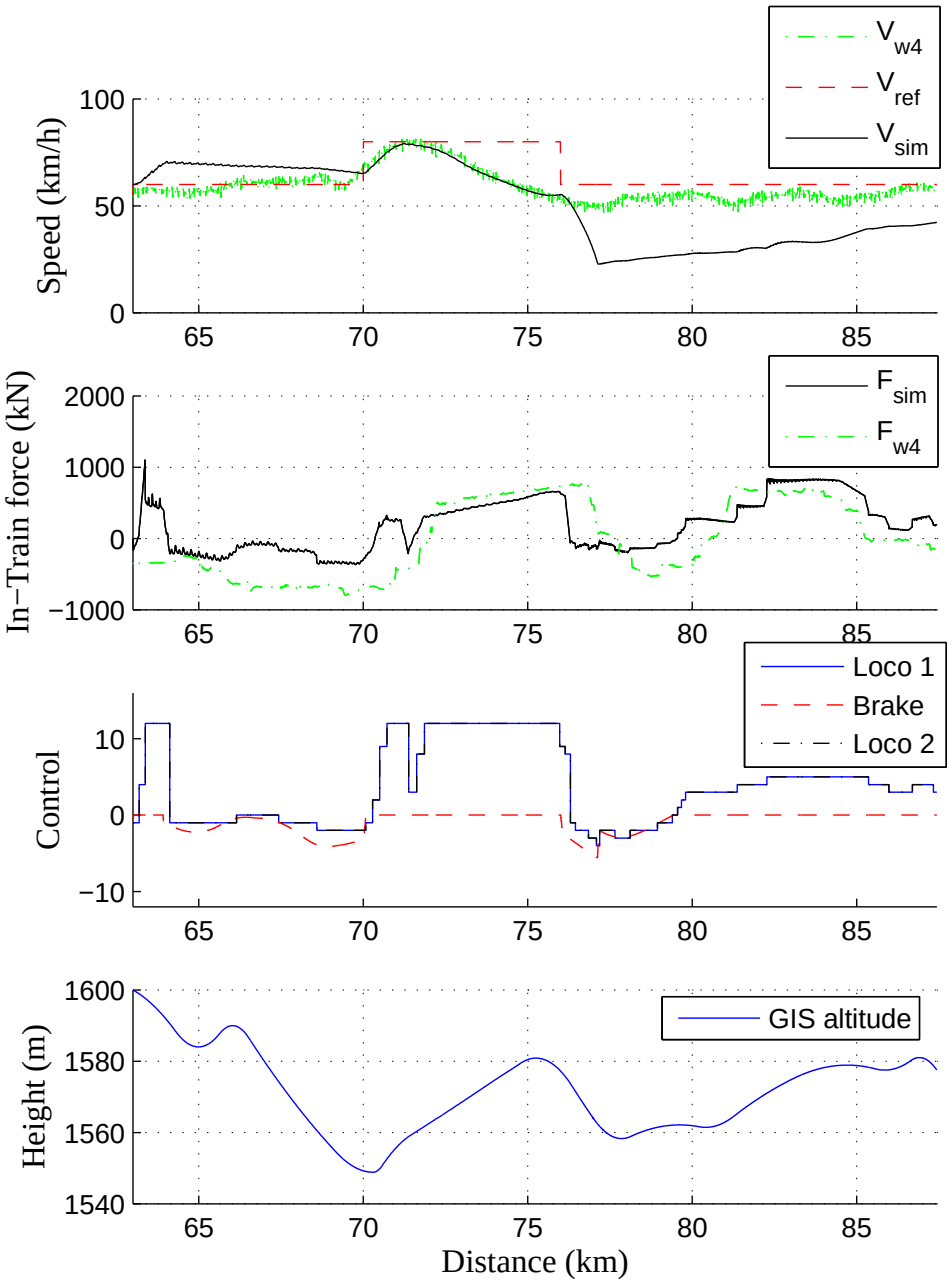


Figure 7.2: Open-loop controller with transient control.

velocity signals, it remains interesting to compare the range of the values for practicality for some of these controllers.

### 7.2.1 Generic set

The same train configuration is used as previous setup, with the same reference speed signal. The difference is that transient control is disabled and closed-loop control is added.

The LQR tuning parameters are set such that the weights $r_l$ and $r_w$ are used for all the locomotives and wagons respectively in the weight $\mathbf{R}$. All in-train forces have the same weight $q_1$, while velocity regulation is split into two groups, $q_{2_l}$ for locomotives and $q_{2_w}$ for wagons.

In this generic setup, all $\mathbf{Q}$ and $\mathbf{R}$ parameters are set to 1.

Comparing the previous result Fig. 7.2, closed-loop control improves the velocity regulation, as well as in-train forces, as shown in Fig. 7.3.

The velocity deviations from 70 to 76 km points, as well as around 85 km point, are due to the specification exceeding grades. At these sections, the available traction efforts available from the six 7E1 locomotives are insufficient to maintain the desired speed.

By integrating the control efforts, the energy consumed can be found. Although the actual values will be greater due to less efficiencies of the motors and brakes, these values still provides a good guideline to energy used by different controllers.

The values for the generic run will be used as reference values for the next few experiments. To allow better comparison for some of the results, a second reference simulation run with a lower, but more modulated reference velocity was also used, shown in Fig 7.4.

The performance indices are grouped in Table 7.1.

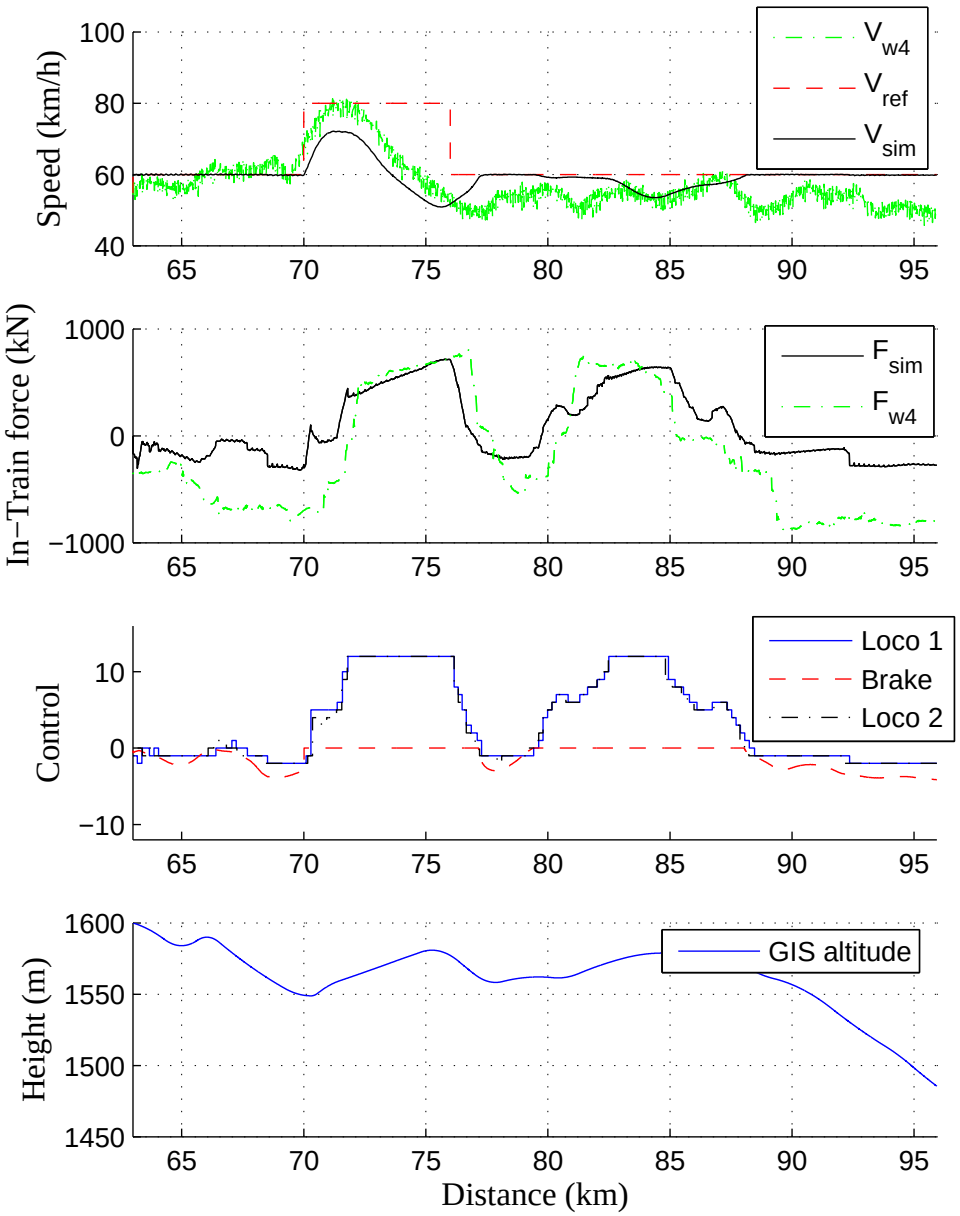


Figure 7.3: Generic closed-loop control with all parameters equal to 1.

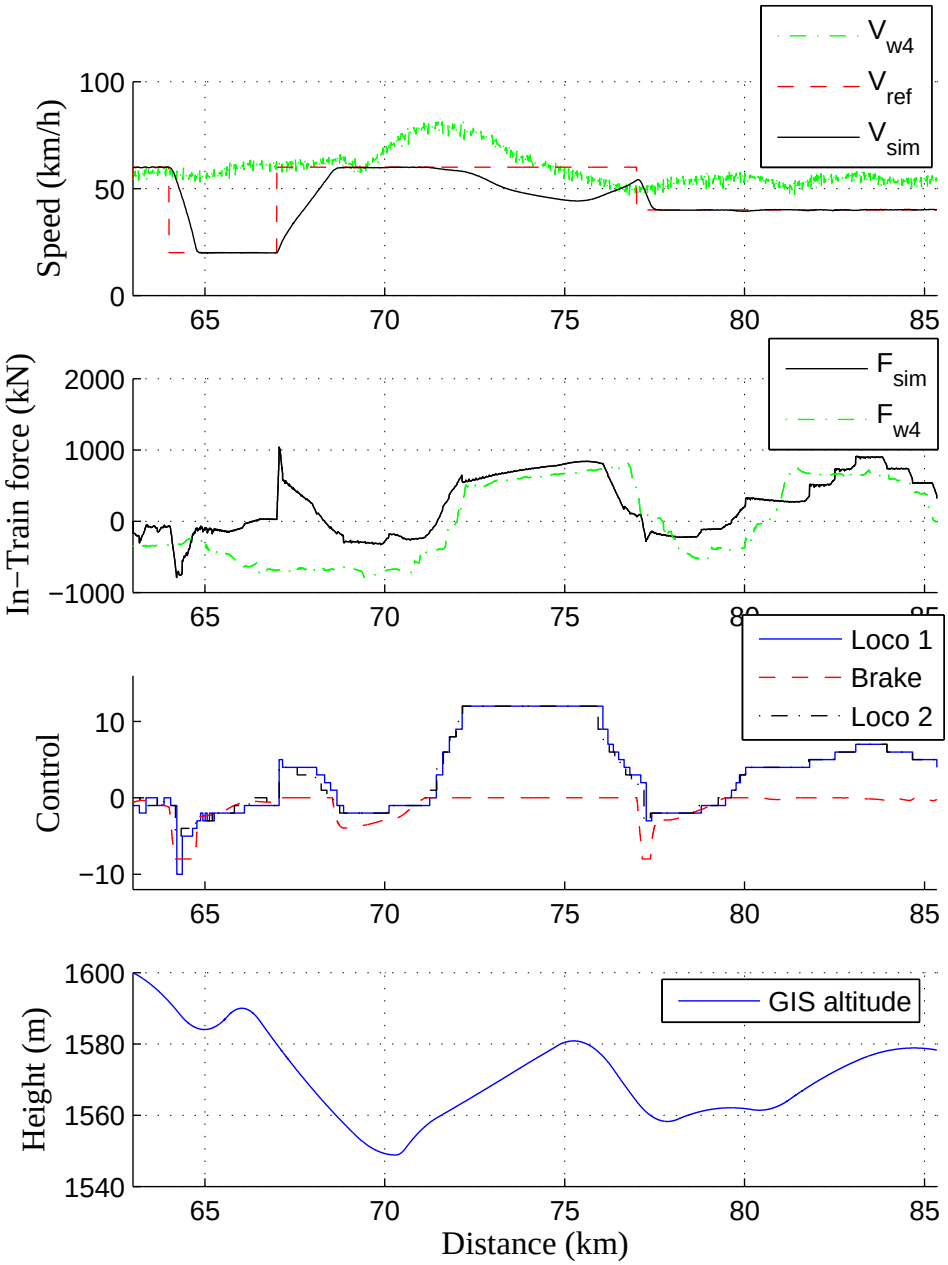


Figure 7.4: Second set of generic closed-loop control with all parameters equal to 1 and a lower, but more modulated reference velocity set.

| | Reference 1 | | Reference 2 | |
|---|---|---|---|---|
| Distance | | | | |
| | 63 - 90 | km | 63 - 82 | km |
| Velocity Deviation | | | | |
| Absolute mean | 5.1649 | km/h | 5.4804 | km/h |
| Mean | -5.1521 | km/h | -3.4834 | km/h |
| In-train force | | | | |
| Minimum | -321.6026 | kN | -788.8906 | kN |
| Maximum | 717.0152 | kN | 1041.2118 | kN |
| Energy consumption | | | | |
| Traction | 698.1804 | MJ | 620.9923 | MJ |
| Dynamic Braking | -87.1825 | MJ | -157.1676 | MJ |

Table 7.1: Performance indices for generic closed-loop simulations.

### 7.2.2 Closed-loop Controller Optimised for Velocity Tracking

The chosen test track together with the chosen reference velocity signals already requires maximum traction force from the locomotives. By increasing $q_1$ and $q_2$ to 12, it is hoped that the velocity regulation performance might even improve further. $r_l$ is slightly increased to 3 to encourage wagon brake usage.

Because of the difficult ruling gradient, velocity regulation improvements are minimal for the first reference set. Steady-state has been reduced slightly, around 80 km point, shown in Fig. 7.5.

The second reference velocity set is more modulated, but at a lower level. Thus the train is able to follow the reference more closely, as shown in Fig. 7.6. Regulation performance has improved slightly, but at the cost of higher energy usage and very large in-train force. The very large in-train force peak around 67 km would have broken the coupler in practice. Thus this result reflects the fact that the weights must be within the acceptable range to ensure reasonable control actions.

| | Current value | | Reference 1 | |
|---|---|---|---|---|
| Velocity Deviation | | | | |
| Absolute mean | 4.4568 | km/h | 5.1649 | km/h |
| Mean | -4.447 | km/h | -5.1521 | km/h |
| In-train force | | | | |
| Minimum | -324.1368 | kN | -321.6026 | kN |
| Maximum | 695.1412 | kN | 717.0125 | kN |
| Energy consumption | | | | |
| Traction | 705.7044 | MJ | 698.1804 | MJ |
| Dynamic Braking | -90.1955 | MJ | -87.1825 | MJ |

Table 7.2: Performance indices for velocity tracking emphasised controller compared to reference 1.

| | Current value | | Reference 2 | |
|---|---|---|---|---|
| Velocity Deviation | | | | |
| Absolute mean | 4.9946 | km/h | 5.4804 | km/h |
| Mean | -2.9909 | km/h | -3.4834 | km/h |
| In-train force | | | | |
| Minimum | -1562.6711 | kN | -788.8906 | kN |
| Maximum | 1640.8775 | kN | 1041.2118 | kN |
| Energy consumption | | | | |
| Traction | 682.77 | MJ | 620.9923 | MJ |
| Dynamic Braking | -190.4987 | MJ | -157.1676 | MJ |

Table 7.3: Performance indices for velocity tracking emphasised controller compared to reference 2.

| | Current value | | Reference 1 | |
|---|---|---|---|---|
| Velocity Deviation | | | | |
| Absolute mean | 6.4368 | km/h | 5.1469 | km/h |
| Mean | -6.433 | km/h | -5.1521 | km/h |
| In-train force | | | | |
| Minimum | -311.9185 | kN | -321.6026 | kN |
| Maximum | 751.014 | kN | 717.0152 | kN |
| Energy consumption | | | | |
| Traction | 690.8597 | MJ | 698.1804 | MJ |
| Dynamic Braking | -87.7121 | MJ | -87.1825 | MJ |

Table 7.4: Performance indices for in-train force emphasised controller compared to reference 1.

The improvements for velocity tracking are not substantial since the generic controller is already very efficient at velocity regulation.

### 7.2.3 Closed-loop Controller Optimised for In-train Force

For in-train force emphasised control, the weights are adjusted as follows: $q_2$ for both locomotive and wagon are reduced to 0.1, while $q_1$ for in-train force is increased to 59. Because of the reduced weights, velocity regulation is expected to deteriorate. $r_l$ is slightly increased to 3 to encourage wagon brake usage.

Fig. 7.7 shows that, again, due to the ruling grade and high reference velocity, improvement are limited. In-train force was not improved, but slightly increased due to the deteriorated velocity regulation. However, the overall in-train force jittering has been reduced; an example would be the minimisation of the peak at 70 km point.

Reference set 2 shows a more interesting picture, shown in Fig. 7.8. Looking at in-train force output at 64 km and 67 km points, one notices that the peaks

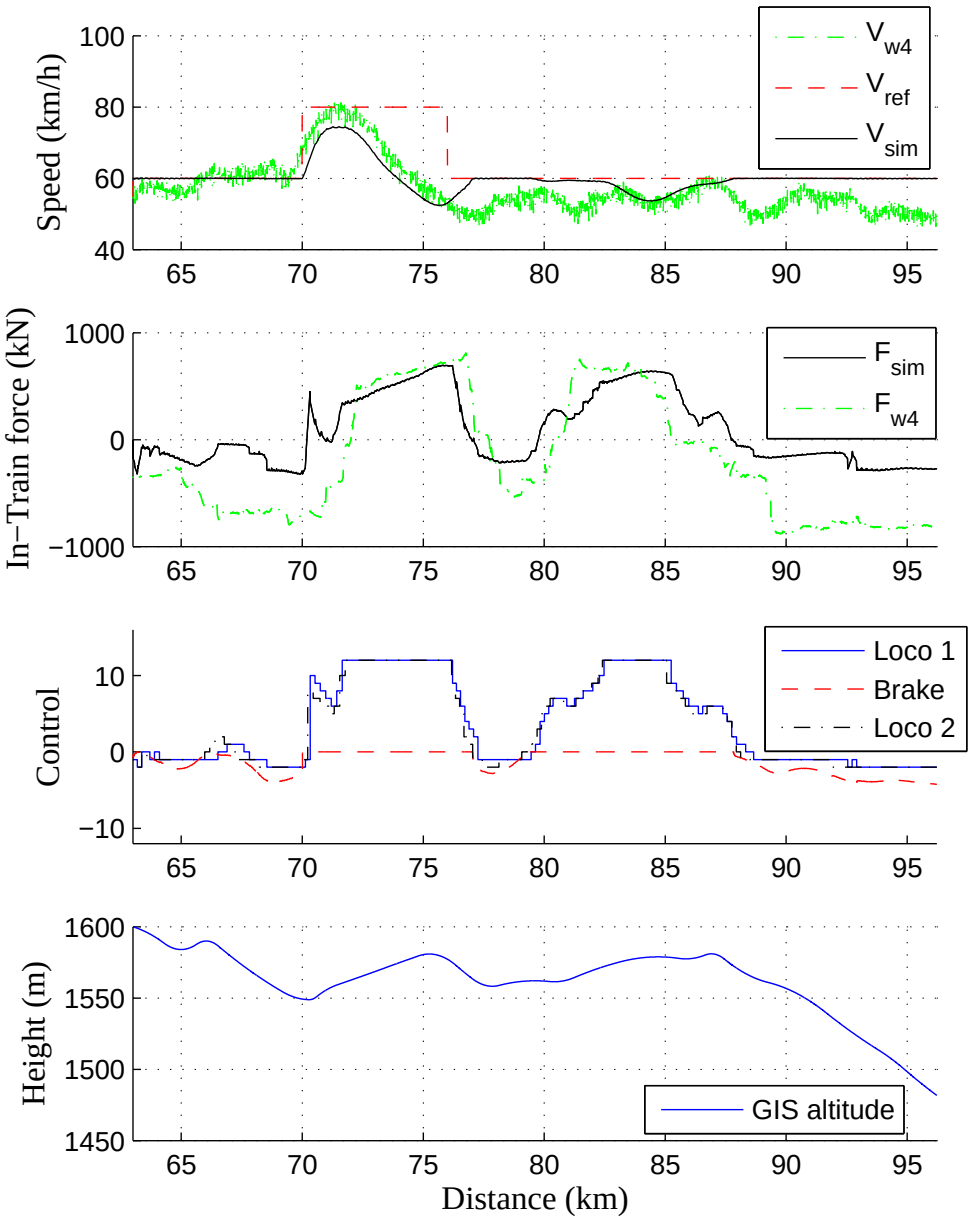


Figure 7.5: Closed-loop controller with emphasis on velocity regulation for reference set 1.

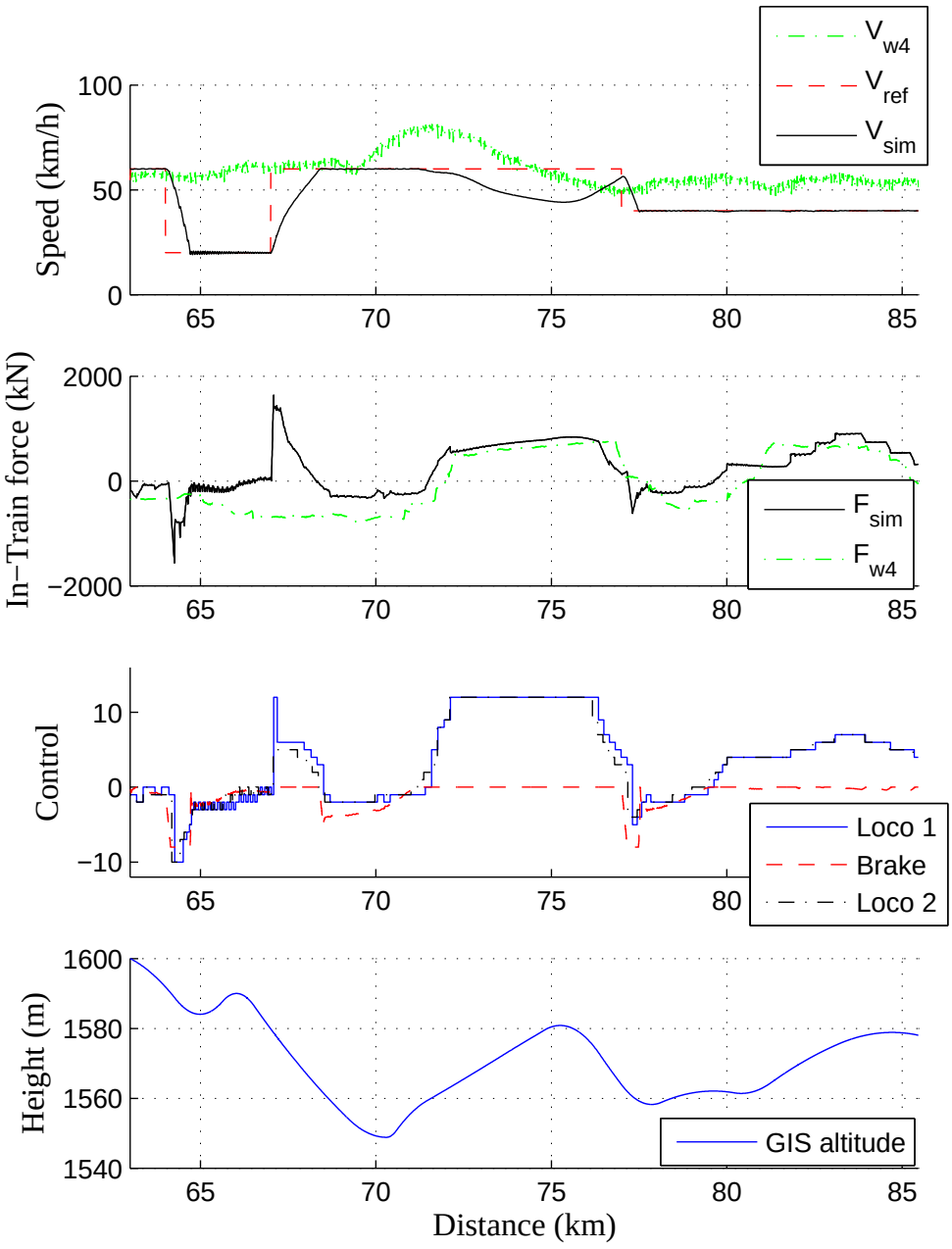


Figure 7.6: Closed-loop controller with emphasis on velocity regulation for reference set 2.

| | Current value | | Reference 2 | |
|---|---|---|---|---|
| Velocity Deviation | | | | |
| Absolute mean | 6.8767 | km/h | 5.4804 | km/h |
| Mean | -4.5972 | km/h | -3.4834 | km/h |
| In-train force | | | | |
| Minimum | -309.4605 | kN | -788.8906 | kN |
| Maximum | 843.6625 | kN | 1041.2118 | kN |
| Energy consumption | | | | |
| Traction | 536.051 | MJ | 620.9923 | MJ |
| Dynamic Braking | -119.9479 | MJ | -157.1676 | MJ |

Table 7.5: Performance indices for in-train force emphasised controller compared to reference 2.

have been greatly reduced, compared to the generic controller in Fig. 7.4. This is evident from the substantial reduction on the minimum in-train force by almost a half.

Additional benefits of reduced in-train force are less control efforts. Looking at the control inputs at 64 and 67 km, one notices that traction demands are greatly reduced, while the peak for brake demands at 77 km is also reduced. Table 7.5 reflects these energy reductions.

Overall, the in-train force and control input patterns are less jittering and smoothened out when compared to the generic controller, at a minimal reduction of velocity tracking error. The advantages are substantial for in-train force emphasised controller.

### 7.2.4 Closed-loop Controller Optimised for Energy Consumption

The last aspect of the weight tuning is on energy reduction. From the results from previous section, one already expects energy consumption reduction will

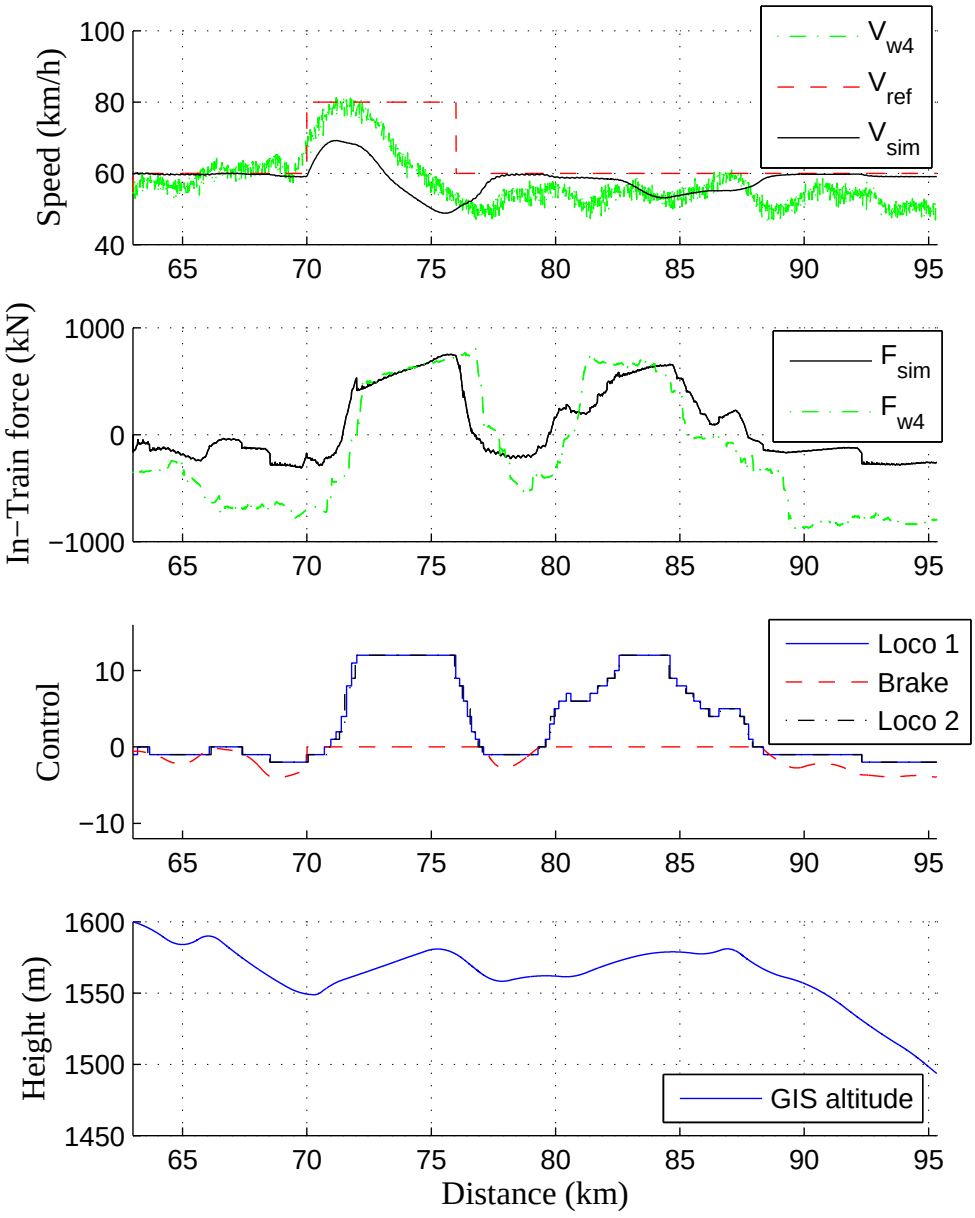


Figure 7.7: Closed-loop controller with emphasis on in-train force reference set 1.

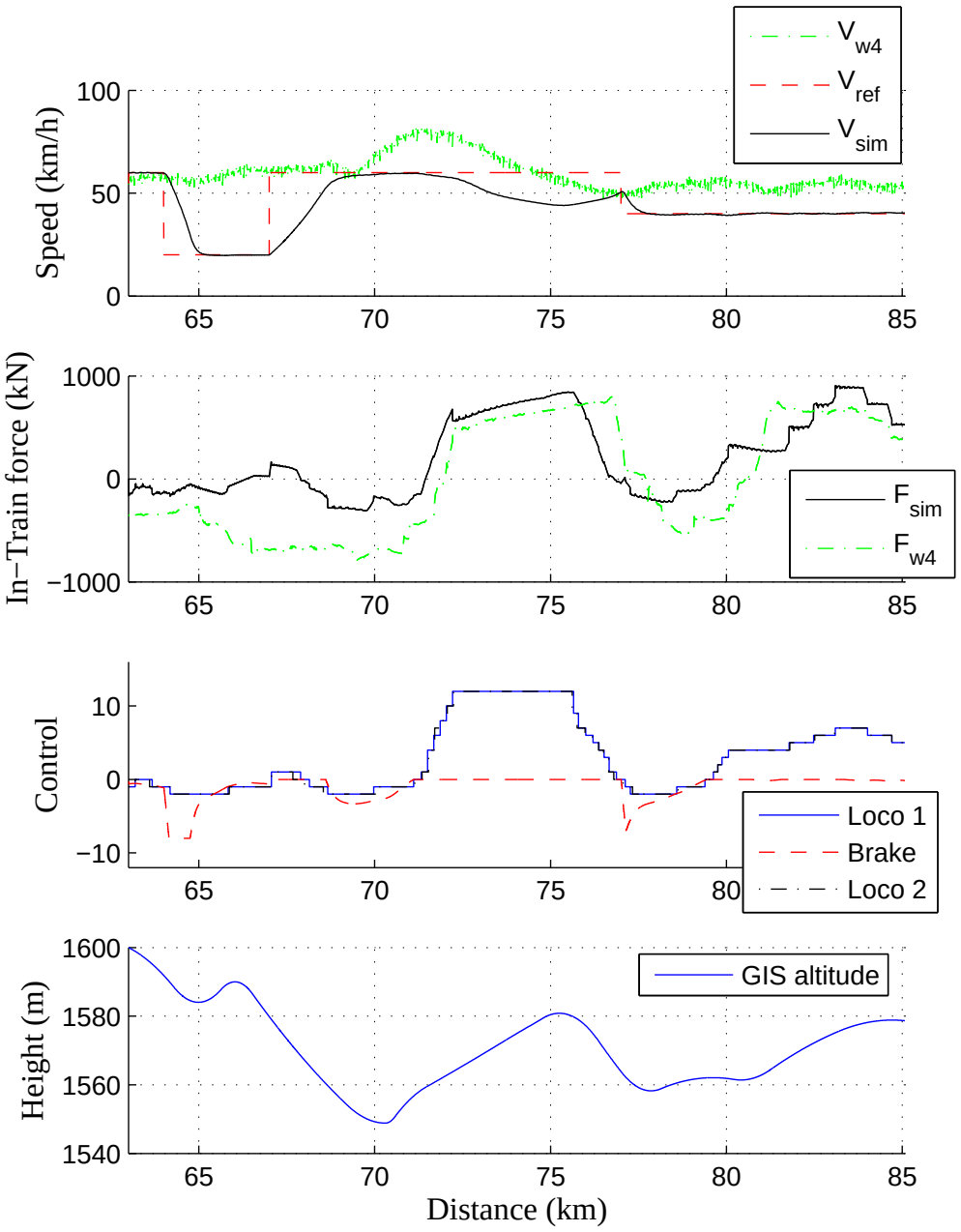


Figure 7.8: Closed-loop controller with emphasis on in-train force reference set 2.

| | Current value | | Reference 1 | |
|---|---|---|---|---|
| Velocity Deviation | | | | |
| Absolute mean | 7.0659 | km/h | 5.1649 | km/h |
| Mean | -7.0623 | km/h | -5.1521 | km/h |
| In-train force | | | | |
| Minimum | -337.6011 | kN | -321.6026 | kN |
| Maximum | 762.546 | kN | 717.0152 | kN |
| Energy consumption | | | | |
| Traction | 698.5708 | MJ | 698.1804 | MJ |
| Dynamic Braking | -96.4332 | MJ | -87.1825 | MJ |

Table 7.6: Performance indices for energy emphasised controller compared to reference 1.

also bring down in-train force.

Weights for velocity tracking $q_2$ are decreased to 0.1, while weights for energy consumption $r$ are increased to 12. It is clear already that velocity tracking will deteriorate slightly.

It is important that Fig. 7.9 and Fig. 7.10 be compared closely, because peak values again does not vary much due to the exceeding ruling grade. Examining the input peaks, one would find that with this controller has minimised all of the short peaks.

The results are smoothened in-train forces and slightly deteriorated velocity tracking.

From Fig 7.8 and Fig. 7.10, it is clear that both controllers only managed to reduce energy consumption, they also improved the overall controller performance.

Control inputs have been even out, with optimal use of gravitational force during downhill, evident in the track section between 63 km and 70 km. The traction demand just after 70km was minimised.

| | Current value | | Reference 2 | |
|---|---|---|---|---|
| Velocity Deviation | | | | |
| Absolute mean | 8.6896 | km/h | 5.4804 | km/h |
| Mean | -4.6265 | km/h | -3.4834 | km/h |
| In-train force | | | | |
| Minimum | -304.03 | kN | -788.8906 | kN |
| Maximum | 854.5669 | kN | 1041.2118 | kN |
| Energy consumption | | | | |
| Traction | 537.9416 | MJ | 620.9923 | MJ |
| Dynamic Braking | -132.5898 | MJ | -157.1676 | MJ |

Table 7.7: Performance indices for energy emphasised controller compared to reference 2.

Because of the smoothened input pattern, in-train force has been improved to the similar level as the previous controller. Comparing values in Table 7.5 and Table 7.7 shows that the in-train force controller is able to reduce around 100 kN more for the minimum peak.

Velocity tracking is slightly better than the in-train force emphasised controller.

## 7.3 A closer look: Dynamic in-train force and train configuration

The in-train force analysed up to now has been the maximum of the static in-train force, *i.e.*, it is the maximum force that a single coupler has to withstand. With the locomotive group concentrated at the front, the coupler that bridges locomotive group and wagon group has to withstand the largest static in-train force. The previous section only considered static in-train force. There exists, however, a dynamic in-train force with the train, which shall be explained next.

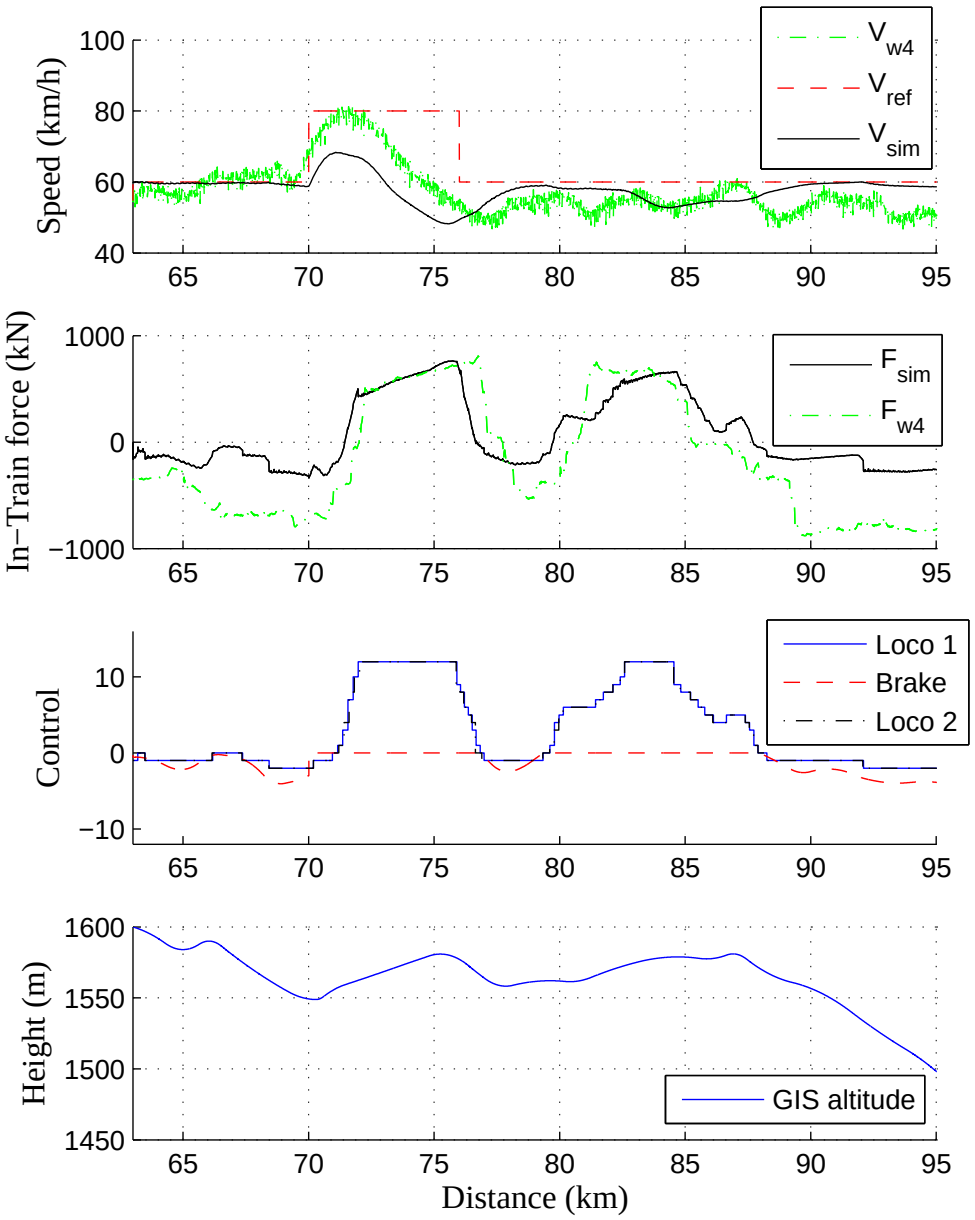


Figure 7.9: Closed-loop controller with emphasis on energy consumption reference set 1.

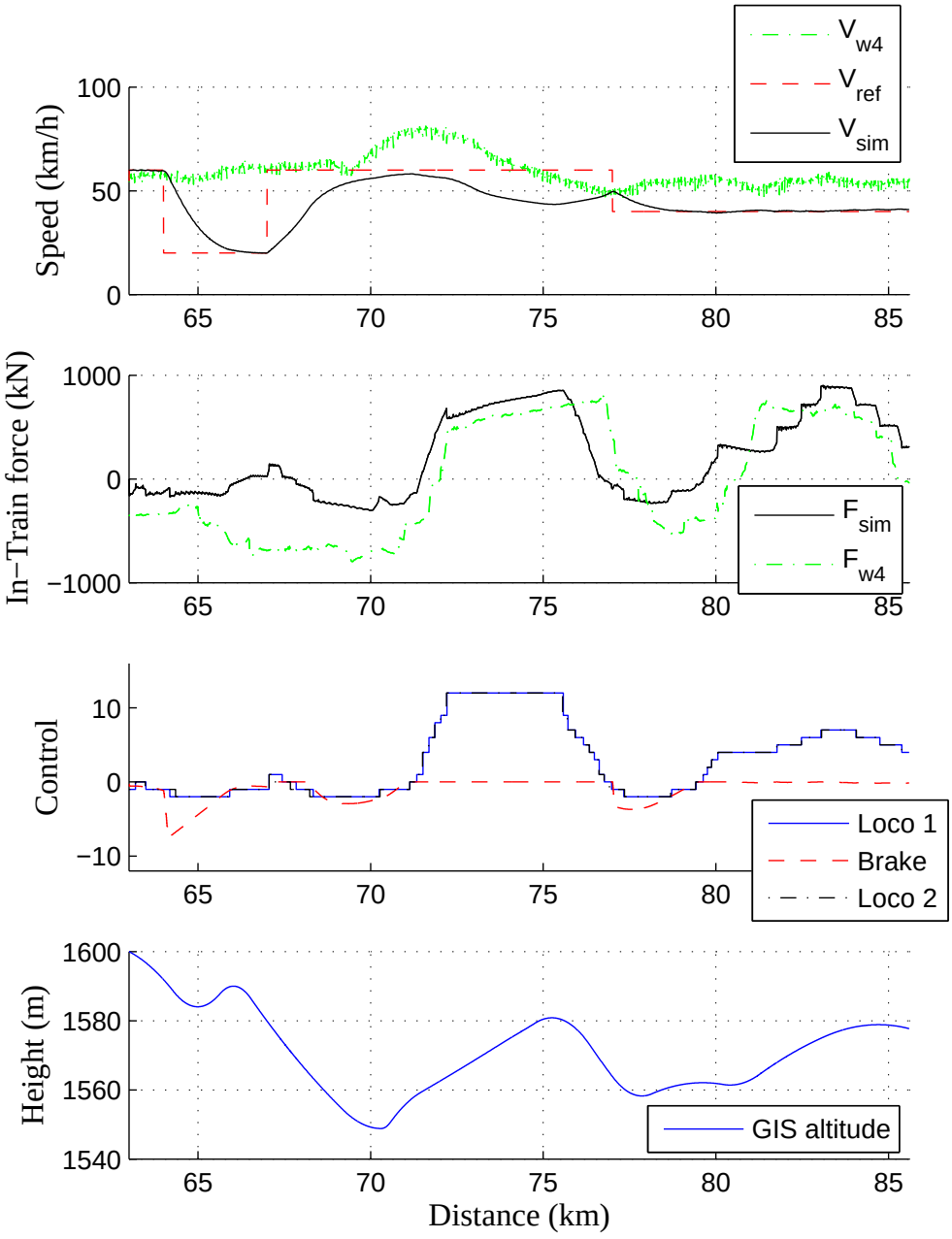


Figure 7.10: Closed-loop controller with emphasis on energy consumption reference set 2.

In Fig. 7.12, the maximum and minimum dynamic in-train forces are plotted along with the static in-train force. Notes these two forces do not belong to a single coupler; they are the maximum and minimum force out of all the couplers at that particular instant of time. Dynamic in-train forces travels across the train in either direction depending on the control inputs and track topology. These sudden peaks of in-train forces cause damage to coupler systems. Due to it propagating properties, it is very difficult to analyse in practice. With simulation, such property can be easily examined.

Train configuration involves closely to the practicality of the application. In practice, all Coallink wagons will become ECP wagons. The same does not necessarily apply to DP conversion of locomotives. Thus, it will be interesting to see if the various combinations of train configuration will affect train performance greatly.

In this section, the objectives is to analyse the effects of different train configurations, especially toward minimising dynamic in-train force. In-train force optimised controller is chosen. From the previous results, it is clear that by improving static in-train force, inputs chattering as well as energy consumption are also improved. The weights are again adjusted as follows: $q_2$ for both locomotive and wagon remain at 1, while $q_1$ for in-train force is increased to 12, with $r_l$ is slightly increased to 3 to encourage wagon brake usage.

The only exception is the fence case, where $q_1$ was slightly perturbed to 12.01 to satisfy the LQR criteria that the weights $\mathbf{Q}$ and $\mathbf{R}$ need to be chosen such that matrix $[\mathbf{Q} \quad \mathbf{N}; \mathbf{N}' \quad \mathbf{R}]$ positive definite, where $\mathbf{N}$ is a zero matrix of dimension $2n \times r$, $r$ is the dimension of matrix $R$.

For this set of comparisons, only velocity reference 2 will be used. This set will allow more subtle dynamics to be observed with its lower reference values.

The train configurations are:

(i) Unified traction and unified ECP control

(ii) DP traction and unified ECP control

(iii) DP traction and limited individual ECP via fencing

| | config 1 | config 2 | config 3 | config 4 |
|---|---|---|---|---|
| Velocity Deviation | | | | |
| Absolute mean (km/h) | 4.9409 | 5.212 | 5.2289 | 6.2383 |
| Mean (km/h) | -3.1756 | -3.4242 | -3.4494 | -3.636 |
| Static In-train force | | | | |
| Minimum (kN) | -550.3345 | -480.1369 | -480.3234 | -312.179 |
| Maximum (kN) | 842.2614 | 910.3569 | 911.342 | 902.7567 |
| Dynamic In-train force | | | | |
| Minimum (kN) | -903.3571 | -934.3943 | -897.5539 | -860.1895 |
| Maximum (kN) | 1034.6011 | 1041.5338 | 1044.6036 | 921.2674 |
| Energy consumption | | | | |
| Traction (MJ) | 926.2305 | 898.9187 | 896.7763 | 870.7232 |
| Dynamic Braking (MJ) | -130.5269 | -137.931 | -137.8525 | -138.8401 |

Table 7.8: Performance indices for the four configurations.

(iv) Full individual traction and brake control

The results are displayed via the configuration order. The three outputs are: velocity regulation in Fig. 7.11, in-train force in Fig. 7.12 and control inputs in Fig. 7.13. The performance indices are given in Table 7.8. The perturbation is less than 1%, for practicality the controllers for all four configurations are assumed to be identical.

From the results, some very interesting observations can be made. Since all four configurations have identical controller structure, the only difference lies in the train configuration.

Looking first at velocity tracking, it is clear that the train with unified traction and unified ECP brake configuration gave the best results, although the differences are minimum.

Analysing static and dynamic in-train force together reveals some insight into the advance train configuration such as individual control. The mono-

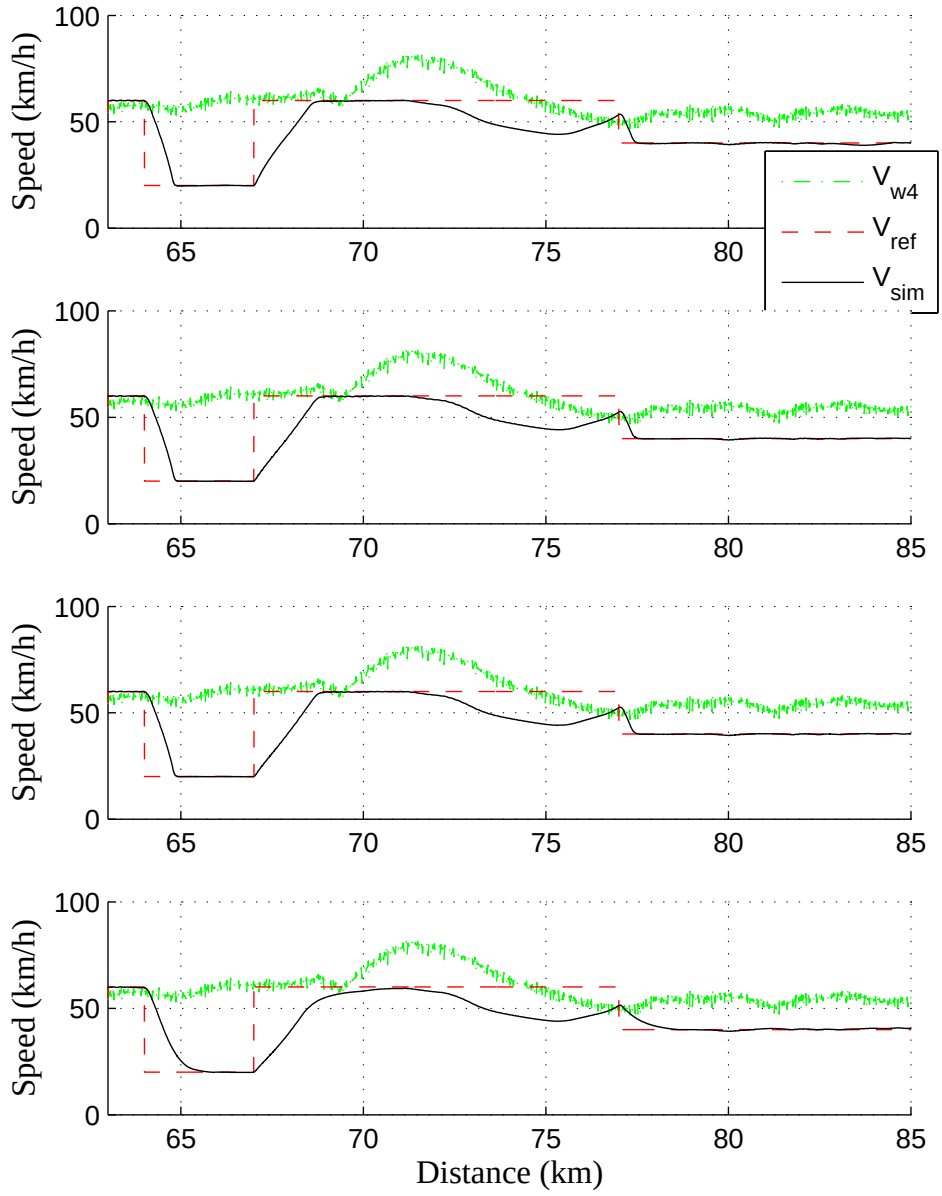


Figure 7.11: Train configuration comparison: velocity tracking (in configuration list order).

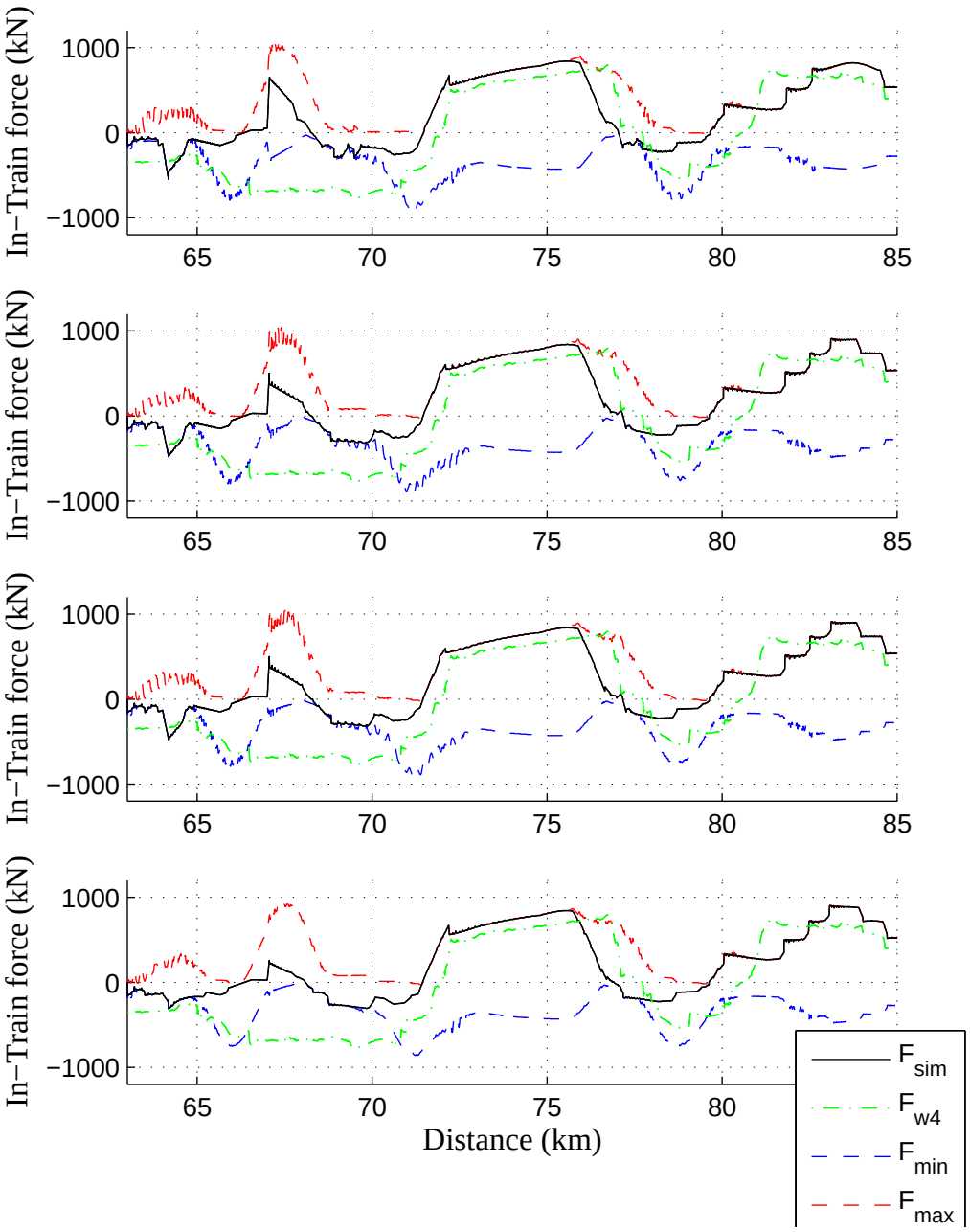


Figure 7.12: Train configuration comparison: dynamic and static in-train force (in configuration list order).

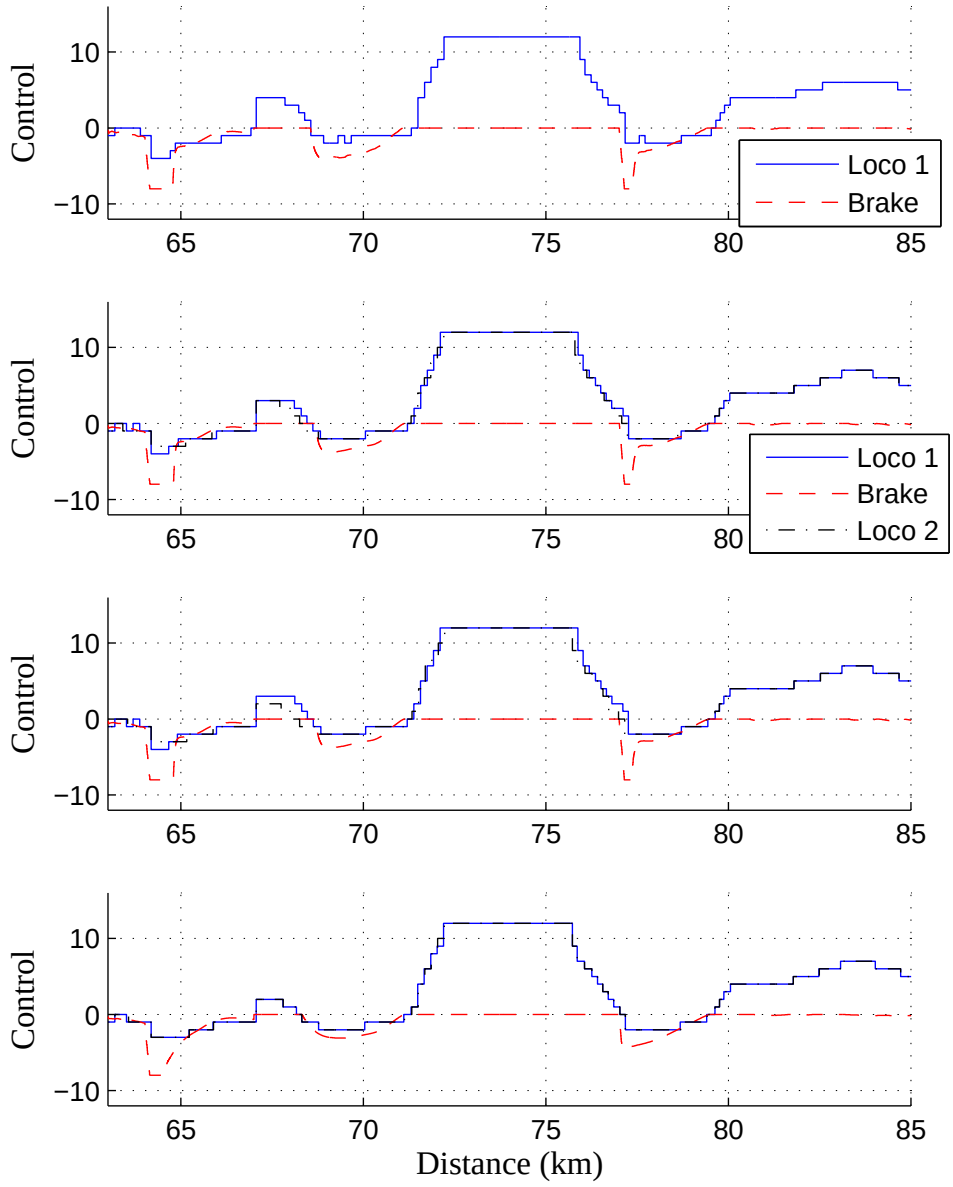


Figure 7.13: Train configuration comparison: control inputs (in configuration list order).

tonic decreasing of minimum peaks from left to right shows that both static and dynamic forces decreases as control inputs increase. The pattern in the maximum peaks is less defined for static in-train force due to the exceeding ruling grade, where all four configurations require similar maximums. The dynamic in-train force peaks, however, exhibits the decreasing pattern similar to those of the minimum peaks. This further demonstrates the improvement of individual controls.

Going to Fig 7.12 shows similar behaviour. From the maximum and minimum peaks between 63 km and 70 km, it is clear that individual control substantially reduces the oscillations in dynamic in-train force.

DP control is an interesting case: from both Fig 7.12 and Table 7.8, it is clear that with the increased inputs, the static in-train force peaks do decrease. Yet the dynamic in-train force does not improve. One possible reason for such behaviour is that the use of two different locomotive groups introduces additional in-train force dynamics.

A mild improvement in energy consumption can be observed for train with multiple brake control.

Observing the general pattern in the Fig 7.12 and Fig 7.13, the advantage of individual control is clear: it smoothens out the inputs, reducing the frequency of notch changes, and thus improve the in-train force behaviours.

From the results, it can be deduced that dynamic in-train force can be reduced via increase in control inputs to train configuration.

## 7.4 Discussion

In this section, the simulated results are compared to the result from the existing studies.

### 7.4.1 Modelling

All existing studies as well as this study assume all the states are available. Gruber and Bayoumi (1982) suggests an observer that calculates the missing wagon velocities by linear interpolation of the locomotive velocities. It should be noted this is neither optimised nor validated, and will result in errors for long trains such as Coallink train where locomotives are only found at the ends of the train.

While the models used in Yang and Sun (2001) and Astolfi and Menini (2002) are very similar to the model used in this study, this research goes a step further by simulating a much longer train and the inclusion of all non-linearities, as well track topology. In comparison, the model used by Gruber and Bayoumi (1982) is very much simplified; track topology was not considered; spring force of the front coupler of every car is ignored; the train is much shorter and has a fixed configuration. In this study, the train configuration is dynamic for different locomotive configurations.

In terms of inputs, all the previous studies ignored power limits and other control signal non-linearities. Even more, in the controller proposed by Gruber and Bayoumi (1982), only two possible traction/brake combinations are considered: pure locomotive traction with no wagon brake and pure locomotive and wagon brake. This greatly reduces control optimality as often long train would apply both brake and traction simultaneous for difficult terrains to reduce in-train forces.

In this study, power limits as well as rate limits are applied to the control signals. The locomotive signals are filtered to reduce input chattering before quantised to the exact locomotive notches.

In the case of limited input channels, this study proposes a dynamic controller structure based on the current track conditions, providing an optimal control structure that can grow and shrink on demand. The paper by Gruber and Bayoumi (1982) only considers simple static grouping of cars into equal groups.

All the previous studies provide theoretical look at train modelling. This study is the only study that has validated the theoretical model with actual data.

### 7.4.2 Controller

In terms of open-loop controller, this study mimics the human driver behaviour by considering the track grade and curvature. No optimisation is performed in this process. Similar schedule is proposed by Gruber and Bayoumi (1982). In comparison, the optimal control propose by Howlett (1996) provides a energy consumption optimised scheduling for the given track. However, only single mass train is assumed. A more complete optimised open-loop control is recently proposed by Zhuan and Xia (2005).

Gruber and Bayoumi (1982) mentioned the need for transient control for additional acceleration and deceleration, but only proposed that closed-loop control be used to handle such needs. In this study, an open-loop transient controller is proposed and demonstrated to operate as expected, as long as the train travels along normal track that falls within specification.

Optimised controllers proposed by Yang and Sun (2001) focused on the velocity regulation and disturbance rejection while Gruber and Bayoumi (1982) focused on velocity regulation and in-train force. However, neither controller offered tunability of control targets. Due to different priorities different operation scenarios may have, in this study the closed-loop controller was designed to allow parameter tuning amongst the three running costs: energy consumption, shorter travelling time via better velocity regulation and lower maintenance cost through lower in-train forces.

Reconfigurable controller through fencing is an interesting control method proposed by this study that showed mild overall improvements, as observed from the results.

The results show that the closed-loop cruise controller proposed in this study is both complete and optimised. Considerations were given to control flexibility and interface problems for implementation. This, together with the validated model, completes the study as a thorough optimised train controller that is applicable to the Coallink train. No other studies have shown such proven modelling as well as controller design that consider the interface problem between theoretical model and the actual train.

# Chapter 8

# Conclusion

In this study, a closed-loop cruise controller that minimises the running costs of heavy-haul train is designed, with optimisations on velocity tracking, in-train forces and energy consumption.

By improving velocity tracking, the train will be travelling at the highest allowed velocity, thus reducing the travelling time. This will increase throughput on the existing lines as well as decrease the chances of receiving heavy fines from the shipping company for late deliveries.

Large in-train forces result in coupler damages and the subsequent high maintenance costs. By reducing the in-train forces, coupler system wears are reduced, thus reducing maintenance costs.

Energy consumption is directly related to the amounts and duration of control efforts used. Thus, controller with efficient control utilisation will reduce energy consumption.

Coallink train with the new train technologies, Distributed Power (DP) traction and Electronically Controlled Pneumatic (ECP) brake system was the target for the research.

The model was validated with Spoornet data. The controllers were designed and tested on the validated model. Validation of the model is important for both future implementation of the controller as well as validation of the research methods employed in this study.

Robustness of the LQR closed-loop controller is guaranteed as long as the parameters are well defined (Lin and Olbrot, 1996). In application, train parameters are entered into the system during the initialisation stage. This reconfigures the controller for that particular train for both performance and robustness.

The control inputs limiters confines the rate of change as well of the extreme values of the control inputs within the acceptable range. This low-pass action eliminates undesired abrupt changes and other high frequency components that could induce large in-train forces as well as excessive oscillation, thus improves on the robustness of the controller.

Individual control of remote consists showed little improvement in the pull-push configuration where locomotive groups are found at the head and the end of the train, unless careful tuning of the parameters were performed. Possible improvement could arise for mid-train consist but the expensive logistic cost could out weight any practical gains from such configuration.

The closed-loop controller behaviour can be redefined online by choosing a different set of weights. This adds flexibility whereby the driver can decide which running costs he wishes to minimise, given the current conditions. Future possibilities include online adaptive parameter tuning whereby the controller improves its performance by adjusting the weights automatically.

In the light of feasibility and logistic costs, this research has demonstrated that unified traction and unified ECP configuration is the most economical when performance, deployment cost and easy tuning are concerned. On the other hand, weight choices for the closed-loop control can affect the performance greatly.

With the completion of this study on closed-loop cruise controller for heavy-haul train, the next step will be the implementation of the controller to improve the efficiency of the current train and working environment for the train drivers.

In this study, it is assumed that all state variables are available. These are usually obtained by designing an observer. In the implementation stage, it is also suggested that state estimates could be obtained from Profiler, a train simulation product of New York Air Brake. A second approach is to install more speed sensors, and then followed by some soft sensors to get more accurate state estimates.

# Bibliography

AAR (2002). Manual of standards and recommended practices, electronically controlled brake system. Technical report. Association of American Railroads.

Astolfi, A. and L. Menini (2002). Input/output decoupling problems for high speed trains. *Proceedings of the American Control Conference* pp. 549–554.

Garg, V.K. and R.V. Dukkipati (1984). *Dynamics of Railway Vehicle Systems*. xiii ed.. Toronto: Academic Press.

Goodwin, G.C., S.F. Graebe and M.E. Salgado (2001). *Control System Design*. New Jersey: Prentice Hall.

Gruber, P. and M.M. Bayoumi (1982). Suboptimal control strategies for multilocomotive powered trains. *IEEE Transaction on Automatic Control* **27**(3), 536–546.

Halder, B. and T. Kailath (1999). Lmi based design of mixed $h_2/h_\infty$ controllers: the state feedback case. *Proceedings of the 1999 American Control Conference, San Diego, USA* pp. 1866–1870.

Howlett, P. (1996). Optimal strategies for the control of a train. *Automatica* **32**(4), 519–532.

Ishikawa, Y. and A. Kawamura (1997). Maximum adhesive force control in super high speed train. *Proceedings of the Power Conversion Conference - Nagaoka* **2**, 951–954.

Khmelnitsky, E. (2000). On an optimal control problem of train operation. *IEEE Transaction of Automatic Control* **45**(7), 1257–1266.

Kull, R.C. (2001). Wabtec ECP system update. *Proceedings of the 2001 IEEE/ASME Joint Railroad Conference* pp. 129 – 134.

Lin, F. and A.W. Olbrot (1996). An LQR approach to robust control of linear systems with uncertain parameters. *Proceesings of the 35th Conference in Decision and Control* pp. 4159–4163.

NYAB (2003). Leader system. Technical report. New York Air Brake.

Scherer, C., P. Gahinet and M. Chilali (1997). Multiobjective output-feedback control via lmi optimization. *IEEE Transactions on Automatic Control* **42**, 896–911.

Slotine, J.J.E. and W. Li (1991). *Applied Nonlinear Control*. New Jersey: Prentice Hall.

Spoornet (2002). Introduction to electronic control pneumatic brake & wire distributived power. Technical report. Spoornet.

Spoornet (2003). Spoornet website. http://www.spoornet.co.za.

Tang, T. and C. Gao (1996). A new train speed automatic control system for chinese railway. *Proceedings of the IEEE International Conference on Industrial Technology* pp. 76–79.

Thelen, G.A. and Y.H. Tse (1990). An automatic speed enforcement system for heavy freight trains. *Railroad Conference* pp. 31–39.

Watanabe, I. and T. Takashige (1994). Advance automatic train protection system. *IEEE Vehicular Technology Conference* **2**, 1126–1129.

Watanabe, T. and M. Yamashita (2001). A novel anti-slip control without speed sensor for electric railway vehicles. *The 27th Annual Conference of the IEEE Industrial Electronics Society* **2**, 1382–1387.

Wu, N. (1995). Control design for reconfigurability. *Proceedings of the American Control Conference* pp. 102–106.

Yang, C.D. and Y.P. Sun (2001). Mixed $H_2/H_\infty$ cruise controller design for high speed train. *International Journal of Control* **74**(9), 905–920.

Zhuan, X. and X. Xia (2005). Cruise control scheduling of heavy haul trains. Technical report. Department of EECE, University of Pretoria.

# Appendix A

# Coallink Handwritten Inputs Notes

Sample copy of the handwritten inputs notes from Coallink test runs are included to show some of the accuracy problems faced during the verification stage.